https://ntrs.nasa.gov/search.jsp?R=19810005831 2020-03-21T14:29:00+00:00Z

NASA
TP
1775
c.1

NASA Technical Paper 1775

LOAN COPY: R
AFWL TECHNI
KIRTLAND AFB
0068097
TECH LIBRARY KAFB, NM

Vibration Characteristics of a Steadily Rotating Slender Ring

Frederick J. Lallman

DECEMBER 1980

NASA

TECH LIBRARY KAFB, NM

0068097

NASA Technical Paper 1775

Vibration Characteristics of a Steadily Rotating Slender Ring

Frederick J. Lallman
Langley Research Center
Hampton, Virginia

NASA
National Aeronautics
and Space Administration

Scientific and Technical
Information Branch

1980

SUMMARY

A system of partial differential equations of motion for a steadily rotating circular ring is derived. The ring is homogeneous with cross-sectional dimensions which are small relative to the overall diameter. Small deflections from the steady-state condition are assumed so that the equations of motion are linear.

Four sets of structural modes are examined. The torsional modes consist of rotations about the line of centroids of the cross section with small deflections perpendicular to the plane of the ring. The out-of-plane bending modes consist of deflections perpendicular to the plane of the ring accompanied by rotations about the line of centroids. The in-plane bending modes consist of radial deflections with small tangential motions. The compression modes consist of stretching and compression of the line of centroids with small radial deflections.

For each mode, the motions are written as sinusoidal functions of time and position around the circumference of the ring. Several low-numbered modes are shown to be rigid body motions which agree with commonly known results of rigid body mechanics. Formulas for the frequencies of vibration and the ratios between different perturbation variables are derived. In many cases the formulas are simplified. For example, for low spin rates the frequencies of vibration of the bending modes approach the frequencies for a linear beam. At high spin rates, these frequencies approach the frequencies for a string under tension.

Several figures are used to demonstrate the spatial and temporal characteristics of the structural modes. The derived formulas are applied to an example problem. The results of the example are plotted to illustrate the effects of spin rate and mode number upon the frequencies of vibration and other parameters which quantify the vibrational characteristics of the spinning ring.

INTRODUCTION

Attitude control of spacecraft is accomplished by generating torques, either externally as may be done by small rocket thrusters or internally by stored momentum control devices. One example of a stored momentum control device is the control moment gyro (CMG). (See ref. 1.) The CMG consists of a momentum wheel which is supported in a gimbal system. Torques applied to the support bearings of the wheel cause it to precess. The precession is used to change the spacecraft attitude. In reference 1, three CMG's are arranged so that the nominal spin axis of each CMG is aligned with one of the spacecraft axes. Another example of a stored momentum control device is the so-called scissors gyro concept described in references 2 and 3. In this approach, two

momentum wheels are arranged so that their nominal spin axes coincide but their spin directions are opposite. Precession of these wheels in opposite directions results in a net transfer of angular momentum to the spacecraft.

The effectiveness of a momentum wheel in a given application depends on the amount of angular momentum which can be produced about its spin axis. The moment of inertia of the wheel and its operating spin rate determine the angular momentum. In general, devices which are to be placed in spacecraft are designed with the least possible mass so that required launch system capabilities are minimized. Meeting the inertia requirement of a momentum wheel while minimizing its mass leads to the annular momentum control device (AMCD). (See ref. 4.) The AMCD consists of a ring (annulus) which is supported by noncontacting magnetic bearings and is spun by a noncontacting electromagnetic motor. For large precessions, the ring and its magnetic bearing assembly can be rotated in a gimbal system. Small accurate precessions may be obtained by varying the magnetic forces in the bearings. An advantage of the AMCD concept over conventional shaft-mounted momentum wheels is that the mass of the center portion of the wheel is eliminated with a relatively small reduction in the moment of inertia.

With the possibility of future spacecraft being gigantic, AMCD's of very large dimensions can be envisioned. As AMCD's increase in overall diameter and decrease in cross-sectional area, their flexibility increases. Thus, structural modes in the device must be considered in the design.

Several analyses of structural vibrations occurring in rotating systems are in the literature. For example, reference 5 examines the flexural vibrations of rotating shafts with various loads, support methods, and unbalance conditions. This work treats high-speed rotary systems in which the shafts rotate at speeds in excess of their critical speeds. When the rotational period approaches the period of transverse flexure modes of the shaft, divergent oscillations occur and cause severe bearing vibrations and possible structural failure. A second type of instability occurring in rotating systems is discussed in reference 6. This work analyzes a self-excited oscillatory helicopter rotor instability. This potentially dangerous phenomenon was shown to be caused by a conversion of the rotational energy of the rotor into oscillatory energy of the blades. Both of the above types of instability can be present in centrifuges. Reference 7 examines the stability characteristics of a centrifuge which is mounted in a large spacecraft. The shaft critical-speed instability arises because the mass of the centrifuge is concentrated along the arm connecting the gondala and counterbalance with the hub. The second oscillatory instability is associated with flexure of the arm and movement of the hub. The speed ranges within which these instabilities occur can be adjusted by altering the mass distribution, stiffness properties, and damping characteristics of the centrifuge.

Circular rings and arches have long been employed in construction (buildings, aqueducts, bridges, etc.) and in cylindrical vessel designs (tanks, pipelines, aircraft, etc.). The strength, rigidity, and possibility of buckling are considerations in these designs. Calculated static stresses, deflections, and elastic stability characteristics of circular rings and arches with various loading conditions can be found in reference 8. A brief analysis of the

stresses within a steadily rotating hollow disk can be found in reference 9. This work does not include vibrations or structural modes.

An early analysis of the vibrations of a circular ring can be found in reference 10. This analysis considers a slender ring which has a circular cross section, is not spinning, and has no external influences (forces) acting upon it. The linear analysis produces formulas for the frequencies of oscillation for flexural vibrations in the plane of the ring, flexural vibrations perpendicular to the plane of the ring, and extensional vibrations along the line of centroids of the ring. Reference 11 examines the forced response characteristics of the flexural vibrations perpendicular to the plane of the ring. Forcing terms are added to the analysis of reference 10 and generalized coordinates are used in developing the response of the vibrational modes to externally applied forces. A corresponding analysis of the forced response characteristics of the flexural vibrations and the extensional vibrations in the plane of the ring is also developed in reference 11. The analysis of the flexural vibrations is validated by a physical experiment. A nonlinear analysis of the flexural vibrations in the plane of the ring is developed in reference 12. Nonlinear resonance curves which demonstrate a nonlinearity of the softening type are developed. The analysis is supported by physical experiment. An analysis of the forced vibrations of a ring which is spinning is presented in reference 13. The linearized structural mode dynamics are developed in terms of generalized coordinates by means of Lagrange's equations. This work considers a thin, flexible ring with flexural and extensional vibrations in the plane of the ring and flexural vibrations perpendicular to the plane of the ring.

The present paper derives linearized equations of motion of a spinning circular ring by application of Newton's law and Euler's equation following the method of reference 14. The resulting set of linear partial differential equations describe the small-amplitude dynamics of the flexural and extensional motions in the plane of the ring, the flexural motions perpendicular to the plane of the ring, and the twisting motions about the centroid of the ring. The vibration frequencies and modal characteristics of the freely vibrating ring are examined in detail with emphasis on physical interpretation of the mathematical results.

The equations of motion are developed in appendix A. These equations are examined in the main text. The individual vibration modes are identified and simple expressions for their characteristic properties (for example, vibration frequencies) are derived. The spatial and temporal characteristics of each vibration mode are illustrated in several figures. Formulas developed in this paper are applied to an example ring and numerical results are presented.

SYMBOLS

A area of ring cross section, m^2

$A_j, B_j, C_j, \ldots, H_j$ modal amplitudes of homogeneous solutions of wave equations

C_A ratio between amplitudes of twist angle and out-of-plane deflection, rad/m

E	modulus of elasticity, Pa
E_G	nondimensional constant equal to EI_r/GJ
$\hat{e}_1,\hat{e}_2,\hat{e}_3$	unit direction vectors of curvilinear coordinate system
$\hat{e}_r,\hat{e}_\theta,\hat{e}_z$	unit direction vectors of cylindrical coordinate system
$\bar{F}$	force vector acting on cross section
F_1,F_2,F_3	components of $\bar{F}$ in curvilinear coordinate system
G	shear modulus, Pa
G_F	ratio between amplitudes of tangential perturbation and radial perturbation, nondimensional
I_p	polar moment of inertia of ring cross section, m^4
I_r,I_z	area moments of inertia of ring cross section, m^4
$\hat{i},\hat{j},\hat{k}$	unit direction vectors of inertial coordinate system
J	torsional constant of ring cross section, m^4
j	mode number
$\bar{M}$	moment vector acting on cross section
M_1,M_2,M_3	components of $\bar{M}$ in curvilinear coordinate system
R	radius of unstressed ring, m
ΔR	radius change caused by centrifugal force
$\bar{R}$	radius change caused by a small increment in spin rate
$\bar{r}_c$	location of ring centroid in inertial space
$\bar{r}_f$	location of ring fiber in inertial space
S_J	nondimensional constant equal to $\sqrt{J/AR^2}$
S_p	nondimensional constant equal to $\sqrt{I_p/AR^2}$
S_r	nondimensional constant equal to $\sqrt{I_r/AR^2}$
S_z	nondimensional constant equal to $\sqrt{I_z/AR^2}$
s	arc length from reference point on ring to any other point on ring

$T_a, T_b, T_c, \ldots$ polynomial coefficients

t time, sec

u radial perturbation variable, m

u_j in-plane nodal frequency, rad/sec

v tangential perturbation variable, m

v_j in-plane nodal velocity, m/sec

v_r velocity of transverse sound waves, equal to $\sqrt{G/\rho}$, m/sec

v_s velocity of longitudinal sound waves, equal to $\sqrt{E/\rho}$, m/sec

$\bar{W}$ externally applied control force density, N/m

W_1, W_2, W_3 components of $\bar{W}$ in curvilinear coordinate system

w out-of-plane deflection perturbation variable, m

X, Y, Z inertial coordinate axes

x, y, z components of displacement for rigid body translation modes

$\dot{x}, \dot{y}, \dot{z}$ components of velocity for rigid body translation modes

x_f radial location of fiber with respect to centroid

x_{min} radial location of the innermost fiber with respect to centroid

z_f axial location of fiber with respect to centroid

β angle-of-twist perturbation variable, rad

γ shearing strain, nondimensional

ε strain, nondimensional

ε_{max} maximum strain occurring among fibers caused by centrifugal force

ε_o strain of line of centroids caused by centrifugal force

θ, ϕ, ψ angular components for rigid body rotation modes, rad

$\dot{\theta}, \dot{\phi}, \dot{\psi}$ angular rate components for rigid body rotation modes, rad/sec

θ_p, ϕ_p angular components for rigid body precession modes, rad

λ tangential distance from X-axis to fixed observation point

ρ mass density of unstressed ring, kg/m^3

σ stress, Pa

σ_a maximum allowable stress, Pa

σ_{max} maximum stress occurring among fibers caused by centrifugal force, Pa

τ shearing stress, Pa

Ω spin rate of ring, rad/sec

Ω_a spin rate required to produce the maximum allowable stress σ_a, rad/sec

Ω_L limiting spin rate for static stability, rad/sec

ω frequency of oscillation, rad/sec

ω_r velocity of transverse sound waves divided by the radius of the ring, rad/sec

ω_s velocity of longitudinal sound waves divided by the radius of the ring, rad/sec

Subscripts:

B in-plane bending mode

C in-plane compression mode

D out-of-plane bending mode

j mode number

P progressive wave

R regressive wave

S relative to inertial space

T torsional mode

u in-plane mode

w out-of-plane mode

Special symbols:

A dot over a variable (e.g., $\dot{v}$) denotes differentiation with respect to time.

A prime after a variable (e.g., v') denotes a spatial derivative with respect to s.

Vertical bars enclosing a vector quantity (e.g., $|\bar{r}_c|$) denote the length of the vector.

EQUATIONS OF MOTION

The linearized equations of motion for a steadily rotating slender ring are derived in appendix A. The properties of the ring and the assumptions used in the derivation are as follows:

1. The ring is circular and has a uniform cross section.

2. One principal axis of the cross section is parallel to the spin axis. The other principal axis lies in the plane of the ring.

3. The ring is rotating about its axis at a constant rate.

4. Perturbations of the ring from its steady state are small so that products of the perturbation variables with each other may be neglected.

5. Externally applied forces are small so that products of these forces with the perturbation variables may be neglected.

6. The stress-strain relationships of the material of the ring are linear.

7. The damping of the material of the ring is negligible.

8. Deformations caused by transverse shear are ignored.

9. Rotary inertia terms are included.

10. The relative change in the radius of the ring caused by its steady rotation is small.

11. The rate of rotation is small relative to the speed of sound traveling around the circumference of the ring.

The small-perturbation equations of motion derived in appendix A (eqs. (A54) to (A57)) are

$$\ddot{u} - 2\Omega\dot{v} - \Omega^2 u = \frac{W_1}{\rho A} - \omega_s^2 S_z^2 (R^4 u'''' + 2R^2 u'' + u) - \omega_s^2 (Rv' + u)$$
$$+ \Omega^2 (R^2 u'' - Rv') + S_z^2 (R^2 \ddot{u}'' - R\ddot{v}') \tag{1}$$

$$\ddot{v} + 2\Omega\dot{u} = \frac{W_2}{\rho A} + \omega_s^2 (Ru' + R^2 v'') + \Omega^2 Ru' + S_z^2 (R\ddot{u}' - \ddot{v}) \tag{2}$$

$$\ddot{w} = \frac{W_3}{\rho A} - \omega_s^2 S_r^2 (R^4 w'''' - R^3 \beta'') + \omega_r^2 S_J^2 (R^2 w'' + R^3 \beta'')$$
$$+ \Omega^2 R^2 w'' + S_r^2 R^2 (\ddot{w}'' - 2\Omega\dot{\beta}' - \Omega^2 w'') \tag{3}$$

$$S_p^2 (\ddot{\beta} + \Omega\dot{w}') + \left(S_r^2 - S_z^2\right)\Omega(\dot{w}' - \Omega\beta) = \omega_r^2 S_J^2 (R^2 \beta'' + Rw'')$$
$$+ \omega_s^2 S_r^2 (Rw'' - \beta) \tag{4}$$

where

Ω is spin rate.

R is the radius of the unstressed ring.

A is the area of the ring cross section.

ρ is the mass density of the unstressed ring.

u is a small-perturbation displacement in the radial direction.

v is a small-perturbation displacement in the tangential direction.

w is a small-perturbation displacement perpendicular to the plane of the ring.

β is the small-perturbation angle of rotation about the line of centroids.

W_1, W_2, and W_3 are external distributed force densities (force per unit length) acting in the radial direction, tangential direction, and perpendicular to the plane of the ring, respectively.

u, v, w, W_1, W_2, and W_3 are functions of s and t.

t is time.

s is the arc length from a reference point on the ring to any other point on the ring.

A dot over a variable denotes differentiation with respect to time.

A prime after a variable denotes a spatial derivative with respect to s.

The constants appearing in equations (1) through (4) are defined as follows:

$$\omega_s = \sqrt{\frac{E}{\rho R^2}} \tag{5}$$

$$\omega_r = \sqrt{\frac{G}{\rho R^2}} \tag{6}$$

$$S_J = \sqrt{\frac{J}{AR^2}} \tag{7}$$

$$S_p = \sqrt{\frac{I_p}{AR^2}} \tag{8}$$

$$S_r = \sqrt{\frac{I_r}{AR^2}} \tag{9}$$

$$S_z = \sqrt{\frac{I_z}{AR^2}} \tag{10}$$

where

E is the modulus of elasticity.

G is the shear modulus.

I_p is the polar moment of the ring cross section.

J is the torsional constant of the cross section.

I_r and I_z are the area moments of inertia of the cross section with respect to the radial direction and the spin axis, respectively.

ω_s is the speed of propagation of longitudinal sound waves divided by the radius of the ring.

ω_r is the speed of propagation of transverse sound waves divided by the radius of the ring.

S_J, S_p, S_r, and S_z are analogous to the inverse of the slenderness ratio used in the design of columns.

More specific information concerning the definition of the variables and constants used above may be found in appendix A.

STATIC STABILITY

This section examines the possibility of a static instability occurring in the spinning ring. Given an increase in the radius of the ring ΔR, if the tension change required to balance the centrifugal force is greater than the increase in tension caused by stretching, then the radius will grow without bound. Given the unperturbed spinning ring, the tension caused by stretching derived in appendix A is

$$F_2 = EA\left(1 + \frac{I_z}{AR^2}\right)\frac{\Delta R}{R} \tag{11}$$

Also from appendix A (eq. (A48)), the tension required to balance centrifugal force is

$$F_2 = \rho A\left(1 + \frac{\Delta R}{R}\right)(R\Omega)^2 \tag{12}$$

The equilibrium strain in the ring is obtained by equating equations (11) and (12):

$$\varepsilon_o = \frac{\Delta R}{R} = \frac{(R\Omega)^2}{\frac{E}{\rho}\left(1 + \frac{I_z}{AR^2}\right) - (R\Omega)^2} \tag{13}$$

The limiting spin rate Ω_L, below which the ring is statically stable and above which the ring is unstable, is obtained by differentiating equations (11) and (12) with respect to the change in radius and equating the results:

$$\Omega_L = \frac{1}{R}\sqrt{\frac{E}{\rho}\left(1 + \frac{I_z}{AR^2}\right)} \tag{14}$$

Therefore, the instability occurs when the spin rate exceeds the speed of sound in the material of the ring divided by the radius of the unstressed ring.

To determine whether this limiting spin rate would be achieved in practice, the spin rate Ω_a required to produce the maximum allowable stress in the material σ_a can be computed and compared with Ω_L. The maximum stress in the steadily spinning ring is obtained from equations (A11) and (A12) of appendix A:

$$\sigma_{max} = E\varepsilon_{max} = \frac{E\varepsilon_o}{1 + \frac{x_{min}}{R}} \tag{15}$$

where the perturbation variables are all zero and x_{min} is the radial distance between the innermost fiber and the centroid and has a negative value. Substitution of equation (13) into equation (15), letting the maximum strain equal the allowable strain, and solving for the spin rate yield the maximum allowable spin rate based on the maximum allowable strain and the dimensions of the ring:

$$\Omega_a = \frac{1}{R}\sqrt{\frac{\sigma_a}{\rho}\left(1 + \frac{I_z}{AR^2}\right)\left[\frac{1 + \frac{x_{min}}{R}}{1 + \frac{\sigma_a}{E}\left(1 + \frac{x_{min}}{R}\right)}\right]} \tag{16}$$

For example, let the ring have a square cross section of dimension a on each side with $a < R/10$. For this case,

$$\frac{I_z}{AR^2} = \frac{a^2}{12R^2} < \frac{1}{1200} << 1 \tag{17}$$

$$\frac{x_{min}}{R} = \frac{a}{2R} < \frac{1}{20} << 1 \tag{18}$$

Also, consider the ring to be fabricated from steel for which (ref. 15)

$$\frac{\sigma_a}{E} \approx 0.7 \times 10^{-3} << 1 \tag{19}$$

Applying the approximations of equations (17), (18), and (19) to equation (16) yields an approximate formula for the allowable spin rate based on the allowable stress of the material:

$$\Omega_a \approx \frac{1}{R}\sqrt{\frac{\sigma_a}{\rho}} \tag{20}$$

Comparing equations (20) and (14),

$$\frac{\Omega_a}{\Omega_L} \approx \sqrt{\frac{\sigma_a}{E}} \approx 0.026 \tag{21}$$

which implies that the ring would experience structural failure well before the limit of equation (14). This result applies to all relatively rigid materials for which $E >> \sigma_a$.

OUT-OF-PLANE HOMOGENEOUS SOLUTIONS

The out-of-plane vibration modes (deflection perpendicular to the plane of the ring and twisting about its centroid) are examined in this section. The equations of motion of the out-of-plane modes are given by equations (3) and (4). In the absence of external influences (control forces and gravity), the distributed force acting perpendicular to the plane of the ring W_3 is zero. Because of the geometry of the ring, the structural perturbation variables are periodic in the variable s, that is,

$$w(s + 2\pi R) = w(s) \tag{22}$$

$$\beta(s + 2\pi R) = \beta(s) \tag{23}$$

for all s. As in all wave equations, there is a family of solutions to equations (3) and (4) which satisfy the constraints of equations (22) and (23). Assume that each mode has the solution

$$w(s,t) = A_j \cos\left(\frac{js}{R} + \omega_{wj}t\right) + B_j \sin\left(\frac{js}{R} + \omega_{wj}t\right) \tag{24}$$

$$\beta(s,t) = C_j \cos\left(\frac{js}{R} + \omega_{wj}t\right) + D_j \sin\left(\frac{js}{R} + \omega_{wj}t\right) \tag{25}$$

where the mode number j is a nonnegative integer and ω_{wj} is the vibration frequency.

Substitution of equations (24) and (25) into equations (3) and (4) with $W_3 = 0$ yields the following algebraic equations:

$$\left(1 + j^2 S_r^2\right)\omega_{wj}^2 - j^2\left(j^2 E_G + 1\right)\omega_r^2 S_J^2 - \left(1 - S_r^2\right)j^2\Omega^2 = \left[j^2 R(E_G + 1)\omega_r^2 S_J^2 - 2jRS_r^2\Omega\omega_{wj}\right]C_{Aj} \tag{26}$$

$$\left[S_p^2\omega_{wj}^2 - \left(j^2 + E_G\right)\omega_r^2 S_J^2 + \left(S_r^2 - S_z^2\right)\Omega^2\right]C_{Aj} = \frac{j^2}{R}\left(1 + E_G\right)\omega_r^2 S_J^2 - 2\,\frac{j}{R}\,S_r^2\Omega\omega_{wj} \tag{27}$$

where

$$E_G = \frac{EI_r}{GJ} \qquad C_{Aj} = \frac{C_j}{A_j} = \frac{D_j}{B_j}$$

The constant E_G relates the out-of-plane bending stiffness to the torsional stiffness, and C_{Aj} is the ratio between the amplitudes of the angle of rotation of the cross section and the deflection of the centroid perpendicular to the plane of the ring.

Solving equations (26) and (27) by eliminating C_{Aj} yields a polynomial in the out-of-plane vibration frequency ω_{wj}:

$$T_a\omega_{wj}^4 - T_b\omega_{wj}^2 + T_c\omega_{wj} + T_d = 0 \tag{28}$$

where

$$T_a = \left(1 + j^2S_r^2\right)S_p^2$$

$$T_b = \left[\left(1 + j^2S_r^2 + j^4S_p^2\right)E_G + j^2\left(1 + j^2S_r^2 + S_p^2\right)\right]\omega_r^2S_J^2 + \left[S_z^2 - S_r^2 + j^2\left(S_p^2 + 2S_r^4\right)\right]\Omega^2$$

$$T_c = 4j^3(1 + E_G)S_r^2\omega_r^2S_J^2\Omega$$

$$T_d = j^2(j^2 - 1)^2E_G\left(\omega_r^2S_J^2\right)^2 + j^2\left[\left(j^2 + E_G\right)\left(1 - S_r^2\right) + \left(j^2E_G + 1\right)\left(S_z^2 - S_r^2\right)\right]\omega_r^2S_J^2\Omega^2 + j^4\left(S_z^2 - S_r^2\right)\left(1 - S_r^2\right)\Omega^4$$

The roots of equation (28) are the vibration frequencies of the out-of-plane modes. The proportionality constants C_{Aj} between the twist and the out-of-plane deflection for each of these modes are obtained by substituting the values of the frequencies into either equation (26) or (27).

The remainder of this section first examines the vibration characteristics when the spin rate is zero. Then the modes with mode numbers of zero and one with nonzero spin rate are examined. Finally, the vibration characteristics of the higher numbered modes with nonzero spin rate are examined.

Zero Spin Rate

If the spin rate Ω is zero, then equation (28) reduces to

$$T_a \omega_{wj}^4 - T_b \omega_{wj}^2 + T_d = 0 \tag{29}$$

where

$$T_a = \left(1 + j^2 S_r^2\right) S_p^2$$

$$T_b = \left[\left(1 + j^2 S_r^2 + j^4 S_p^2\right) E_G + j^2\left(1 + j^2 S_r^2 + S_p^2\right)\right] \omega_r^2 S_J^2$$

$$T_d = j^2 (j^2 - 1)^2 E_G \left(\omega_r^2 S_J^2\right)^2$$

The two roots of equation (29) of greatest magnitude may be calculated by the quadratic formula:

$$\omega_{Tj}^2 = \frac{T_b}{2T_a}\left(1 + \sqrt{1 - \frac{4T_a T_d}{T_b^2}}\right) \tag{30}$$

Since the expression under the radical is never negative, the values of ω_{Tj} are real. For slender rings, the values of S_r and S_p are much less than one. Consider the range of mode numbers j such that $j^2 S_r^2$, $j^2 S_p^2$, and $j^2 S_p^2 E_G$ are much less than one. For this range, equation (30) becomes

$$\omega_{Tj} = \pm\sqrt{\frac{J}{I_p}\left(j^2 + E_G\right)}\,\omega_r \tag{31}$$

Substitution of equation (31) into equation (26) yields the ratio of the out-of-plane deflection $w(s,t)$ to the angle of twist $\beta(s,t)$:

$$C_{ATj}^{-1} = \frac{I_p}{AR}\,\frac{j^2(1 + E_G)}{j^2 + E_G} \tag{32}$$

Equations (31) and (32) describe the out-of-plane modes which consist primarily of twisting motion about the line of centroids accompanied by a small deflection perpendicular to the plane of the ring. An example of this type of mode is illustrated in figure 1. In this case the deflection of the centroid and the rotation about the centroid combine to produce rotation of the cross section

about a point which is near the outer edge of the ring. Therefore, the outer surface appears to be relatively undistorted, while the inner surface shows a large distortion.

The two roots of equation (29) of least magnitude may be calculated by the quadratic formula:

$$\omega_{Dj}^2 = \frac{2T_d}{T_b\left(1 + \sqrt{1 - \frac{4T_aT_d}{T_b^2}}\right)} \tag{33}$$

For the range of mode numbers such that $j^2S_r^2$ and $j^2S_p^2E_G$ are much less than one, equation (33) becomes

$$\omega_{Dj} = \pm \frac{j(j^2 - 1)}{\sqrt{j^2 + E_G}} S_r\omega_s \tag{34}$$

Substitution of equation (34) into equation (27) yields the ratio of the angle of twist $\beta(s,t)$ to the out-of-plane deflection $w(s,t)$:

$$C_{ADj} = -\frac{1}{R}\left(\frac{1 + E_G}{1 + E_G/j^2}\right) \tag{35}$$

Equations (34) and (35) describe the out-of-plane modes which consist primarily of deflection perpendicular to the plane of the ring accompanied by a small twisting motion about the line of centroids. An example of this type of mode is illustrated in figure 2.

For mode numbers within the range considered above but significantly greater than $\sqrt{E_G}$, equations (31), (32), (34), and (35) simplify to the following:

$$\omega_{Tj} = \pm j\sqrt{\frac{J}{I_p}}\,\omega_r \tag{36}$$

$$C_{ATj}^{-1} = \frac{I_p}{AR}(1 + E_G) \tag{37}$$

$$\omega_{Dj} = \pm j^2S_r\omega_s \tag{38}$$

$$C_{ADj} = -\frac{1}{R}(1 + E_G) \tag{39}$$

where $j^2 >> E_G$.

Mode Number of Zero

If the mode number j is zero, then equation (28) becomes

$$T_a \omega_{w0}^4 - T_b \omega_{w0}^2 = 0 \tag{40}$$

where

$$T_a = S_p^2$$

$$T_b = S_r^2 \omega_s^2 + \left(S_z^2 - S_r^2\right)\Omega^2$$

The two nonzero roots of equation (40) correspond to a uniform rotation of the ring about the line of centroids which has a frequency of oscillation of

$$\omega_{T0} = \pm \sqrt{\frac{S_r^2 \omega_s^2 + \left(S_z^2 - S_r^2\right)\Omega^2}{S_p^2}} \tag{41}$$

The dynamics of this case may be written as

$$w(s,t) = 0 \tag{42}$$

$$\beta(s,t) = C_{T0} \cos \omega_{T0} t + D_{T0} \sin \omega_{T0} t$$

The frequency of this mode is affected by the spin rate. If $I_z > I_r$, then the frequency increases with increasing spin rate and has a stiffening effect. If $I_z < I_r$, the frequency decreases.

Figure 3 illustrates this mode in a ring with a rectangular cross section. The long axis of the cross section in figure 3(a) is nominally in the radial direction. As the ring spins, the centrifugal force is greater on the outer edge of the ring than on the inner edge. This produces a couple which tends to force the ring back to its rest condition and thus stiffens the vibration mode.

The long axis of the cross section in figure 3(b) is nominally parallel to the spin axis. In this case, the couple has an effect opposite to stiffening.

The couple may overpower the elastic restoring forces if the frequencies given by equation (41) become complex. This occurs when

$$\Omega > \frac{\omega_s}{\sqrt{1 - \frac{I_z}{I_r}}} \tag{43}$$

and $I_r > I_z$. When these conditions are satisfied, the mode is dynamically unstable. The lowest spin-rate limit imposed by equation (43) occurs when $I_z = 0$. For this case the limiting spin rate is ω_s which is identical to that given by equation (14) for static stability.

For $j = 0$, the mode frequency given by equation (40) has a double solution of zero which implies a solution form different than equations (24) and (25). The dynamics of this case may be written as

$$w(s,t) = z + \dot{z}t \tag{44}$$

$$\beta(s,t) = 0$$

This solution is rigid body translation along the inertial z-direction which nominally coincides with the axis of the ring as is shown in figure 4. The constant z is the initial displacement and $\dot{z}$ is the rate of displacement.

Mode Number of One

If the mode number j is one, then equation (28) becomes

$$T_a\omega_{w1}^4 - T_b\omega_{w1}^2 + T_c\omega_{w1} + T_d = 0 \tag{45}$$

where

$$T_a = \left(1 + S_r^2\right)S_p^2$$

$$T_b = \left(1 + S_z^2 + 2S_r^2\right)(1 + E_G)\omega_r^2 S_J^2 + 2\left(S_z^2 + S_r^4\right)\Omega^2$$

$$T_c = 4(1 + E_G)S_r^2\omega_r^2 S_J^2\Omega$$

$$T_d = \left(1 + S_z^2 - 2S_r^2\right)(1 + E_G)\omega_r^2 S_J^2\Omega^2 + \left(S_z^2 - S_r^2\right)\left(1 - S_r^2\right)\Omega^4$$

Equation (45) can be factored into

$$(\omega_{w1} - \Omega)\left(\tilde{T}_a\omega_{w1}^3 + \tilde{T}_b\omega_{w1}^2 - \tilde{T}_c\omega_{w1} - \tilde{T}_d\right) = 0 \tag{46}$$

where

$$\tilde{T}_a = \left(1 + S_r^2\right)S_p^2$$

$$\tilde{T}_b = \left(1 + S_r^2\right)S_p^2\Omega$$

$$\tilde{T}_c = \left(1 + 2S_r^2 + S_z^2\right)(1 + E_G)\omega_r^2 S_J^2 + \left(1 - S_r^2\right)\left(S_z^2 - S_r^2\right)\Omega^2$$

$$\tilde{T}_d = \left(1 - 2S_r^2 + S_z^2\right)(1 + E_G)\omega_r^2 S_J^2\Omega + \left(1 - S_r^2\right)\left(S_z^2 - S_r^2\right)\Omega^3$$

If the ring is very slender such that S_r^2 and S_z^2 are very small relative to unity, equation (46) may be factored into

$$\left(\omega_{w1}^2 - \Omega^2\right)\left[S_p^2\omega_{w1}^2 - (1 + E_G)\omega_r^2 S_J^2 - \left(S_z^2 - S_r^2\right)\Omega^2\right] = 0 \tag{47}$$

Two of the roots of equation (47) correspond to the twisting mode which has a frequency of oscillation of

$$\omega_{T1} = \pm\sqrt{\frac{(1 + E_G)S_J^2\omega_r^2 + \left(S_z^2 - S_r^2\right)\Omega^2}{S_p^2}} \tag{48}$$

Substituting equation (48) into equation (26) with $j = 1$, assuming that S_r^2 and S_p^2 are very small relative to unity, and assuming that the spin rate is much less than ω_r, yield the proportionality constant between the out-of-plane deflection $w(s,t)$ and the angle of twist $\beta(s,t)$:

$$C_{AT1}^{-1} = \frac{I_p}{AR} \tag{49}$$

which is small for slender rings. The spin rate has a small effect on the frequency of this mode.

For the remaining roots of equation (47), two different cases may be considered. If the spin rate is zero, then the mode frequency has a double solution of zero. The dynamics of this case may be written as

$$w(s,t) = R(\theta + \dot{\theta}t) \cos\left(\frac{s}{R}\right) + R(\phi + \dot{\phi}) \sin\left(\frac{s}{R}\right) \tag{50}$$

$$\beta(s,t) = -(\theta + \dot{\theta}t) \cos\left(\frac{s}{R}\right) - (\phi + \dot{\phi}) \sin\left(\frac{s}{R}\right) \tag{51}$$

This solution is a rigid body rotation of the ring about a line lying in the XY-plane which nominally coincides with the plane of the ring, as shown in figure 5. The constant θ is the initial rotation angle about the Y-axis and $\dot{\theta}$ is the rate of rotation about the Y-axis. The constant ϕ is the initial rotation angle about the X-axis and $\dot{\phi}$ is the rate of rotation about the X-axis. These angles correspond to the pitch and roll angles of Eulerian mechanics so long as their values are small.

If the spin rate is not zero, then the mode frequency has solutions equal to plus and minus the spin rate. The dynamics of this case may be written as:

$$w(s,t) = R\theta \cos\left(\frac{s}{R} + \Omega t\right) + R\phi \sin\left(\frac{s}{R} + \Omega t\right) + R\theta_p \cos\left(\frac{s}{R} - \Omega t\right) + R\theta_p \sin\left(\frac{s}{R} - \Omega t\right) \tag{52}$$

$$\beta(s,t) = -\theta \cos\left(\frac{s}{R} + \Omega t\right) - \phi \sin\left(\frac{s}{R} + \Omega t\right) - \theta_p \cos\left(\frac{s}{R} - \Omega t\right) - \phi_p \sin\left(\frac{s}{R} - \Omega t\right) \tag{53}$$

The first pair of terms of equations (52) and (53) correspond to a constant inclination of the ring axis determined by the angles θ and ϕ as shown in figure 6. The second pair of terms of equations (52) and (53) describe a gyroscopic precession shown in figure 7. The initial orientation of the ring is determined by a rotation about the Y-axis of angle θ_p and a rotation about the X-axis of angle ϕ_p.

Mode Numbers of Two and Greater

This section examines the vibration characteristics of the out-of-plane modes for mode numbers of two and greater when the spin rate is substantially less than ω_s and the ring is very slender so that the quantities $j^2 s_r^2$,

$j^2 S_z^2$, and $j^4 S_p^2$ are much less than unity. With these conditions, equation (28) can be approximated by

$$T_a \omega_{wj}^4 - T_b \omega_{wj}^2 + T_c \omega_{wj} + T_d = 0 \tag{54}$$

where

$$T_a = S_p^2$$

$$T_b = \left(j^2 + E_G\right) \omega_r^2 S_J^2$$

$$T_c = 4j^3 (1 + E_G) S_r^2 \omega_r^2 S_J^2 \Omega$$

$$T_d = j^2 (j^2 - 1)^2 E_G \left(\omega_r^2 S_J^2\right)^2 + j^2 \left(j^2 + E_G\right) \omega_r^2 S_J^2 \Omega^2$$

As described in appendix B, the solutions of equation (54) may be expressed in the form

$$\omega_{wj} = u_{wj} \pm \omega_{Dj}, \quad -u_{wj} \pm \omega_{Tj} \tag{55}$$

where

$$u_{wj} = 2j^3 \left(\frac{1 + E_G}{j^2 + E_G}\right) S_r^2 \Omega \tag{56}$$

$$\omega_{Dj}^2 = j^2 \left[\frac{(j^2 - 1)^2}{j^2 + E_G} S_r^2 \omega_s^2 + \Omega^2\right] \tag{57}$$

$$\omega_{Tj}^2 = \left(j^2 + E_G\right) \frac{J}{I_p} \omega_r^2 \tag{58}$$

Since the out-of-plane nodal frequency u_{wj} is much smaller than the vibration frequencies, ω_{Dj} and ω_{Tj}, it is ignored in the following discussion. This effectively ignores the presence of T_c in equation (54).

Equation (58) is the formula for the frequency of vibration of the out-of-plane mode which consists primarily of twisting motion about the line of centroids with small deflection perpendicular to the plane of the ring. The ratio

of the out-of-plane deflection to the angle of twist is found by substituting equation (58) into equation (26):

$$C_{ATj}^{-1} = \frac{I_p}{AR} \frac{j^2(1 + E_G)}{j^2 + E_G} \tag{59}$$

The phase velocity relative to the rotating ring is obtained by multiplying the modal frequency ($\omega_{Tj}/2\pi$) by the wavelength ($2\pi R/j$):

$$v_{Tj} = \mp \sqrt{\left(1 + \frac{E_G}{j^2}\right)\frac{J}{I_p}}\, v_r \tag{60}$$

where v_r is the velocity of transverse sound waves. The signs of equation (60) are chosen so that the velocities of the traveling waves which move around the ring in the same direction as the spin rotation have positive values. In this paper, these waves are called progressive. Those waves which move in the opposite direction are called regressive. Since the velocities given by equation (60) are much larger than the velocity of the ring $R\Omega$, the apparent frequency of oscillation and the phase velocity which would be observed from inertial space are effectively the same as those given by equations (58) and (60).

Equation (57) is the formula for the frequency of vibration of the out-of-plane mode which consists primarily of deflection perpendicular to the plane of the ring with small rotation about the line of centroids. The ratio of the angle of twist to the out-of-plane deflection is found by substituting equation (57) into equation (27):

$$C_{ADj} = -\frac{1}{R} \frac{j^2(1 + E_G)}{j^2 + E_G} \tag{61}$$

The phase velocity relative to the rotating ring is obtained by multiplying the modal frequency by the wavelength:

$$v_{Dj} = \mp \sqrt{\frac{(j^2 - 1)^2}{j^2 + E_G} S_r^2 v_s^2 + (R\Omega)^2} \tag{62}$$

where v_s is the velocity of longitudinal sound waves.

The phase velocity relative to inertial space is obtained by adding the nominal velocity of a point on the ring $R\Omega$ to the phase velocity relative to the ring:

$$v_{SDj} = R\Omega \mp \sqrt{\frac{(j^2 - 1)^2}{j^2 + E_G} S_r{}^2 v_s{}^2 + (R\Omega)^2} \tag{63}$$

The apparent frequency of oscillation observed at a point fixed in inertial space is obtained by dividing the apparent phase velocity by the wavelength:

$$\omega_{SDj} = -j\left[\Omega \mp \sqrt{\frac{(j^2 - 1)^2}{j^2 + E_G} S_r{}^2 \omega_s{}^2 + \Omega^2}\right] \tag{64}$$

For small rotation rates Ω, the modal frequencies and phase velocities are determined mainly by the ring's material properties (E, G, and ρ) and the geometric parameters (I_r, J, A, and R). For large rotation rates, the modal frequencies and phase velocities approach the following values:

$$\omega_{Dj} = \mp j\Omega \tag{65}$$

$$v_{Dj} = \mp R\Omega \tag{66}$$

$$v_{SDj} = -\frac{S_r{}^2 v_s{}^2}{2R\Omega} \frac{(j^2 - 1)^2}{j^2 + E_G}, \quad +2R\Omega \tag{67}$$

$$\omega_{SDj} = \frac{S_r{}^2 \omega_s{}^2}{R\Omega} \frac{j(j^2 - 1)^2}{j^2 + E_G}, \quad -2j\Omega \tag{68}$$

where Ω is significantly larger than $jS_r\omega_s$.

The restoring forces caused by the tension in the ring are large in comparison to the restoring forces caused by material strain so that given a sufficiently high rotation rate, the out-of-plane deflection modes of the ring approach the solutions for a spinning loop of string (which has $I_r = 0$). Equation (66) shows that the phase velocities relative to the material approach the linear velocity of the edge of the ring in both the progressive and regressive waves. Equation (67) shows that the phase velocities relative to inertial space approach a value twice the ring speed for the progressive wave and a very slow velocity for the regressive wave.

The material of the ring has a velocity of $R\Omega$. The progressive wave travels around the ring in advance of the material at a total velocity of $2R\Omega$ as shown in figure 8. The regressive wave shape is almost stationary in space with a slight retrograde movement. To an observer, the material of the ring would appear to be following a track which is almost fixed in space as shown in figure 9.

The following development examines the out-of-plane structural modes in a more conventional manner than was done above. Application of trigonometric identities to equations (24) and (25) yields the following alternative form for the modal equations:

$$w(s,t) = \sum_{j=2}^{\infty} \left(\tilde{A}_j \cos \frac{js}{R} \cos \omega_{Dj} t + \tilde{B}_j \cos \frac{js}{R} \sin \omega_{Dj} t + \tilde{C}_j \sin \frac{js}{R} \sin \omega_{Dj} t + \tilde{D}_j \sin \frac{js}{R} \cos \omega_{Dj} t \right) \tag{69}$$

$$\beta(s,t) = \sum_{j=2}^{\infty} C_{ADj} \left(\tilde{A}_j \cos \frac{js}{R} \cos \omega_{Dj} t + \tilde{B}_j \cos \frac{js}{R} \sin \omega_{Dj} t + \tilde{C}_j \sin \frac{js}{R} \sin \omega_{Dj} t + \tilde{D}_j \sin \frac{js}{R} \cos \omega_{Dj} t \right) \tag{70}$$

where the modal frequencies ω_{Dj} are given by equation (57) and the proportionality constant between the twist angle and the out-of-plane deflection C_{ADj} is given by equation (61) and where

$$\left.\begin{aligned} \tilde{A}_j &= A_j + C_j & \tilde{B}_j &= B_j - D_j \\ \tilde{C}_j &= C_j - A_j & \tilde{D}_j &= B_j + D_j \end{aligned}\right\} \tag{71}$$

Therefore, the out-of-plane structural modes may be represented as the sum of products of sinusoidal functions of s (mode shapes) and sinusoidal functions of time (oscillations). Since the mode shapes are a function of s only, standing waves do not move with respect to the material of the ring; that is, the nodes of the standing waves are fixed in the material.

Consider, for example, any one of the terms of equation (69):

$$w(s,t) = \tilde{A}_j \cos \frac{js}{R} \cos \omega_{Dj} t \tag{72}$$

Consider an observation point fixed in inertial space and located at a distance λ along the circumference of the ring measured from the X-axis. The deflection of the ring observed at this point is the deflection at

$$s = \lambda - R\Omega t \tag{73}$$

Substituting equation (73) into equation (72) yields the motion of an out-of-plane standing wave relative to the inertial coordinate system:

$$w(s,t) = \tilde{A}_j \cos \frac{j}{R}(\lambda - R\Omega t) \cos \omega_{Dj} t \tag{74}$$

In the limit for $\Omega \to \infty$, equation (65) may be substituted into equation (74). Subsequent trigonometric manipulations yield the following representation for the modal behavior of the ring at high spin rates as seen by a fixed observer:

$$w(\lambda,t) = \frac{\tilde{A}_j}{2}\left[\cos \frac{j}{R} \lambda + \cos \frac{j}{R}(\lambda - 2R\Omega t)\right] \tag{75}$$

This equation consists of two terms. The first is a sinusoidal shape of the ring which is fixed in time. The second is a sinusoidal shape which travels around the ring at twice the rim speed. Figure 10 illustrates the motion of a standing wave described by equation (75) as would be viewed by a fixed observer. The ring achieves its maximum deflection in figures 10(a) and 10(g) with intermediate positions in figures 10(b) through 10(f). The square symbol on these figures identifies the reference point fixed in the ring at $s = 0$. Although the crest and troughs (at maximum deflection) alternate when viewed relative to a point which is fixed to the ring, they always occur at the same locations in inertial space, as can be seen by comparing figures 10(a) and 10(g).

The analysis of this section has been limited to a range of mode numbers for which the quantities $j^2S_r^2$, $j^2S_z^2$, $j^2S_p^2$, and $j^4S_p^2$ are much less than unity. Since the effects of transverse shear upon the deformation of the ring are neglected in the development of the equations of motion of appendix A, the equations derived above may give inaccurate results for mode numbers beyond the indicated range. However, for large mode numbers within the range, several of the equations can be simplified to the following:

$$\omega_{Tj} = \pm j \sqrt{\frac{J}{I_p}}\, \omega_r \tag{76}$$

$$C_{ATj}^{-1} = \frac{I_p}{AR}(1 + E_G) \tag{77}$$

$$v_{Tj} = \mp \sqrt{\frac{J}{I_p}}\, v_r \tag{78}$$

$$\omega_{Dj} = \pm j \sqrt{j^2 S_r^2 \omega_s^2 + \Omega^2} \tag{79}$$

$$C_{ADj} = -\frac{1 + E_G}{R} \tag{80}$$

$$v_{Dj} = \mp\sqrt{j^2 S_r{}^2 v_s{}^2 + (R\Omega)^2} \tag{81}$$

$$\omega_{SDj} = -j\left(\Omega \mp \sqrt{j^2 S_r{}^2 \omega_s{}^2 + \Omega^2}\right) \tag{82}$$

$$v_{SDj} = R\Omega \mp \sqrt{j^2 S_r{}^2 v_s{}^2 + (R\Omega)^2} \tag{83}$$

where $j^2 >> E_G$.

For high spin rates, equations (82) and (83) become

$$\omega_{SDj} = \frac{j^3 S_r{}^2 \omega_s{}^2}{2\Omega}, \quad -2j\Omega \tag{84}$$

$$v_{SDj} = -j^2 \frac{S_r{}^2 v_s{}^2}{2R\Omega}, \quad +2R\Omega \tag{85}$$

IN-PLANE HOMOGENEOUS SOLUTIONS

The characteristics of the in-plane vibration modes (deflections in the radial and tangential directions) are examined in this section. The equations of motion of the in-plane modes are given by equations (1) and (2). In the absence of external influences (control forces and gravity), the distributed forces acting in the plane of the ring, W_1 and W_2, are zero. As in the out-of-plane case, the structural perturbation variables are periodic in the variable s, that is,

$$u(s + 2\pi R) = u(s) \tag{86}$$

$$v(s + 2\pi R) = v(s) \tag{87}$$

for all s. As in all wave equations, there is a family of solutions of equations (1) and (2) which satisfy the constraints of equations (86) and (87). Assume that each mode has the solution

$$u(s,t) = E_j \cos\left(\frac{js}{R} + \omega_{uj}t\right) + F_j \sin\left(\frac{js}{R} + \omega_{uj}t\right) \tag{88}$$

$$v(s,t) = G_j \cos\left(\frac{js}{R} + \omega_{uj}t\right) + H_j \sin\left(\frac{js}{R} + \omega_{uj}t\right) \tag{89}$$

where the mode number j is a nonnegative integer.

Substitution of equations (88) and (89) into equations (1) and (2) yields the following simultaneous algebraic equations:

$$\left[(j^2 - 1)^2 S_z^2 \omega_s^2 + \omega_s^2 + (j^2 - 1)\Omega^2\right] - \left(1 + j^2 S_z^2\right)\omega_{uj}^2 = \left[j\left(\omega_s^2 + \Omega^2\right) - 2\Omega\omega_{uj} - jS_z^2\omega_{uj}^2\right]G_{Fj} \tag{90}$$

$$\left[j^2\omega_s^2 - \left(1 + S_z^2\right)\omega_{uj}^2\right]G_{Fj} = j\left(\omega_s^2 + \Omega^2\right) - 2\Omega\omega_{uj} - jS_z^2\omega_{uj}^2 \tag{91}$$

where

$$G_{Fj} = \frac{G_j}{F_j} = -\frac{H_j}{E_j}$$

The constant G_{Fj} is the ratio between the amplitudes of tangential deflection of the centroid and its radial deflection.

Solving equations (90) and (91) by eliminating G_{Fj} yields a polynomial in the in-plane vibration frequency ω_{uj}:

$$T_a\omega_{uj}^4 - T_b\omega_{uj}^3 - T_c\omega_{uj}^2 + T_d\omega_{uj} + T_e = 0 \tag{92}$$

where

$$T_a = 1 + (j^2 + 1)S_z^2$$

$$T_b = 4j\Omega S_z^2$$

$$T_c = (j^3 + 3)\Omega^2 + (j^2 + 1)\left(\omega_s^2 - S_z^2\Omega^2\right) + \left(2 + S_z^2\right)(j^2 - 1)^2 S_z^2\omega_s^2$$

$$T_d = 4j\Omega\left(\omega_s^2 + \Omega^2\right)$$

$$T_e = j^2\left[(j^2 - 1)^2 S_z^2\omega_s^4 + (j^2 - 3)\omega_s^2\Omega^2 - \Omega^4\right]$$

The roots of equation (92) are the vibration frequencies of the in-plane modes. The ratios of the amplitudes of the tangential and radial deflections for each of these modes are obtained by substituting the values of the frequencies into either equation (90) or (91).

The remainder of this section first examines the vibration characteristics when the spin rate is zero. Then the modes with mode number equal to zero and one with nonzero spin rate are examined. Finally, the vibration characteristics of the higher numbered modes with nonzero spin rate are examined.

Zero Spin Rate

If the spin rate Ω is zero, then equation (92) reduces to

$$T_a \omega_{uj}^4 - T_c \omega_{uj}^2 + T_e = 0 \tag{93}$$

where

$$T_a = 1 + (j^2 + 1) S_z^2$$

$$T_c = \left[j^2 + 1 + \left(2 + S_z^2 \right) (j^2 - 1)^2 S_z^2 \right] \omega_s^2$$

$$T_e = j^2 (j^2 - 1)^2 S_z^2 \omega_s^4$$

The two roots of equation (93) of greatest magnitude may be calculated by the quadratic formula:

$$\omega_{Cj}^2 = \frac{T_c}{2T_a} \left(1 + \sqrt{1 - \frac{4T_a T_c}{T_c^2}} \right) \tag{94}$$

Since the expression under the radical is never negative, the values of ω_{Cj} are real. For slender rings, S_z is much less than one. Consider the range of mode numbers j such that $j^2 S_z^2$ is much less than one. For this range, equation (94) becomes

$$\omega_{Cj} = \pm \sqrt{j^2 + 1}\ \omega_s \tag{95}$$

Substitution of equation (95) into equation (91) yields the ratio of the tangential deflection $v(s,t)$ to the radial deflection $u(s,t)$:

$$G_{FCj} = -j \tag{96}$$

Equations (95) and (96) describe the in-plane modes which consist primarily of compression and stretching of the line of centroids with little bending. An example of this type of mode is illustrated in figure 11.

The two roots of equation (93) of least magnitude may be calculated by the quadratic formula

$$\omega_{Bj}^2 = \frac{2T_c}{T_c\left(1 + \sqrt{1 - \frac{4T_aT_e}{T_c^2}}\right)} \tag{97}$$

For the range of mode numbers such that $j^2S_z^2$ is much less than one, equation (97) becomes

$$\omega_{Bj} = \pm \frac{j(j^2 - 1)}{\sqrt{j^2 + 1}} S_z\omega_s \tag{98}$$

Substitution of equation (98) into equation (91) yields the ratio of the radial deflection $u(s,t)$ to the tangential deflection $v(s,t)$:

$$G_{FCj}^{-1} = j \tag{99}$$

Equations (98) and (99) describe the in-plane modes which consist primarily of bending of the line of centroids with little compression and stretching. An example of this type of mode is illustrated in figure 12.

For mode numbers within the range considered above but significantly greater than one, equations (95) and (98) reduce to the following:

$$\omega_{Cj} = \pm j\omega_s \tag{100}$$

$$\omega_{Bj} = \pm j^2S_z\omega_s \tag{101}$$

where $j^2 >> 1$.

Mode Number of Zero

If the mode number j is zero, then equation (92) becomes

$$T_a\omega_{u0}^4 - T_c\omega_{u0}^2 = 0 \tag{102}$$

where

$$T_a = \left(1 + S_z{}^2\right)$$

$$T_c = \left(1 + S_z{}^2\right)^2 \omega_s{}^2 + \left(3 - S_z{}^2\right)\Omega^2$$

For slender rings, the constant $S_z{}^2$ may be ignored. The two nonzero roots of equation (102) correspond to a radial oscillation of the ring with no bending which has a frequency of oscillation of

$$\omega_{C0} = \pm\sqrt{\omega_s{}^2 + 3\Omega^2} \tag{103}$$

Substitution of equation (103) into equation (91) yields the ratio of tangential deflection to radial deflection:

$$G_{FC0} = \pm \frac{2\Omega}{\sqrt{\omega_s{}^2 + 3\Omega^2}} \tag{104}$$

The relative magnitudes and phasing of the radial and tangential terms are such that the angular momentum of the ring is constant.

The radial oscillation mode is illustrated in figure 13. For this figure the parameter F_{C0} (eq. (88)) is zero. Figure 13(a) shows the ring at its initial condition ($t = 0$). The radius is increased by the amount E_{C0}. The tangential velocity of the ring is the sum of the nominal velocity, $R\Omega$, and the time derivative of the variable $v(s,t)$. Since the radius of the ring is larger than the nominal radius at $t = 0$, the ring rotates at a speed less than nominal. Figure 13(b) shows the ring after one-quarter cycle of oscillation ($t = \pi/2\omega_{C0}$). The radius of the ring equals the nominal radius and is decreasing. Because the ring was rotating at a slower than nominal rate previously, it has retarded by an amount $G_{FC0}E_{C0}$. This retardation is shown by the location of the mass element at $s = 0$ (denoted by the dark square fixed to the ring) relative to its nominal location (denoted by the light square). The ring is now rotating at its nominal rate and is decelerating. Figure 13(c) shows the ring after one-half cycle of oscillation ($t = \pi/\omega_{C0}$). The radius of the ring is now less than nominal by the amount E_{C0}; the ring is rotating at a rate which is greater than nominal and the previous retardation has been canceled. Figure 13(d) shows the ring after three-quarters cycle of oscillation ($t = 3\pi/2\omega_{C0}$). The radius of the ring is now equal to its nominal value; the ring is rotating at its nominal rate and is decelerating. The indicated mass element has progressed ahead of its nominal circumferential location.

The double root at zero in equation (102) implies a solution which is not of the form of equations (88) and (89). For this case, the following form may be used:

$$u(s,t) = R \tag{105}$$

$$v(s,t) = \psi + \dot{\psi}t \tag{106}$$

Substituting equations (105) and (106) into equations (1) and (2) yields

$$R = \frac{2\Omega}{\left(1 + S_z^2\right)\omega_s^2 - \Omega^2}\,\dot{\psi} \tag{107}$$

$$\psi = \text{Arbitrary value} \tag{108}$$

The parameter ψ specifies an arbitrary angular displacement of the ring about its spin axis. The parameter $\dot{\psi}$ specifies a constant increment in the spin rate of the ring; that is, the actual spin rate is equal to $\Omega + \dot{\psi}/R$. The parameter R is the change in the radius of the ring caused by the change in centripetal force acting on the ring.

Mode Number of One

If the mode number j is one, then equation (92) may be written in the factored form

$$(\omega_{u1} - \Omega)^2\left[\left(1 + 2S_z^2\right)\omega_{u1}^2 + 2\Omega\omega_{u1} - \left(\Omega^2 + 2\omega_s^2\right)\right] = 0 \tag{109}$$

The roots of the quadratic term of equation (109) are

$$\omega_{C1} = \frac{-\Omega \pm \sqrt{\Omega^2 + \left(1 + 2S_z^2\right)\left(\Omega^2 + 2\omega_s^2\right)}}{1 + 2S_z^2} \tag{110}$$

Substitution of equation (110) in equation (91) yields the ratio of the tangential deflection to the radial deflection:

$$G_{FC1} = -1 \tag{111}$$

Assuming that the spin rate is substantially less than ω_s and that the parameter S_z^2 is much less than unity reduces equation (110) to

$$\omega_{C1} = \pm\sqrt{2}\,\omega_s \tag{112}$$

This solution is a compression mode in which the ring maintains its circular shape but moves in such a way as to keep its center of mass fixed in space. This mode for the negative value of equation (112) and F_{C1} (eq. (88)) equal to zero is illustrated in figure 14. At time zero (fig. 14(a)), the shape of the ring is shifted in the positive x-direction while most of the mass is displaced in the negative x-direction. After one-half cycle of oscillation (fig. 14(c)), the ring's shape has rotated counterclockwise to the negative x-direction and the mass has accumulated in the positive x-direction. For the positive value of equation (112), the motion is similar except that the ring's shape rotates clockwise. The sum of these two modes produces the standing-wave motion of figure 15 where the ring is oscillating from side to side. Figures 14 and 15 which illustrate this mode for zero spin rate are representative of the motion of this mode for nonzero spin rate because the frequency of oscillation of the mode is so much greater than Ω.

The double root in equation (109) implies a solution which is not of the form of equations (88) and (89). For this case, the following form may be used:

$$u(s,t) = (x + \dot{x}t) \cos\left(\frac{s}{R} + \Omega t\right) + (y + \dot{y}t) \sin\left(\frac{s}{R} + \Omega t\right) \tag{113}$$

$$v(s,t) = (y + \dot{y}t) \cos\left(\frac{s}{R} + \Omega t\right) - (x + \dot{x}t) \sin\left(\frac{s}{R} + \Omega t\right) \tag{114}$$

These solutions represent rigid body translations and rates in the plane of the ring. They are illustrated in figure 16.

Mode Numbers of Two and Greater

This section examines the vibration characteristics of the in-plane modes for mode numbers of two and greater when the spin rate is substantially less than ω_s and the ring is very slender so that $j^2 S_z^2$ is much less than unity. In addition, assume that the roots of equation (92) are each much greater than $4j\Omega S_z^2$. With these assumptions, equation (92) can be approximated by

$$\omega_{uj}^4 - T_c \omega_{uj}^2 + T_d \omega_{uj} + T_e = 0 \tag{115}$$

where

$$T_c = (j^2 + 1)\omega_s^2$$

$$T_d = 4j\Omega\omega_s^2$$

$$T_e = j^2\left[(j^2 - 1)^2 S_z^2 \omega_s^2 + (j^2 - 3)\Omega^2\right]\omega_s^2$$

As described in appendix B, the solutions of equation (115) may be expressed in the form

$$\omega_{uj} = u_j \pm \omega_{Bj}, \quad -u_j \pm \omega_{Cj} \tag{116}$$

where

$$u_j = \frac{2j}{j^2 + 1}\,\Omega \tag{117}$$

$$\omega_{Bj} = \frac{j(j^2 - 1)}{j^2 + 1}\sqrt{(j^2 + 1)S_z{}^2\omega_s{}^2 + \Omega^2} \tag{118}$$

$$\omega_{Cj} = \sqrt{j^2 + 1}\,\omega_s \tag{119}$$

Define the values of ω_{uj} which are solutions of equation (115) as follows:

$$\omega_{BRj} = \omega_{Bj} + u_j \tag{120}$$

$$\omega_{BPj} = -\omega_{Bj} + u_j \tag{121}$$

$$\omega_{CRj} = \omega_{Cj} - u_j \tag{122}$$

$$\omega_{CPj} = -\omega_{Cj} - u_j \tag{123}$$

Equations (120) and (121) with equations (117) and (118) are the formulas for the frequencies of vibration of the in-plane modes which consist primarily of bending of the line of centroids with little compression and stretching. The ratios of the amplitudes of the tangential movement $v(s,t)$ to the radial deflection $u(s,t)$ are found by substituting equations (120) and (121) into equation (91):

$$G_{FBRj} = \frac{1}{j} \tag{124}$$

$$G_{FBPj} = \frac{1}{j} \tag{125}$$

where G_{FBRj} and G_{FBPj} are the ratios corresponding to the frequencies ω_{BRj} and ω_{BPj}, respectively.

The phase velocities relative to the rotating ring are obtained by multiplying the modal frequencies ($\omega_{BRj}/2\pi$ and $\omega_{BPj}/2\pi$) by the wavelength ($2\pi R/j$):

$$v_{BRj} = -\frac{(j^2 - 1)\sqrt{(j^2 + 1)S_z{}^2 v_s{}^2 + (R\Omega)^2} + 2R\Omega}{j^2 + 1} \tag{126}$$

$$v_{BPj} = \frac{(j^2 - 1)\sqrt{(j^2 + 1)S_z{}^2 v_s{}^2 + (R\Omega)^2} - 2R\Omega}{j^2 + 1} \tag{127}$$

where v_s is the velocity of longitudinal sound waves. The signs of equations (126) and (127) are chosen so that the velocities of the traveling waves which move around the ring in the same direction as the spin rotation (progressive waves) have positive values.

Consider the solution of equations (88) and (89) where $F_j = 0$, $\omega_{uj} = \omega_{BPj}$, and $\Omega << S_z\omega_s$. Substitution of equation (121) into equations (88) and (89) and using equations (117), (118), and (125) yield the following:

$$u(s,t) = E_j \cos\left[\frac{js}{R} - (\omega_{Bj} - u_j)t\right] \tag{128}$$

$$v(s,t) = \frac{E_j}{j} \sin\left[\frac{js}{R} - (\omega_{Bj} - u_j)t\right] \tag{129}$$

where

$$u_j = \frac{2j}{j^2 + 1}\Omega \tag{130}$$

$$\omega_{Bj} = \frac{j(j^2 - 1)}{\sqrt{j^2 + 1}} S_z\omega_s \tag{131}$$

Equations (128) and (129) describe a sinusoidal traveling wave which progresses ahead of the nominal material motion with the relative velocity

$$v_{BPj} = v_{Bj} - v_j \tag{132}$$

where

$$v_{Bj} = \frac{(j^2 - 1)}{\sqrt{j^2 + 1}} S_z v_s \tag{133}$$

$$v_j = \frac{2}{j^2 + 1} R\Omega \tag{134}$$

This mode consists mainly of bending of the line of centroids with little compression and stretching. Since the spin rate is substantially less than $S_z\omega_s$, the vibration frequencies and phase velocities are primarily functions of the geometric and material properties of the ring (E, ρ, A, I_z, and R) and the mode numbers. Figure 17 illustrates this mode for $j = 2$.

Similarly, consider the solution of equations (88) and (89) where $F_j = 0$, $\omega_{uj} = \omega_{BRj}$, and $\Omega << S_z\omega_s$. Substitution of equation (120) into equations (88) and (89) and using equations (117), (118), and (124) yield the following:

$$u(s,t) = E_j \cos\left[\frac{js}{R} + (\omega_{Bj} + u_j)t\right] \tag{135}$$

$$v(s,t) = \frac{E_j}{j} \sin\left[\frac{js}{R} + (\omega_{Bj} + u_j)t\right] \tag{136}$$

where u_j and ω_{Bj} are given by equations (130) and (131).

Equations (135) and (136) describe a sinusoidal traveling wave which regresses behind the nominal material motion with the relative velocity

$$v_{BRj} = v_{Bj} + v_j \tag{137}$$

where v_{Bj} and v_j are given by equations (133) and (134). Figure 18 shows this mode for $j = 2$.

Since ω_{Bj} is substantially larger than the spin rate for mode numbers of two and greater, the apparent phase velocities, v_{SBPj} and v_{SBRj}, and the apparent vibration frequencies, ω_{SBPj} and ω_{SBRj}, which would be seen by a stationary observer are essentially equal to v_{BPj}, v_{BRj}, ω_{BPj}, and ω_{BRj}, respectively.

Given that the ring has both progressive and regressive in-plane bending modes of equal amplitude, the resultant motion would have a standing-wave character. Adding the two traveling waves described by equations (128), (129), (135), and (136) and applying trigonometric identities yield the following equations for the in-plane bending-mode standing waves:

$$u(s,t) = \tilde{E}_j \cos\left(\frac{js}{R} + u_j t\right) \cos \omega_{Bj} t \tag{138}$$

$$v(s,t) = \frac{\tilde{E}_j}{j} \sin\left(\frac{js}{R} + u_j t\right) \cos \omega_{Bj} t \tag{139}$$

where u_j and ω_{Bj} are given by equations (130) and (131), $\tilde{E}_j = 2E_j$, and $\Omega << S_z\omega_s$. Following the above analysis, using $E_j = 0$ yields equations

similar to equations (138) and (139) except for interchanges in the sine and cosine operators. Therefore, the in-plane structural bending modes may be represented by the sum of products of sinusoidal functions of time (oscillations) and sinusoidal functions of distance along the ring s and time (mode shapes). Since the mode shapes are functions of time as well as s, the standing waves move with respect to the material of the ring. The nodes of the standing waves may be said to move along the ring at some nodal velocity. The nodal velocity of the bending standing waves is equal to v_j (eq. (134)) in the direction opposite to the rotation of the ring. In other words, the modes regress at the velocity v_j relative to the material. At time equal to zero, the deformation variables as seen by a fixed observer can be plotted as shown in the upper two curves of figure 19. The radial displacement u is greater than the tangential displacement v by the factor j. After one-quarter cycle of oscillation, the plots for both variables collapse to zero, corresponding to an undeformed ring (not shown). After one-half cycle of oscillation ($t = \pi/\omega_{Bj}$), the variables u and v attain the plots shown in the lower two curves of figure 19. The ring and the s coordinate system have moved by the amount $R\Omega t$. The nodes of the mode shape have lagged behind by an amount $v_j t$. Figure 20 shows the ring with a bending-mode standing wave for $j = 2$. After one full cycle of oscillation ($t = 2\pi/\omega_{Bj}$), the ring has rotated through an angle of Ωt and the structural mode shape has lagged behind by an angle of $(v_j/R)t$.

For higher spin rates, the character of the bending modes changes. The above analysis considered low spin rates for which $\Omega << S_z\omega_s$. The following analysis examines higher spin rates for which $S_z\omega_s << \Omega << \omega_s$. For this range of spin rates, the above development applies except for the formulas for ω_{Bj} and v_{Bj} which become

$$\omega_{Bj} = \frac{j(j^2 - 1)}{j^2 + 1}\,\Omega \tag{140}$$

$$v_{Bj} = \frac{j^2 - 1}{j^2 + 1}\,R\Omega \tag{141}$$

where $S_z\omega_s << \Omega << \omega_s$. The frequencies and phase velocities of the bending modes are now functions of the tension in the ring caused by centrifugal force.

The progressive bending-mode traveling wave described by equations (128) and (129) for high spin rate and $j = 2$ is illustrated in figure 21. This figure is similar to the figure for low spin rate (fig. 17) except for the speed of rotation of the ring's shape and the movement of the ring's material relative to the ring's shape. For low spin rates, the ring's shape rotated at a relatively slow rate which was significantly faster than the nominal rotation rate of the ring. For high spin rates, the ring's shape rotates at a relatively high rate which is at most twice as fast as the nominal rotation rate of the ring. For $j = 2$ (shown in fig. 21), the relative phase velocity v_{BPj} is a fraction of the material velocity. The ring may thus appear to have a fixed distortion and to be rotating as a rigid body. This illusion diminishes with increasing mode number.

The regressive bending-mode traveling wave described by equations (135) and (136) for high spin rate and $j = 2$ is illustrated in figure 22. This figure is similar to figure 18 for low spin rate except that now the speed of the wave shape relative to the material is equal to the speed of the material in the opposite direction. Therefore, the shape of the ring is fixed in space and the material moves around this fixed contour.

The phase velocities of these modes relative to inertial space, v_{SBPj} and v_{SBRj}, are obtained by adding the nominal velocity of the ring $R\Omega$ to the phase velocities relative to the ring, v_{BPj} and v_{BRj}, given by equations (126) and (127):

$$v_{SBRj} = -(j^2 - 1)\frac{S_z^2 v_s^2}{2R\Omega} \tag{142}$$

$$v_{SBPj} = 2\left(\frac{j^2 - 1}{j^2 + 1}\right)R\Omega \tag{143}$$

The apparent frequencies of oscillation, ω_{SBPj} and ω_{SBRj}, observed from inertial space are obtained by dividing the apparent phase velocities by the wavelength:

$$\omega_{SBRj} = j(j^2 - 1)\frac{S_z^2 \omega_s^2}{2\Omega} \tag{144}$$

$$\omega_{SBPj} = -2\left(\frac{j^2 - 1}{j^2 + 1}\right)j\Omega \tag{145}$$

Given that the ring has both progressive and regressive in-plane bending modes of equal amplitude and $S_z\omega_s << \Omega << \omega_s$, equations (138) and (139) apply except that ω_{Bj} is given by equation (140). Figure 23 shows the deformation variable as seen by a fixed observer at time equal to zero and after one-half cycle of oscillation. Using equation (140), the time for one-half cycle of oscillation is

$$t = \frac{\pi}{\omega_{Bj}} = \frac{j^2 + 1}{j(j^2 - 1)}\frac{\pi}{\Omega} \tag{146}$$

The material of the ring has moved a distance equal to

$$R\Omega t = \frac{j^2 + 1}{j(j^2 - 1)} R\pi \tag{147}$$

Using equation (134), the distance that the mode of the standing wave has regressed relative to the material is

$$v_j t = \frac{2}{j(j^2 - 1)} R\pi \tag{148}$$

Subtracting equation (148) from (147) gives the spatial displacement of the mode of the standing wave:

$$R\Omega t - v_j t = \frac{R}{j} \pi \tag{149}$$

which is equal to one-half of the wavelength of the structural deformation. Therefore, the peaks and valleys of the structural vibrations occur at the same locations in space and do not interchange as was the case for very low spin rates shown in figure 19. Figure 24 shows the ring with a bending-mode standing wave for $j = 2$.

Equations (122) and (123) with equations (117) and (119) are the formulas for the frequencies of vibration of the in-plane modes which consist primarily of compression and stretching of the line of centroids with little bending. The ratios of the amplitudes of the tangential movement $v(s,t)$ to the radial deflection $u(s,t)$ are found by substituting equations (122) and (123) into equation (91):

$$G_{FCRj} = -j \tag{150}$$

$$G_{FCPj} = -j \tag{151}$$

where G_{FCRj} and G_{FCPj} are the ratios corresponding to the frequencies ω_{CRj} and ω_{CPj}, respectively.

The phase velocities relative to the rotating ring are obtained by multiplying the modal frequencies ($\omega_{CRj}/2\pi$ and $\omega_{CPj}/2\pi$) by the wavelength ($2\pi R/j$):

$$v_{CRj} = -\sqrt{1 + \frac{1}{j^2}}\, v_s + \frac{2R\Omega}{j^2 + 1} \tag{152}$$

$$v_{CPj} = \sqrt{1 + \frac{1}{j^2}}\, v_s + \frac{2R\Omega}{j^2 + 1} \tag{153}$$

Since these velocities are much larger than the velocity of the ring $R\Omega$, the apparent frequencies of oscillation, ω_{SCPj} and ω_{SCRj}, and the apparent phase

velocities, v_{SCPj} and v_{SCRj}, that would be observed from inertial space are effectively the same as those given by equations (122), (123), (152), and (153).

Consider the solution of equations (88) and (89) where $F_j = 0$, $\omega_{uj} = \omega_{CPj}$, and $\Omega << \omega_s$. Substitution of equation (123) into equations (88) and (89) and using equations (117), (119), and (151) yield the following:

$$u(s,t) = E_j \cos\left[\frac{js}{R} - (\omega_{Cj} + u_j)t\right] \tag{154}$$

$$v(s,t) = -jE_j \sin\left[\frac{js}{R} - (\omega_{Cj} + u_j)t\right] \tag{155}$$

where

$$u_j = \frac{2j}{j^2 + 1}\,\Omega \tag{156}$$

$$\omega_{Cj} = \sqrt{j^2 + 1}\;\omega_s \tag{157}$$

Equations (154) and (155) describe a sinusoidal traveling wave which progresses ahead of the nominal material motion with the relative velocity

$$v_{CPj} = v_{Cj} + v_j \tag{158}$$

where

$$v_{Cj} = \sqrt{1 + \frac{1}{j^2}}\;v_s \tag{159}$$

$$v_j = \frac{2}{j^2 + 1}\,R\Omega \tag{160}$$

This mode consists mainly of tension and compression distortions with very little bending of the ring's material. The phase velocity is primarily a function of the material and geometric properties of the ring.

Similarly, consider the solution of equations (88) and (89) where $F_j = 0$, $\omega_{uj} = \omega_{CRj}$, and $\Omega << \omega_s$. Substitution of equation (122) into equations (88) and (89) and using equations (117), (119), and (150) yield the following:

$$u(s,t) = E_j \cos\left[\frac{js}{R} + (\omega_{Cj} - u_j t)\right] \tag{161}$$

$$v(s,t) = -jE_j \sin\left[\frac{js}{R} + (\omega_{Cj} - u_j t)\right] \tag{162}$$

where u_j and ω_{Cj} are given by equations (156) and (157). Equations (161) and (162) describe a sinusoidal traveling wave which regresses behind the nominal material motion with the relative velocity

$$v_{CRj} = v_{Cj} - v_j \tag{163}$$

where v_{Cj} and v_j are given by equations (159) and (160).

Given that the ring has both progressive and regressive in-plane compression modes of equal amplitude, the resultant motion would have a standing-wave character. Adding the two traveling waves described by equations (154), (155), (161), and (162) and applying trigonometric identities yield the following equations for the compression-mode standing waves:

$$u(s,t) = \tilde{E}_j \cos\left(\frac{js}{R} - u_j t\right) \cos \omega_{Cj} t \tag{164}$$

$$v(s,t) = \frac{\tilde{E}_j}{j} \sin\left(\frac{js}{R} - u_j t\right) \cos \omega_{Cj} t \tag{165}$$

where u_j and ω_{Cj} are given by equations (156) and (157), $\tilde{E}_j = 2E_j$, and $\Omega << \omega_s$. Since the mode shapes are functions of time as well as s, the standing waves move with respect to the material of the ring. The nodal velocity of the compression standing waves is equal to v_j (eq. (160)) in the direction of rotation of the ring. In other words, the modes progress at the velocity v_j relative to the material.

At time equal to zero, the deformation variables as seen by a fixed observer can be plotted as shown in the upper two curves of figure 25. The tangential displacement v is greater than the radial displacement u by the factor j. After one-quarter cycle of oscillation, the plots for both variables collapse to zero, corresponding to an undeformed ring (not shown). After one-half cycle of oscillation ($t = \pi/\omega_{Cj}$), the variables u and v attain the plots shown in the lower two curves of figure 25. The ring and the s coordinate system have moved by the amount $R\Omega t$. The mode shape has moved an additional amount $v_j t$. Figure 26 shows the ring which has a compression-mode standing wave for $j = 3$. After one full cycle of oscillation ($t = 2\pi/\omega_{Cj}$), the ring has rotated through an angle of Ωt and the structural mode shape has moved through an additional angle of $(v_j/R)t$.

The analysis of this section has been limited to a range of mode numbers for which $j^2 S_z^2$ is much less than unity. Since the effects of transverse shear upon the deformation of the ring are neglected in the development of the

equations of motion of appendix A, the equations derived above may give inaccurate results for mode numbers beyond the indicated range. However, for large mode numbers within the range, several of the equations can be simplified to the following:

$$u_j = \frac{2}{j}\Omega \tag{166}$$

$$\omega_{Bj} = j\sqrt{j^2 S_z{}^2 \omega_s{}^2 + \Omega^2} \tag{167}$$

$$\omega_{Cj} = j\omega_s \tag{168}$$

$$v_{BRj} = -\sqrt{j^2 S_z{}^2 v_s{}^2 + (R\Omega)^2} \tag{169}$$

$$v_{BPj} = \sqrt{j^2 S_z{}^2 v_s{}^2 + (R\Omega)^2} \tag{170}$$

$$v_{CRj} = -v_s \tag{171}$$

$$v_{CPj} = v_s \tag{172}$$

where $j^2 >> 1$. For low spin rates, the formulas for the bending modes become

$$\omega_{Bj} = j^2 S_z \omega_s \tag{173}$$

$$v_{BRj} = -jS_z v_s \tag{174}$$

$$v_{BPj} = jS_z v_s \tag{175}$$

where $j^2 >> 1$ and $\Omega << S_z\omega_s$. For higher spin rates, the formulas for the bending modes become

$$\omega_{Bj} = j\Omega \tag{176}$$

$$v_{BRj} = -R\Omega \tag{177}$$

$$v_{BPj} = R\Omega \tag{178}$$

$$v_{SBRj} = \frac{-j^2 S_z{}^2 v_s{}^2}{2R\Omega} \tag{179}$$

$$v_{SBPj} = 2R\Omega \tag{180}$$

$$\omega_{SBRj} = \frac{j^2 S_z{}^2 \omega_s{}^2}{2\Omega} \tag{181}$$

$$\omega_{SBPj} = -2j\Omega \tag{182}$$

where $j^2 >> 1$ and $S_z\omega_s << \Omega << \omega_s$.

EXAMPLE

Solutions for an example ring were computed using the formulas of the previous sections. The example ring has a radius of 360 m and a 1.4-cm-square cross section. The mass density of the material is 1.8 g/cm^3, Young's modulus is 280 GPa, and the shearing modulus is 110 GPa. The other physical characteristics of the ring are given in table I.

The highest spin rate considered for this example is 1 rad/sec. This spin rate produces a steady-state strain of the line of centroids of $\varepsilon_o = 8.338 \times 10^{-4}$ as computed by equation (13). The maximum steady-state stress is $\sigma_{max} = 0.2335$ GPa as computed by equation (15). The validity of the approximations of equations (A50) through (A53) used in deriving the equations of motion in appendix A have been checked.

The out-of-plane frequencies, u_{wj}, ω_{Tj}, and ω_{Dj}, were computed from equation (28) using the procedure of appendix B. The nodal frequencies u_{wj} are plotted in figure 27. The vibration frequencies of the torsional modes ω_{Tj} and of the out-of-plane deflection modes ω_{Dj} are plotted in figure 28. The ratios of the out-of-plane deflection to the twist angle for the torsional modes C_{ATj}^{-1} were computed by equation (26). The ratios of the twist angle to the out-of-plane deflection for the deflection modes C_{ADj} were computed by equation (27). These ratios for $\Omega = 1$ rad/sec are plotted in figure 29. The phase velocities for the out-of-plane modes are plotted in figures 30 and 31.

The in-plane frequencies, u_j, ω_{Cj}, and ω_{Bj}, were computed from equation (115) using the procedure of appendix B. The nodal frequencies u_j are plotted in figure 32 and the vibration frequencies, ω_{Cj} and ω_{Bj}, are plotted in figure 33. The ratios of the amplitudes of the tangential motions to the amplitudes of the radial deflections were computed from equation (90) for compression modes and from equation (91) for bending modes. These ratios for $\Omega = 1$ rad/sec are plotted in figure 34. The nodal velocities for the in-plane

modes are plotted in figure 35. The phase velocities for the in-plane vibration modes are plotted in figures 36 and 37. These velocities are relative to the nodal velocities.

Note that the quantities plotted in figures 27 through 37 are functions of only integer values of the mode number j. The curves have been faired to improve their readability.

For the example problem being considered here, the out-of-plane nodal frequencies u_{wj} are small and do not significantly contribute to the solution of the problem. The in-plane nodal frequencies substantially contribute to the vibrational behavior of the ring for low-numbered modes.

The frequencies of the torsional modes ω_{Tj} and the compression modes ω_{Cj} are roughly proportional to mode number. Since the cross section of the ring is square ($I_z = I_r$), the frequencies of the torsional modes are independent of spin rate. The phase velocities of the torsional modes v_{Tj} are approximately equal to the speed of transverse sound waves in the material of the ring. The phase velocities of the compression modes v_{Cj} are approximately equal to the speed of longitudinal sound waves.

The frequencies of the out-of-plane deflection modes ω_{Dj} and of the in-plane bending modes ω_{Bj} are functions of both mode number and spin rate. Given low spin rates or high mode numbers, the restoring moments caused by bending are larger than the restoring moments caused by tension in the ring. Under these conditions, the ring vibrates much like a linear beam. The vibration frequencies are proportional to mode number squared j^2 and are independent of spin rate. The phase velocities are proportional to mode number. For high spin rates and low mode numbers, the restoring moments caused by tension dominate so that the ring vibrates much like a flexible string held under tension. The vibration frequencies are proportional to mode number and to spin rate. The phase velocities approach the velocity of the ring $R\Omega$.

The out-of-plane deflection $w(s,t)$ and the twist angle $\beta(s,t)$ vibrate in phase. For the deflection mode, the ratio of the twist angle to the out-of-plane deflection ranges from $-1/R$ to $-(1 + E_G)/R$ rad/m. For the torsional mode, there is very little out-of-plane deflection.

The tangential movement $v(s,t)$ and the radial deflection $u(s,t)$ vibrate in quadrature. For the in-plane bending mode, the ratio between the amplitudes of the tangential movement and the radial deflection is approximately equal to the inverse of the mode number. For the compression mode, this ratio is approximately equal to the mode number.

CONCLUSIONS

Small-amplitude dynamics of a steadily rotating slender ring have been examined. Derived were linear partial differential equations which describe flexural and extensional motions in the plane of the ring (in-plane bending and

compression modes), flexural motions perpendicular to the plane of the ring (out-of-plane bending modes), and twisting motions about the centroid of the ring cross section (torsional modes). The following conclusions were drawn from the investigation:

1. A maximum spin rate, beyond which the ring is statically unstable, has been found. Given an increase in the radius of the ring, if the tension change required to balance the centrifugal force is greater than the increase in tension caused by stretching, then the radius will grow without bound. This instability occurs when the spin rate approaches the speed of longitudinal sound waves divided by the radius of the unstressed ring. For practical materials such as steel, the ring will fail in tension well before this spin rate can be achieved.

2. The spin rate can have an effect upon the vibration frequency of the torsional modes. If the cross section is such that the axis of greatest moment of inertia is parallel to the radius vector from the center of the ring, then the torsional modes are stiffened by increases in spin rate. But, if the axis of greatest moment of inertia is perpendicular to the radius vector, then the torsional modes are softened by increases in spin rate. The torsional mode with mode numbers of zero becomes dynamically unstable at a spin rate which is near the limit for static stability.

3. The spin rate affects the nature of the bending modes of the ring. Given low spin rates or high mode numbers, the ring behaves like a vibrating beam. For high spin rates and low mode numbers, the ring vibrates like a flexible string under tension.

4. Standing waves (mode shapes) move with respect to the ring. For the out-of-plane modes, this nodal motion is insignificant. This motion is significant for in-plane bending modes with low mode numbers.

5. Some modes of a spinning ring would appear to a fixed observer to be surface movement along a fixed, warped, contour. Such modes might pose a problem in the design of an active control system because of difficulties in obtaining the rates of change of the perturbation variables.

Langley Research Center
National Aeronautics and Space Administration
Hampton, VA 23665
November 5, 1980

APPENDIX A

DERIVATION OF EQUATIONS OF MOTION

The linearized equations of motion for a steadily rotating slender ring are derived in this appendix. The deformations of the ring are defined by the three-dimensional displacement of the centroid of the ring's cross section and the angle of twist of the ring about the line of centroids. The stresses within the ring and the linear and angular accelerations of each mass element of the ring are derived as functions of the ring deformations. Deformations caused by shear are not included in this development. Euler's equation and Newton's law are used to obtain a linearized system of partial differential equations which define the dynamics of the perturbation variables with respect to time and location around the circumference of the ring.

Geometry of Ring

The geometry of the ring is shown in figure 38. The ring is a slender piece of material formed into the shape of a hoop with radius R. The ring lies in the plane of the X and Y inertial axes. Choose the point P, which happens to be at the intersection of the ring with the X-axis, as a reference point; then any point Q on the ring may be identified by the variable s which is set equal to the length of the arc PQ. Given a steady spin rate Ω, the wing expands to a new radius, $R + \Delta R$. The angle between line OP and the X-axis is equal to Ωt. Since the ring, being uniform, expands equally in all directions, the angle POQ does not change and the length of the arc PQ becomes $(1 + \Delta R/R)s$.

The displacement of the centroid of the ring caused by structural deformations is shown in figure 39. Given the perturbation variables u, v, and w, the point Q moves a distance v along the arc of the undeformed ring to Q_1, a distance u along a radius to Q_2, and a distance w parallel to the Z-axis to Q_3.

The vector which locates the point Q_3 in inertial space may be written as

$$\bar{r}_c(s,t) = (R + \Delta R + u)\left[\cos\left(\frac{s}{R} + \frac{v}{R + \Delta R} + \Omega t\right)\hat{i} + \sin\left(\frac{s}{R} + \frac{v}{R + \Delta R} + \Omega t\right)\hat{j}\right] + w\hat{k} \qquad (A1)$$

where u, v, and w are functions of s and t and $\hat{i}$, $\hat{j}$, and $\hat{k}$ are unit direction vectors parallel to the X-, Y-, and Z-axes, respectively. Given that u, v, and w are very small, equation (A1) may be written in terms of cylindrical coordinates:

APPENDIX A

$$\bar{r}_c(s,t) = (R + \Delta R + u)\hat{e}_r + v\hat{e}_\theta + w\hat{e}_z \tag{A2}$$

where the cylindrical coordinate system is defined at the point Q as shown in figure 39. The velocity and acceleration are written as follows:

$$\dot{\bar{r}}_c(s,t) = (\dot{u} - \Omega v)\hat{e}_r + \left[\dot{v} + \Omega(R + \Delta R + u)\right]\hat{e}_\theta + \dot{w}\hat{e}_z \tag{A3}$$

$$\ddot{\bar{r}}_c(s,t) = \left[\ddot{u} - 2\Omega\dot{v} - \Omega^2(R + \Delta R + u)\right]\hat{e}_r + \left[\ddot{v} + 2\Omega\dot{u} - \Omega^2 v\right]\hat{e}_\theta + \ddot{w}\hat{e}_z \tag{A4}$$

where a dot over a variable denotes differentiation with respect to time.

Forces and Moments

A curvilinear coordinate system is developed to aid in deriving the stress and strain of the deformed ring. Let the vector $\hat{e}_2$ be defined tangent to the deformed line of centroids of the ring as shown in figure 40. Then,

$$\hat{e}_2 = \frac{\bar{r}_c'}{|\bar{r}_c'|} = \hat{e}_\theta + \frac{R}{R + \Delta R}\left[\left(u' - \frac{v}{R}\right)\hat{e}_r + w'\hat{e}_z\right] \tag{A5}$$

where the prime denotes differentiation with respect to s and where $|\bar{r}_c'|$ has been approximated by

$$\frac{R + \Delta R}{R} + v' + \frac{u}{R}$$

Let the vector $\hat{e}_1$ be defined perpendicular to the vector $\hat{e}_2$ and the vector obtained by rotating $\hat{e}_z$ about $\hat{e}_2$ through β, the angle of twist of the cross section (see fig. 40). Then

$$\hat{e}_1 = \hat{e}_2 \times \left(\hat{e}_z + \beta\hat{e}_r\right) = \hat{e}_r - \frac{R}{R + \Delta R}\left(u' - \frac{v}{R}\right)\hat{e}_\theta - \beta\hat{e}_z \tag{A6}$$

Let the vector $\hat{e}_3$ be defined perpendicular to the vectors $\hat{e}_1$ and $\hat{e}_2$ so that the triad $(\hat{e}_1,\hat{e}_2,\hat{e}_3)$ forms an orthogonal coordinate system:

$$\hat{e}_3 = \hat{e}_1 \times \hat{e}_2 = \hat{e}_z + \beta\hat{e}_r - \frac{R}{R + \Delta R}w'\hat{e}_\theta \tag{A7}$$

APPENDIX A

Equations (A5) through (A7) define vectors which have lengths of unity plus terms which are products of the perturbation variables; that is, $\hat{e}_1$, $\hat{e}_2$, and $\hat{e}_3$ are unit vectors to the first order. Since the perturbation variables are assumed to be small quantities and nonlinear terms are ignored throughout this development of linearized equations, the vectors $\hat{e}_1$, $\hat{e}_2$, and $\hat{e}_3$ are treated as unit direction vectors.

Assume that the cross section of the ring is perpendicular to $\hat{e}_2$ and the principal axes coincide with $\hat{e}_1$ and $\hat{e}_3$. Let the components of the forces acting on the cross section of the ring be (F_1,F_2,F_3) aligned to the $(\hat{e}_1,\hat{e}_2,\hat{e}_3)$ triad. The component F_2 is the tensile force in the ring and F_1 and F_3 are shear forces. Let any externally applied influences be represented by the distributed forces (force per distance) W_1, W_2, and W_3 aligned to the $(\hat{e}_1,\hat{e}_2,\hat{e}_3)$ triad. Given a short segment of the ring of length ds, the sum of forces acting on the segment is

$$dF = \left[\frac{\partial}{\partial s}\left(F_1\hat{e}_1 + F_2\hat{e}_2 + F_3\hat{e}_3\right) + \left(W_1\hat{e}_1 + W_2\hat{e}_2 + W_3\hat{e}_3\right)\right] ds \tag{A8}$$

Ignoring products of u, v, w, and β with F_1', F_2', and F_3' and using the relations of equations (A5) through (A7) yield an expression for the spatial derivative of the total force acting on the ring segment in terms of cylindrical coordinates:

$$\begin{aligned}\frac{d\bar{F}}{ds} = {} & \left\{W_1 + F_1' - \frac{1}{R}F_2 + \frac{R}{R+\Delta R}\left[\left(u' - \frac{v}{R}\right)\left(W_2 + \frac{1}{R}F_1\right) + \left(u'' - \frac{v'}{R}\right)F_2\right] + \beta W_3 + \beta' F_3\right\}\hat{e}_r \\ & + \left\{W_2 + F_2' + \frac{1}{R}F_1 - \frac{R}{R+\Delta R}\left[\left(u' - \frac{v}{R}\right)\left(W_1 - \frac{1}{R}F_2\right) + \left(u'' - \frac{v'}{R}\right)F_1 + w'W_3 + w''F_3\right] + \frac{\beta}{R}F_3\right\}\hat{e}_\theta \\ & + \left[W_3 + F_3' + \frac{R}{R+\Delta R}\left(w'W_2 + w''F_2\right) - \beta W_1 - \beta' F_1\right]\hat{e}_z\end{aligned} \tag{A9}$$

The strain in a fiber of the ring located at $x_f\hat{e}_1 + z_f\hat{e}_3$ relative to the centroid of the cross section is given by

$$\varepsilon(x_f,z_f) = \frac{\bar{r}_f'(x_f,z_f,u,v,w,\beta,\Delta R)}{\bar{r}_f'(x_f,z_f,0,0,0,0,0)} - 1 \tag{A10}$$

where

$$\bar{r}_f = \bar{r}_c + x_f\hat{e}_1 + z_f\hat{e}_3$$

APPENDIX A

An expression for the distributed strain perpendicular to the ring's cross section is obtained by substituting equations (A2), (A6), and (A7) into equation (A10) and using small-value approximations for the perturbation variables:

$$\varepsilon(x_f, z_f) = \frac{\frac{\Delta R}{R} + \frac{u}{R} + v' + \frac{R}{R + \Delta R}\left(\frac{v'}{R} - u''\right)x_f - \left(\frac{R}{R + \Delta R}w'' - \frac{\beta}{R}\right)z_f}{1 + \frac{x_f}{R}} \tag{A11}$$

The stress is assumed to obey Hooke's law:

$$\sigma(x_f, z_f) = E\,\varepsilon(x_f, z_f) \tag{A12}$$

where E is the modulus of elasticity of the material. It is assumed that there is no intrinsic damping in the material of the ring; that is, deformations are conservative. Such damping would appear in equation (A12) as an additional term which could be a function of $\dot{\varepsilon}$. The total tensile force F_2 is obtained by integrating equation (A12) over the cross section:

$$F_2 = E\int_A \varepsilon\, dA \tag{A13}$$

An infinite series expansion of the denominator of equation (A11) is used, all moments of the cross section above the second order are discarded, and cross products of the cross section are ignored to give an expression for F_2:

$$F_2 = EA\left(\frac{\Delta R}{R} + \frac{u}{R} + v'\right) + \frac{EI_z}{R^2}\left[\frac{\Delta R}{R} + \frac{u}{R} + v' + \frac{R}{R + \Delta R}(Ru'' - v')\right] \tag{A14}$$

The second term of equation (A14) arises from the fact that the ring is curved and the elastic center does not coincide with the centroid. For very slender rings, this term may be ignored.

The moments caused by the tensile forces acting on the cross section are obtained by integrating the cross product of the vector from the centroid to each fiber with the stress vector of the fiber:

$$\bar{M} = \int_A (x_f\hat{e}_1 + z_f\hat{e}_3) \times E\varepsilon\hat{e}_2\, dA \tag{A15}$$

Performing this integration, ignoring the moments of the cross section above the second order, and ignoring cross products of the cross section yield

$$\bar{M} = M_1\hat{e}_1 + M_3\hat{e}_3 \tag{A16}$$

where

$$M_1 = EI_r\left(\frac{R}{R + \Delta R}\, w'' - \frac{\beta}{R}\right) \tag{A17}$$

$$M_3 = -EI_z\left[\frac{R}{R + \Delta R}\left(u'' - \frac{v'}{R}\right) + \frac{1}{R}\left(\frac{\Delta R}{R} + \frac{u}{R} + v'\right)\right] \tag{A18}$$

where I_z and I_r are the second moments of the cross section about $\hat{e}_3$ and $\hat{e}_1$, respectively. The second term of equation (A18) arises from the fact that the ring is curved and the elastic center does not coincide with the centroid.

The angle of shear strain caused by twisting of the ring γ can be determined for any fiber in the ring by computing the angle between the fiber and the line of centroids (ref. 15):

$$\gamma(x_f, z_f) = \frac{\left|\bar{r}_f'(x_f, z_f) \times \bar{r}_f'(0,0)\right|}{\left|\bar{r}_f'(x_f, z_f)\right| \cdot \left|\bar{r}_f'(0,0)\right|} \tag{A19}$$

where $\bar{r}_f = \bar{r}_c + x_f\hat{e}_1 + z_f\hat{e}_3$. Noting that $\bar{r}_f'(0,0) = \bar{r}_c'$ and using equation (A5) yield a simpler form for equation (A19):

$$\gamma(x_f, z_f) = \frac{\left(x_f\hat{e}_1' + z_f\hat{e}_3'\right) \times \hat{e}_2}{\left|\bar{r}_f'(x_f, z_f)\right|} \tag{A20}$$

Using equations (A2) and (A5) through (A7) and assuming that there is no warping of the cross section yield an expression for shear strain acting in the ring's cross section:

$$\gamma(x_f, z_f) = \sqrt{x_f^2 + z_f^2}\, \frac{R}{R + \Delta R}\left(\beta' + \frac{w'}{R + \Delta R}\right) \tag{A21}$$

Because of warping, this equation is exact only for circular cross sections.

The shearing stress is obtained by multiplying equation (A21) by the shearing modulus of elasticity G:

$$\tau(x_f, z_f) = G\,\gamma(x_f, z_f) \tag{A22}$$

As above, it is assumed that there is no intrinsic damping in the material of the ring. Such damping could appear in equation (A22) as an additional term which would be a function of $\dot{\gamma}$.

The line of action of the shearing stress is perpendicular to the radius vector from the centroid to the (x_f, z_f) location. The moment produced by twisting is the product of shearing stress and the radius, integrated over the cross section:

$$M_2 = \int_A \sqrt{x_f^2 + z_f^2}\, \tau(x_f, z_f)\, dA \tag{A23}$$

Using equations (A21) and (A22) in equation (A23) yields an expression for the torsional moment in the ring expressed in terms of the perturbation variables:

$$M_2 = GJ \frac{R}{R + \Delta R}\left(\beta' + \frac{w'}{R + \Delta R}\right) \tag{A24}$$

where J is the torsional constant for the cross section. For rings which have circular cross sections, J becomes the polar moment of the cross section. For rings which have noncircular cross sections, J is the torsional constant which accounts for the warping of the cross section. A table of torsional constants J for typical cross sections is given in reference 10.

The relationships between the internal forces and moments of the ring are now derived according to the procedure of reference 9. Consider a short segment of the ring having length ds. Application of Euler's equation to this segment yields the relationship between the angular rate of change of the segment and the forces and moments acting upon this segment, which are depicted in figure 41:

$$I\dot{\bar{\omega}} = \bar{M}(s + ds) - \bar{M}(s) + \bar{r}_c'(s)\, ds \times \bar{F}(s + ds) + \frac{\bar{r}_c'(s)\, ds}{2} \times \bar{W}(s)\, ds \tag{A25}$$

where

$$\bar{\omega} = \omega_1 \hat{e}_1 + \omega_2 \hat{e}_2 + \omega_3 \hat{e}_3$$

$$\bar{M} = M_1 \hat{e}_1 + M_2 \hat{e}_2 + M_3 \hat{e}_3$$

$$\bar{F} = F_1 \hat{e}_1 + F_2 \hat{e}_2 + F_3 \hat{e}_3$$

and I is the inertia tensor of the segment relative to the $(\hat{e}_1,\hat{e}_2,\hat{e}_3)$ axis system. The principal axes of inertia are assumed to coincide with the $(\hat{e}_1,\hat{e}_2,\hat{e}_3)$ axes so that the inertia tensor is diagonal in form. The diagonal elements of I are

$$I_1 = \rho I_r \, ds \tag{A26}$$

$$I_2 = \rho I_p \, ds \tag{A27}$$

$$I_3 = \rho I_z \, \dot{ds} \tag{A28}$$

where I_p is the polar moment of the cross section and ρ is the mass density of the material of the ring when it is at rest.

The components of the angular velocity $\bar{\omega}$ consist of the nominal spin rate $\Omega\hat{k}$ projected onto the $(\hat{e}_1,\hat{e}_2,\hat{e}_3)$ triad and the angular rate of change of the triad with respect to the rotating ring:

$$\omega_1 = -\Omega\beta + \frac{R}{R + \Delta R} \dot{w}' \tag{A29}$$

$$\omega_2 = \frac{R\Omega}{R + \Delta R} w' + \dot{\beta} \tag{A30}$$

$$\omega_3 = \Omega - \frac{R}{R + \Delta R}\left(\dot{u}' - \frac{\dot{v}}{R}\right) \tag{A31}$$

The left side of equation (A25) may be written as

$$I\dot{\bar{\omega}} = I_1 \frac{d}{dt}(\omega_1\hat{e}_1) + I_2 \frac{d}{dt}(\omega_2\hat{e}_2) + I_3 \frac{d}{dt}(\omega_3\hat{e}_3) \tag{A32}$$

Equations (A5) through (A7) and (A26) through (A31) are substituted into equation (A32), the indicated differentiations are performed, and products of the perturbation variables are dropped to yield a linearized equation for $I\dot{\bar{\omega}}$ in terms of the perturbation variables:

$$\dot{\bar{I\omega}} = \left\{\left[I_r\left(\frac{R}{R + \Delta R}\,\ddot{w}' - \Omega\dot{\beta}\right) + (I_z - I_p)\Omega\left(\frac{R\Omega}{R + \Delta R}\,w' + \dot{\beta}\right)\right]\hat{e}_r\right.$$

$$+ \left[I_p\left(\ddot{\beta} + \frac{R\Omega}{R + \Delta R}\,\dot{w}'\right) + (I_r - I_z)\Omega\left(\frac{R}{R + \Delta R}\,\dot{w}' - \Omega\beta\right)\right]\hat{e}_\theta$$

$$\left. - I_z\,\frac{R}{R + \Delta R}\left(\ddot{u}' - \frac{\ddot{v}}{R}\right)e_z\right\}\rho\ ds \qquad \text{(A33)}$$

The first two terms of the right side of equation (A25) may be approximated by

$$\bar{M}(s + ds) - \bar{M}(s) \approx \frac{\partial}{\partial s}\left(M_1\hat{e}_1 + M_2\hat{e}_2 + M_3\hat{e}_3\right) ds \qquad \text{(A34)}$$

Equations (A5) through (A7) are substituted into equation (A34) and the indicated differentiation is performed. Because M_1 and M_2 as given by equations (A17) and (A24) consist of terms which are proportional to the perturbation variables w and β, and M_3 as given by equation (A18) consists of terms which are proportional to the perturbation variables u and v, products of the perturbation variables and the quantities M_1, M_2, M_1', M_2', and M_3' are dropped for a linearized solution:

$$\bar{M}(s + ds) - \bar{M}(s) \approx \left\{\left[M_1' - \frac{1}{R}\,M_2 + \left(\beta' + \frac{1}{R + \Delta R}\,w'\right)M_3\right]\hat{e}_r\right.$$

$$\left. + \left[M_2' + \frac{1}{R}\,M_1 + \left(\frac{\beta}{R} - \frac{R}{R + \Delta R}\,w''\right)M_3\right]\hat{e}_\theta + M_3'\hat{e}_z\right\} ds \qquad \text{(A35)}$$

Using the definition of $\hat{e}_2$ in equation (A5) and ignoring second order terms in the variable ds, the third term of the right side of equation (A25) may be written as

$$\bar{r}_c'(s)\ ds \times \bar{F}(s + ds) = |r_c'(s)|\left[F_3(s)\ \hat{e}_1 - F_1(s)\ \hat{e}_3\right] ds \qquad \text{(A36)}$$

APPENDIX A

Equations (A5) through (A7) are substituted into equation (A36) and products of the perturbation variables are dropped to obtain

$$\bar{r}_c'(s)\,ds \times \bar{F}(s + ds) = \left\{ \left[\left(\frac{R + \Delta R}{R} + v' + \frac{u}{R} \right) F_3 - \frac{R + \Delta R}{R} \beta F_1 \right] \hat{e}_r \right.$$
$$+ \left[w' F_1 - \left(u' - \frac{v}{R} \right) F_3 \right] \hat{e}_\theta$$
$$\left. - \left[\left(\frac{R + \Delta R}{R} + v' + \frac{u}{R} \right) F_1 + \frac{R + \Delta R}{R} \beta F_3 \right] \hat{e}_z \right\} ds \qquad \text{(A37)}$$

Three equations which relate the internal forces and moments with inertia effects are obtained by substituting equations (A33), (A35), and (A37) into equation (A25). Since the last term of the right side of equation (A25) is second order in the variable ds, it is dropped:

$$\rho I_r \left(\frac{R}{R + \Delta R} \ddot{w}' - \Omega \dot{\beta} \right) + \rho (I_z - I_p) \Omega \left(\frac{R\Omega}{R + \Delta R} w' + \dot{\beta} \right)$$
$$= M_1' - \frac{1}{R} M_2 + \left(\beta' + \frac{1}{R + \Delta R} w' \right) M_3$$
$$+ \left(\frac{R + \Delta R}{R} + v' + \frac{u}{R} \right) F_3 - \frac{R + \Delta R}{R} \beta F_1 \qquad \text{(A38)}$$

$$\rho I_p \left(\ddot{\beta} + \frac{R\Omega}{R + \Delta R} \dot{w}' \right) + \rho (I_r - I_z) \Omega \left(\frac{R}{R + \Delta R} \dot{w}' - \Omega \beta \right)$$
$$= M_2' + \frac{1}{R} M_1 + \left(\frac{\beta}{R} - \frac{R}{R + \Delta R} w'' \right) M_3 + w' F_1 - \left(u' - \frac{v}{R} \right) F_3 \qquad \text{(A39)}$$

$$-\rho I_z \frac{R}{R + \Delta R} \left(\ddot{u}' - \frac{\ddot{v}}{R} \right) = M_3' - \left(\frac{R + \Delta R}{R} + v' + \frac{u}{R} \right) F_1 - \frac{R + \Delta R}{R} \beta F_3 \qquad \text{(A40)}$$

Substituting equations (A17), (A18), and (A24) into equations (A38) through (A40) and using small-value approximations for the perturbation variables yield the following relations:

$$\frac{R + \Delta R}{R} F_3 = -EI_r\left(\frac{R}{R + \Delta R}\right)\left(w''' - \frac{\beta'}{R}\right) + \left(\frac{GJ}{R + \Delta R} + \frac{EI_z\,\Delta R}{R^2}\right)\left(\beta' + \frac{w'}{R + \Delta R}\right)$$

$$+ \rho I_r\left(\frac{R}{R + \Delta R}\ddot{w}' - \Omega\dot{\beta}\right) + \rho(I_z - I_p)\Omega\left(\frac{R\Omega}{R + \Delta R} w' + \dot{\beta}\right) \qquad \text{(A41)}$$

$$\rho I_p\left(\ddot{\beta} + \frac{R\Omega}{R + \Delta R}\dot{w}'\right) + \rho(I_r - I_z)\Omega\left(\frac{R}{R + \Delta R}\dot{w}' - \Omega\beta\right)$$

$$= \frac{GJR}{R + \Delta R}\beta'' - E\left(\frac{R}{R + \Delta R} I_r + \frac{\Delta R}{R} I_z\right)\frac{\beta}{R^2}$$

$$+ \left[\frac{R}{R + \Delta R} GJ + E\left(I_r + \frac{\Delta R}{R} I_z\right)\right]\frac{w''}{R + \Delta R} \qquad \text{(A42)}$$

$$\frac{R + \Delta R}{R} F_1 = -EI_z\left[\frac{R}{R + \Delta R}\left(u''' - \frac{v''}{R}\right) + \frac{1}{R}\left(\frac{u'}{R} + v''\right)\right] + \rho I_z\left(\ddot{u}' - \frac{\ddot{v}}{R}\right) \qquad \text{(A43)}$$

Equations (A41) and (A43) are formulas for the shear forces acting across the cross section as functions of the perturbation variables. Equation (A42) is the relationship between the angle of twist β and the out-of-plane deflection w.

Equations of Motion

Given a small segment of the ring, its motion obeys Newton's law which is described by

$$\ddot{\bar{r}}_c \rho A\, ds = d\bar{F} \qquad \text{(A44)}$$

Substitution of equations (A4) and (A9) into equation (A44) yields a system of partial differential equations:

$$\rho A\left[\ddot{u} - 2\Omega\dot{v} - \Omega^2(R + \Delta R + u)\right] = W_1 + F_1' - \frac{F_2}{R} + \frac{R}{R + \Delta R}\left[\left(u' - \frac{v}{R}\right)W_2\right.$$

$$\left. + \frac{1}{R}\left(u' - \frac{v}{R}\right)F_1 + \left(u'' - \frac{v'}{R}\right)F_2\right] + \beta W_3 + \beta' F_3 \qquad \text{(A45)}$$

APPENDIX A

$$\rho A\left[\ddot{v} + 2\Omega\dot{u} - \Omega^2 v\right] = W_2 + F_2' + \frac{F_1}{R} - \frac{R}{R + \Delta R}\left[\left(u' - \frac{v}{R}\right)W_1 + w'W_3 + \left(u'' - \frac{v'}{R}\right)F_1 - \frac{1}{R}\left(u' - \frac{v}{R}\right)F_2 + w''F_3\right] + \frac{\beta}{R}F_3 \tag{A46}$$

$$\rho A\ddot{w} = W_3 + F_3' + \frac{R}{R + \Delta R}\left(w'W_2 + w''F_2\right) - \beta W_1 - \beta' F_1 \tag{A47}$$

Solving the quiescent case of equation (A45) where the externally applied forces $\bar{W}$ and the perturbation variables are zero yields an expression for the equilibrium tension in the ring:

$$F_2 = \rho A\left(1 + \frac{\Delta R}{R}\right)(R\Omega)^2 \tag{A48}$$

The equilibrium strain in the ring is obtained by equating equations (A48) and (A14) where the perturbation variables are set to zero:

$$\varepsilon_o = \frac{\Delta R}{R} = \frac{(R\Omega)^2}{\frac{E}{\rho}\left(1 + \frac{I_z}{AR^2}\right) - (R\Omega)^2} \tag{A49}$$

Let the externally applied force densities W_1, W_2, and W_3 be small perturbation quantities. Substitutions of equations (A14), (A41), and (A43) into equations (A45), (A46), and (A47) and using equations (A42) and (A48) yield a system of partial differential equations of the perturbation variables for a steadily spinning ring with small external forces. In addition, if the assumptions

$$\varepsilon_o = \frac{\Delta R}{R} << 1 \tag{A50}$$

$$(R\Omega)^2 << \frac{E}{\rho}\left(1 + \frac{I_z}{AR^2}\right) \tag{A51}$$

$$\varepsilon_o << \frac{GJ}{EI_z} \tag{A52}$$

$$\varepsilon_o << \frac{I_r}{I_z} \tag{A53}$$

are used and we note that $I_p^2 = I_r^2 + I_z^2$, then the resulting system of equations is

$$\ddot{u} - 2\Omega\dot{v} - \Omega^2 u = \frac{W_1}{\rho A} - \omega_s^2 S_z^2 (R^4 u'''' + 2R^2 u'' + u) - \omega_s^2 (Rv' + u) + \Omega^2 (R^2 u'' - Rv') + S_z^2 (R^2 \ddot{u}'' - R\ddot{v}') \tag{A54}$$

$$\ddot{v} + 2\Omega\dot{u} = \frac{W_2}{\rho A} + \omega_s^2 (Ru' + R^2 v'') + \Omega^2 Ru' + S_z^2 (R\ddot{u}' - \ddot{v}) \tag{A55}$$

$$\ddot{w} = \frac{W_3}{\rho A} - \omega_s^2 S_r^2 (R^4 w'''' - R^3 \beta'') + \omega_r^2 S_J^2 (R^2 w'' + R^3 \beta'') + \Omega^2 R^2 w'' + S_r^2 R^2 (\ddot{w}'' - 2\Omega\dot{\beta}' + \Omega^2 w'') \tag{A56}$$

$$S_p^2 (\ddot{\beta} + \Omega\dot{w}') + \left(S_r^2 - S_z^2\right)\Omega(\dot{w}' - \Omega\beta) = \omega_r^2 S_J^2 (R^2 \beta'' + Rw'') + \omega_s^2 S_r^2 (Rw'' - \beta) \tag{A57}$$

where

$$\omega_s = \sqrt{\frac{E}{\rho R^2}} \tag{A58}$$

$$\omega_r = \sqrt{\frac{G}{\rho R^2}} \tag{A59}$$

$$S_z = \sqrt{\frac{I_z}{AR^2}} \tag{A60}$$

$$S_r = \sqrt{\frac{I_r}{AR^2}} \tag{A61}$$

$$S_p = \sqrt{\frac{I_p}{AR^2}} \tag{A62}$$

$$S_J = \sqrt{\frac{J}{AR^2}} \tag{A63}$$

The terms ω_s and ω_r may be interpreted to be the speed of longitudinal and transverse sound waves in the material divided by the ring radius, and S_z, S_r, S_p, and S_J are geometric characteristics which are analogous to the inverse of the slenderness ratio used in the design of columns (ref. 9).

Equations (A54) through (A57) form a system of partial differential equations which describe the small-perturbation dynamic behavior of a steadily spinning slender ring which is influenced by small external forces. Equations (A54) and (A55) describe the coupled radial and tangential motions for which the ring remains in its original plane. Equations (A56) and (A57) describe the coupled out-of-plane deflection and ring twisting motions. The out-of-plane and the in-plane motions are uncoupled from each other.

Because of the absence of structural damping terms in the stress-strain relationships of equations (A12) and (A22), the homogeneous solutions of the above equations are periodic in time. If damping were considered, the solutions would include exponentially decaying functions. It is expected that any practical ring would be very lightly damped so that the development of this paper would apply at least for short-term behavior.

APPENDIX B

SOLUTION OF VIBRATION FREQUENCY EQUATION

During the development of the characteristics of the structural dynamics of the ring performed in the main text, equations defining the vibration frequencies of the structural modes were found to be of the form

$$f(\omega) = \omega^4 - a\omega^2 + b\omega + c = 0 \tag{B1}$$

where ω is the frequency of vibration; a, b, and c are positive real values; and b has a small value. If the roots of $f(\omega) = 0$ are real, then the motions of the ring are periodic in time. If any of the roots are complex, then the structural vibrations of the ring are unstable. This appendix presents a procedure for calculating the roots of $f(\omega) = 0$. A sufficient condition for the existence of four real roots is also presented.

Conditions on the values of a, b, and c in equation (B1) are found so that if these conditions are satisfied, then there are no complex roots of $f(\omega) = 0$. Consider the special case of equation (B1) where the value of b is zero:

$$g(\omega) = \omega^4 - a\omega^2 + c \tag{B2}$$

The roots of $g(\omega) = 0$ are easily found to be

$$\omega = \pm\sqrt{\frac{1}{2}\left(a \pm \sqrt{a^2 - 4c}\right)} \tag{B3}$$

These roots are all real and distinct if $a^2 > 4c$.

From equations (B1) and (B2), the roots of $f(\omega) = 0$ satisfy the following equation:

$$g(\omega) = -b\omega \tag{B4}$$

A typical curve for $g(\omega)$ where $a^2 > 4c$ is presented in figure 42. The intersections of $g(\omega)$ and a straight line passing through the origin with slope $-b$ occur at the roots of $f(\omega) = 0$. For sufficiently small values of b, four intersections occur implying the existence of four distinct real roots. For sufficiently large values of b, only two intersections occur implying the existence of two real roots and two complex roots. The line $-b_c\omega$ in figure 42 has two intersections and is tangent at a third point on the $g(\omega)$ curve. In this case, there exists a double real root at the tangent. For $b > b_c$, there exist complex roots, and for $b < b_c$, there exist only real roots

of $f(\omega) = 0$. Therefore, the value of b_c is the greatest lower bound on the values of b for which there are complex roots of $f(\omega) = 0$.

Consider the line $-b_L\omega$ in figure 42 which passes through an extremum of $g(\omega)$. The value of b_L is given by

$$b_L = \frac{a^2 - 4c}{\sqrt{8a}} \tag{B5}$$

The value of b_L being less than b_c is a lower bound on the values of b for which there may be complex roots of $f(\omega) = 0$. Therefore, if

$$a^2 > 4c \tag{B6}$$

and

$$b \leqq \frac{a^2 - 4c}{\sqrt{8a}} \tag{B7}$$

then all roots are real and distinct. If b is nonzero and $a^2 = 4c$ or if $a^2 < 4c$, then there exist complex roots of equation (B1). If equation (B6) is satisfied but equation (B7) is not, then a more detailed analysis is required to determine whether the roots are all real.

The roots of the quartic polynomial equation $f(\omega) = 0$ can be calculated by algebraic techniques, for example, Ferrari's method (ref. 16). However, a different procedure is used in the following analysis.

Given that $f(\omega)$ has four real roots, then it can be factored into the form

$$f(\omega) = (\omega - \omega_0 - \omega_1)(\omega - \omega_0 + \omega_1)(\omega + \omega_0 - \omega_2)(\omega + \omega_0 + \omega_2) \tag{B8}$$

where ω_0, ω_1, and ω_2 are real numbers.

Multiplying out equation (B8) and equating coefficients with equation (B1) yield a set of simultaneous nonlinear equations in ω_0, ω_1, and ω_2:

$$\omega_1^2 + \omega_2^2 + 2\omega_0^2 = a \tag{B9}$$

$$2\left(\omega_2^2 - \omega_1^2\right)\omega_0 = b \tag{B10}$$

$$\left(\omega_0^2 - \omega_1^2\right)\left(\omega_0^2 - \omega_2^2\right) = c \tag{B11}$$

APPENDIX B

Solving equation (B9) for ω_2^2 and substituting the result into equation (B10) yield an equation for ω_1^2 as a function of ω_0:

$$\omega_1^2 = \frac{a}{2} - \omega_0^2 - \frac{b}{4\omega_0} \tag{B12}$$

Similarly, solving equation (B9) for ω_1^2 and substituting the result into equation (B10) yield an equation for ω_2^2 as a function of ω_0:

$$\omega_2^2 = \frac{a}{2} - \omega_0^2 + \frac{b}{4\omega_0} \tag{B13}$$

Substitution of equations (B12) and (B13) into equation (B11) yields a polynomial in ω_0:

$$\omega_0^6 - \frac{a}{2}\omega_0^4 + \left(\frac{a^2 - 4c}{16}\right)\omega_0^2 - \frac{b^2}{64} = 0 \tag{B14}$$

The roots of this equation may be found by application of Tartaglia's method (ref. 16). In this paper only those roots of equation (B14) with the smallest magnitude are considered. Assuming that the magnitudes of these roots are much smaller than the magnitudes of the remaining roots, an approximate solution may be obtained by ignoring the first term of equation (B14):

$$\omega_0^2 = \frac{\frac{1}{2}b^2}{(a^2 - 4c) + \sqrt{(a^2 - 4c)^2 - 8ab^2}} \tag{B15}$$

For more precision, an iterative procedure may be used for solving equation (B14) by substituting an estimate (or previous solution) for ω_0^2 for the first term of the equation and solving as if it were part of the constant term as follows:

$$\left(\omega_0^2\right)_{i+1} = \frac{\frac{1}{2}\left[b^2 - 64\left(\omega_0^2\right)_i^3\right]}{(a^2 - 4c) + \sqrt{(a^2 - 4c)^2 - 8a\left[b^2 - 64\left(\omega_0^2\right)_i^3\right]}} \tag{B16}$$

where the subscript i denotes the ith solution of the iteration and $\left(\omega_0^2\right)_0 = 0$.

Without loss of generality, only positive values of ω_0 are considered. With this condition, examination of equations (B12) and (B13) shows that the

magnitude of ω_2 is larger than the magnitude of ω_1. Solving equation (B9) for ω_2^2 and substituting the result into equation (B11) yield a polynomial in ω_1^2:

$$\omega_1^4 - \left(a - 2\omega_0^2\right)\omega_1^2 + \left[c + \omega_0^2\left(a - 3\omega_0^2\right)\right] = 0 \tag{B17}$$

Similarly solving equation (B9) for ω_1^2 and substituting the result into equation (B11) yield an identical polynomial in ω_2^2. Equations (B12) and (B13) show that there are only two solutions for ω_1 and two solutions for ω_2. Since $|\omega_2| > |\omega_1|$, the two larger roots of equation (B17) are values of ω_2 and the two smaller roots are values of ω_1:

$$\omega_2^2 = \frac{\left(a - 2\omega_0^2\right) + \sqrt{\left(a - 2\omega_0^2\right)^2 - 4\left[c + \omega_0^2\left(a - 3\omega_0^2\right)\right]}}{2} \tag{B18}$$

$$\omega_1^2 = \frac{2\left[c + \omega_0^2\left(a - 3\omega_0^2\right)\right]}{\left(a - 2\omega_0^2\right) + \sqrt{\left(a - 2\omega_0^2\right)^2 - 4\left[c + \omega_0^2\left(a - 3\omega_0^2\right)\right]}} \tag{B19}$$

From equation (B8), the four roots of $f(\omega) = 0$ where $f(\omega)$ is given by equation (B1) are $\omega = \omega_0 \pm \omega_1$, $-\omega_0 \pm \omega_2$ where ω_0 is calculated by the approximate equation (B14) or the iteration equation (B16), ω_2 is calculated by equation (B18), and ω_1 is calculated by equation (B19). All the roots are real if the conditions of equations (B6) and (B7) are satisfied. However, there are cases which have all real roots but which violate the condition of equation (B7).

REFERENCES

1. Kurzhals, Peter R.; and Grantham, Carolyn: A System for Inertial Experiment Pointing and Attitude Control. NASA TR R-247, 1966.

2. Kennedy, H. B.: A Gyro Momentum Exchange Device for Space Vehicle Attitude Control. AIAA J., vol. 1, no. 5, May 1963, pp. 1110-1118.

3. Montgomery, Raymond C.; and Johnson, C. Richard, Jr.: The Dual-Momentum Control Device for Large Space Systems. A Collection of Technical Papers - AIAA/NASA Conference on Advanced Technology for Future Space Systems, May 1979, pp. 366-374. (Available as AIAA Paper 79-0923.)

4. Anderson, Willard W.; and Groom, Nelson J.: The Annular Momentum Control Device (AMCD) and Potential Applications. NASA TN D-7866, 1975.

5. Dimentberg, F. M.: Flexural Vibrations of Rotating Shafts. Butterworths, 1961.

6. Coleman, Robert P.; Feingold, Arnold M.; and Brooks, George W.: Theory of Self-Excited Mechanical Oscillations of Helicopter Rotors With Hinged Blades. NACA Rep. 1351, 1958.

7. Sleeper, Robert K.; and Lester, Harold C.: A Stability Study and Modal Analysis of a Space-Station-Centrifuge Configuration. NASA TN D-5801, 1970.

8. Roark, Raymond J.; and Young, Warren C.: Formulas for Stress and Strain. Fifth ed. McGraw-Hill, Inc., c.1975.

9. Sechler, Ernest E.: Elasticity in Engineering. John Wiley & Sons, Inc., c.1952.

10. Love, A. E. H.: A Treatise on the Mathematical Theory of Elasticity. Fourth ed. Dover Publ., 1927. (First ed., 1892.)

11. Greensite, Arthur L.: Control Theory: Volume II - Analysis and Design of Space Vehicle Flight Control Systems. Spartan Books, c.1970.

12. Lang, T. E.: Vibration of Thin Circular Rings. Part I. Solutions for Modal Characteristics and Forced Excitation. Tech. Rep. No. 32-261 (Contract No. NAS7-100), Jet Propulsion Lab., C.I.T., July 1, 1962.

13. Öz, H.; and Meirovitch, L.: Dynamics of the AMCD Ring. Dynamics and Control of Large Flexible Spacecraft, L. Meirovitch, ed., American Inst. Aeronaut. & Astronaut., 1979, pp. 523-544.

14. Fox, E. A.: Mechanics. Harper & Row Publ., c.1967.

15. Popov, E. P.: Mechanics of Materials. Prentice-Hall, Inc., c.1952.

16. Brink, Raymond W.: College Algebra. Second ed. Appleton-Century-Crofts, Inc., c.1951.

TABLE I.- CHARACTERISTICS OF EXAMPLE RING

Symbol	Value	Symbol	Value
R	360 m	S_z	1.12×10^{-5}
A	1.96 cm^2	S_r	1.12×10^{-5}
I_z	0.320 cm^4	S_p	1.59×10^{-5}
I_r	0.320 cm^4	S_J	1.46×10^{-5}
I_p	0.640 cm^4	E_G	1.52
J	0.538 cm^4	v_s	12.5 km/sec
ρ	1.8 g/cm^3	v_r	7.8 km/sec
E	280 GPa	ω_s	34.7 rad/sec
G	110 GPa	ω_r	21.7 rad/sec

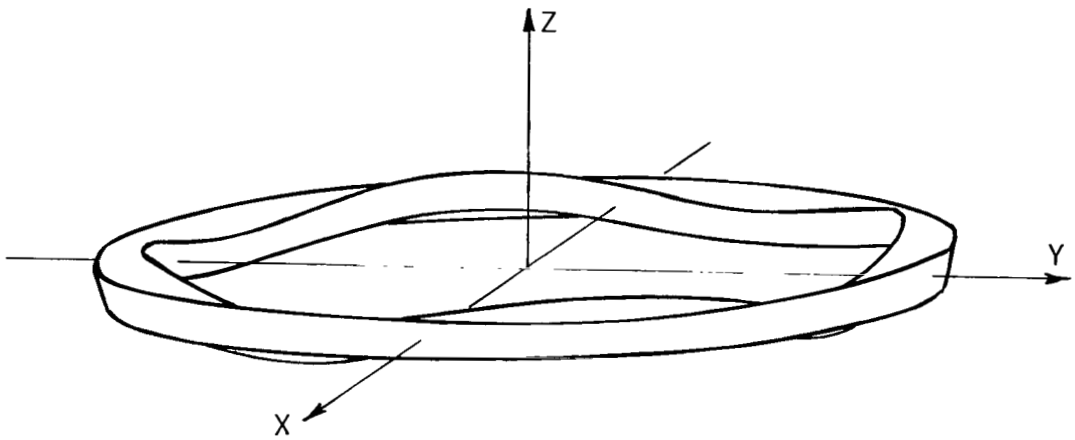

Figure 1.- Torsional mode. j = 4.

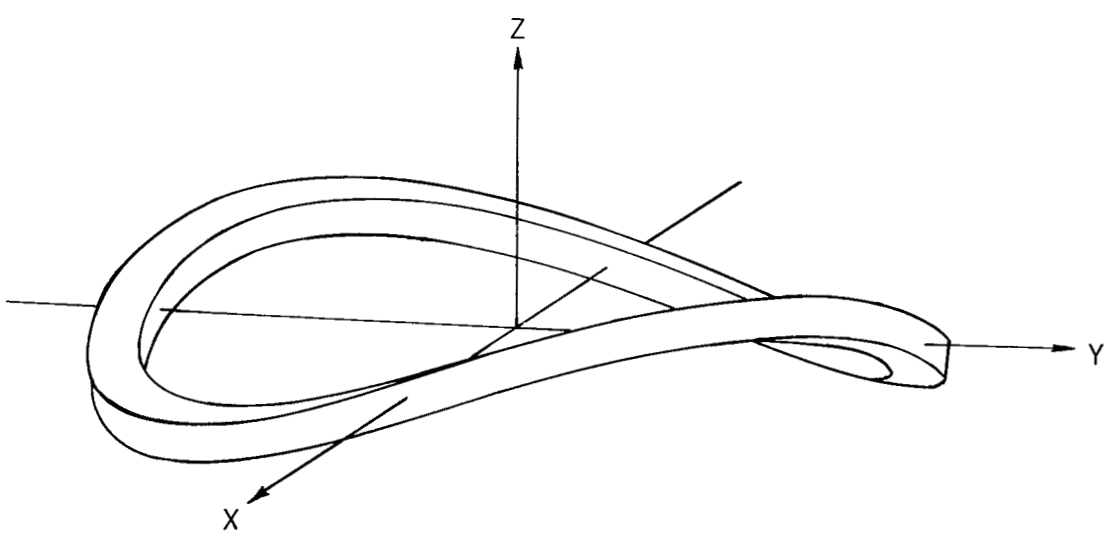

Figure 2.- Out-of-plane bending mode. j = 2.

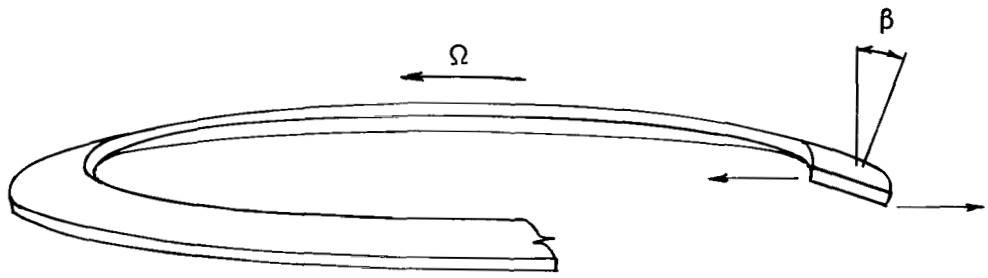

(a) Stiffening couple, $I_r < I_z$.

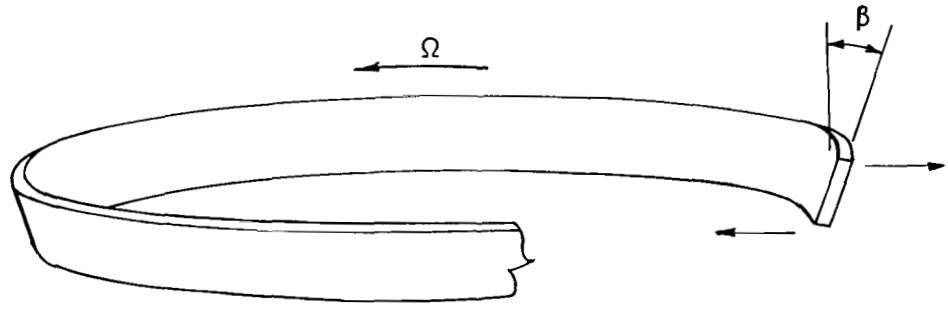

(b) Destabilizing couple, $I_r > I_z$.

Figure 3.- Torsional couples produced in spinning ring. j = 0.

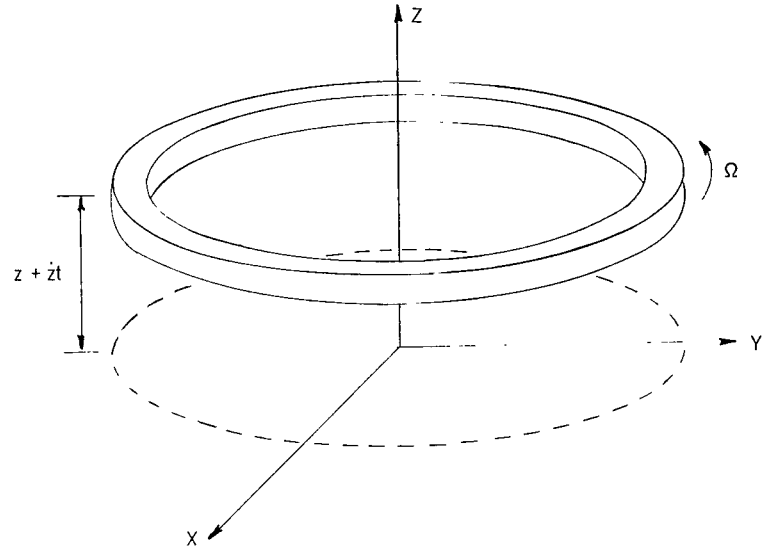

Figure 4.- Out-of-plane translation. j = 0.

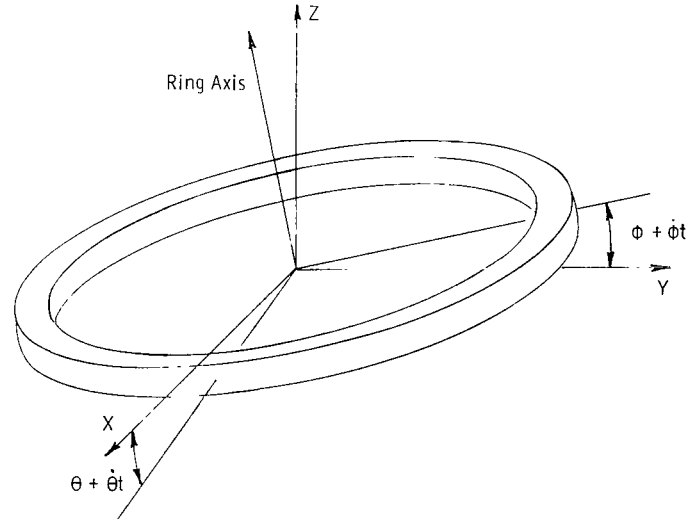

Figure 5.- Out-of-plane rotation. j = 1.

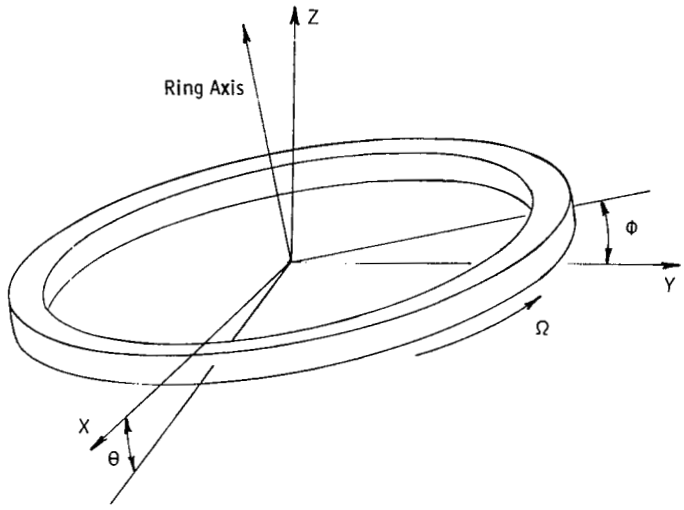

Figure 6.- Axis inclination. j = 1.

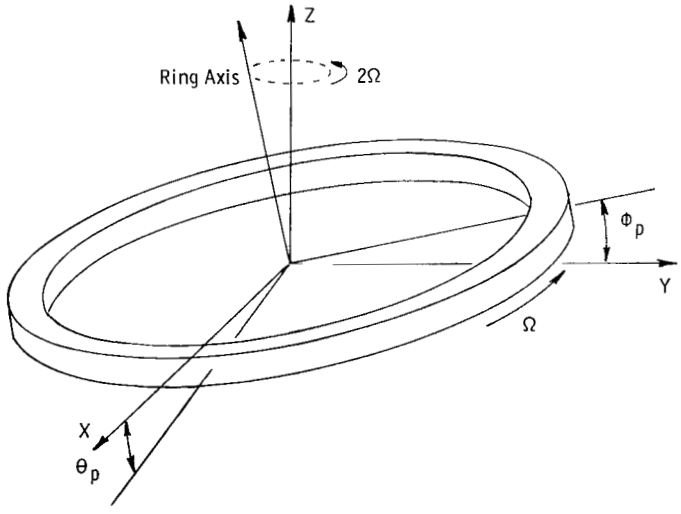

Figure 7.- Gyroscopic precession. j = 1.

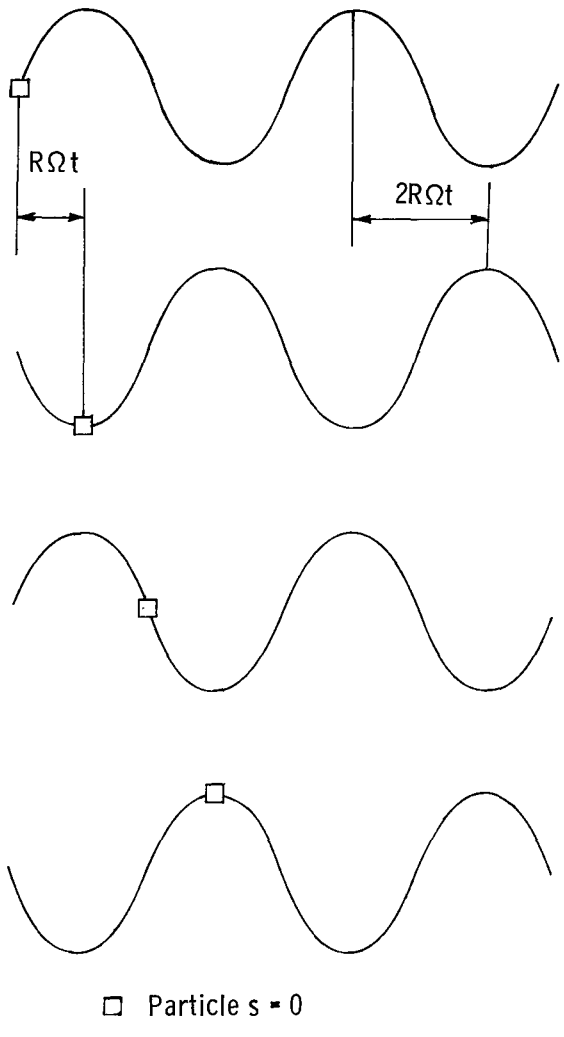

Figure 8.- Out-of-plane progressive wave motion for high spin rate.

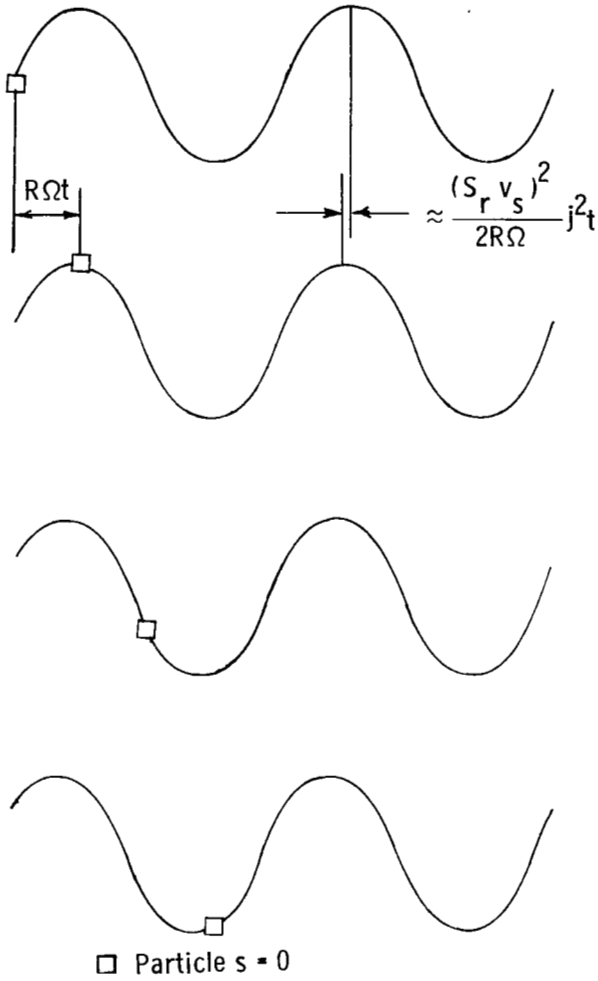

Figure 9.- Out-of-plane regressive wave motion for high spin rate.

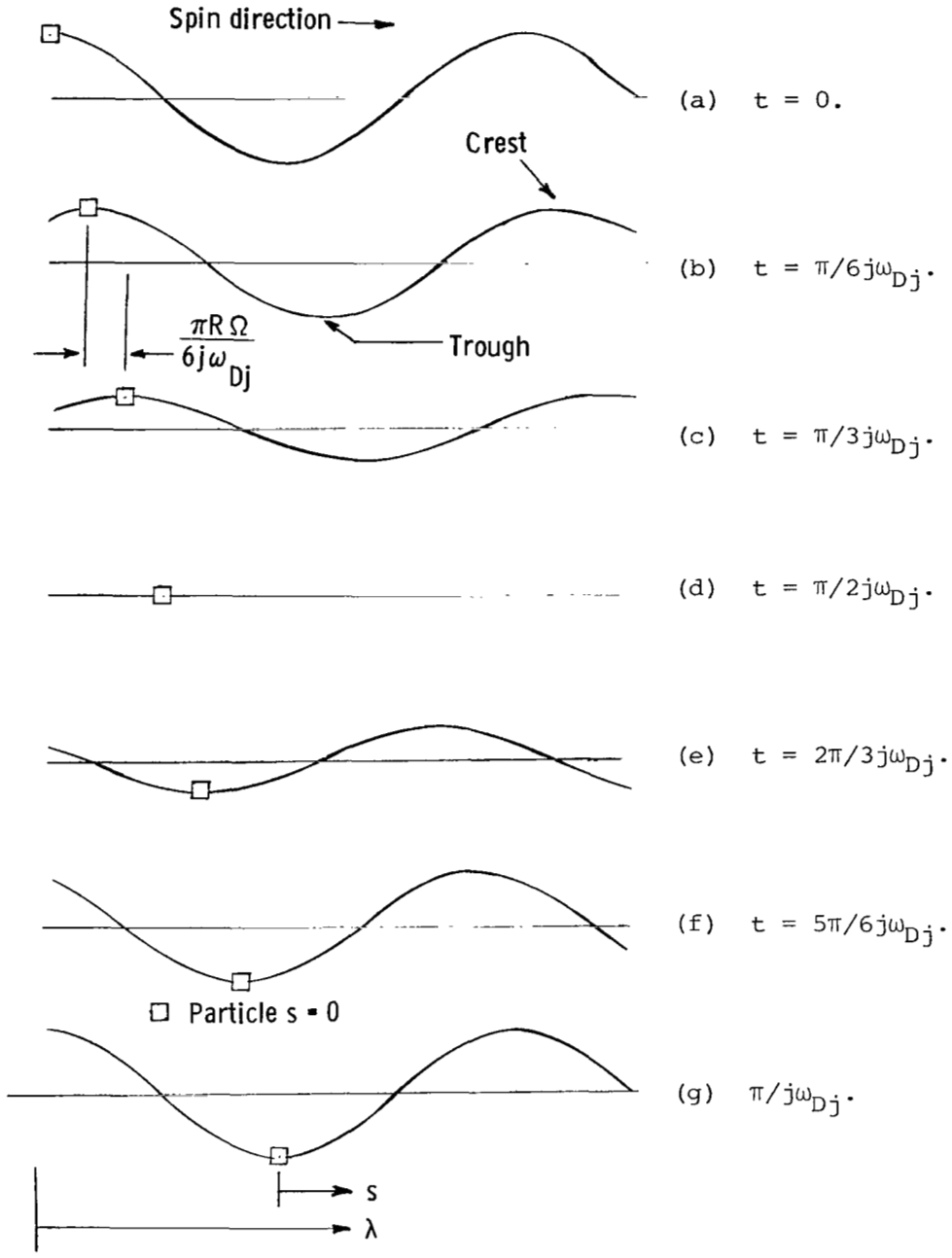

Figure 10.- Out-of-plane standing wave motion for high spin rate.

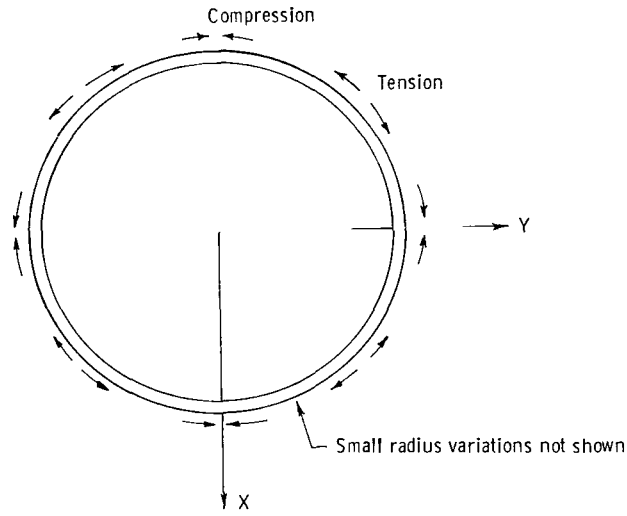

Figure 11.- In-plane compression mode. j = 4.

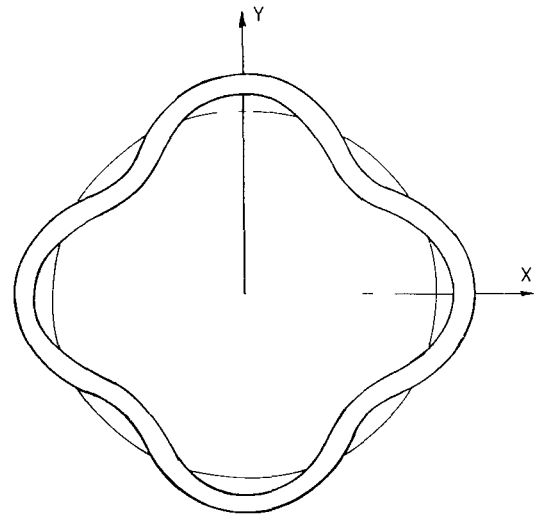

Figure 12.- In-plane bending mode. j = 4.

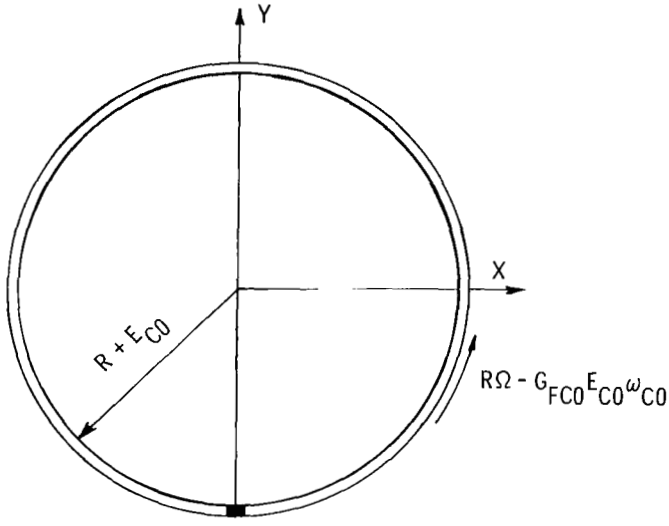

(a) Initial condition, $t = 0$.

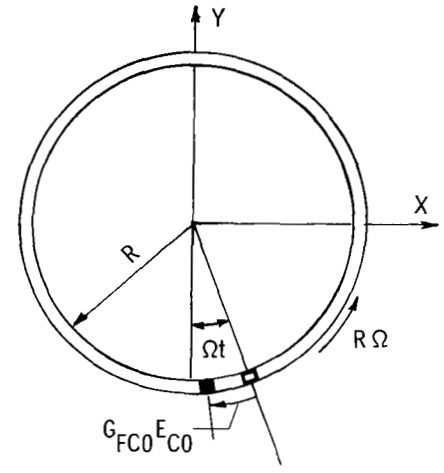

(b) $t = \pi/2\omega_{C0}$.

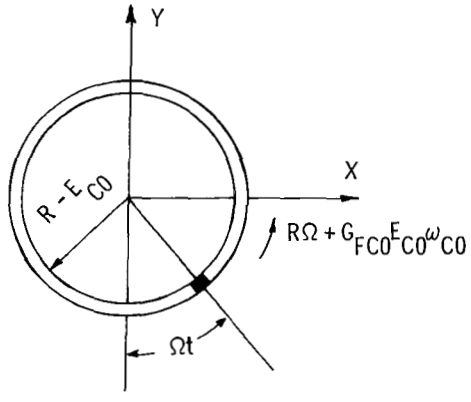

(c) $t = \pi/\omega_{C0}$.

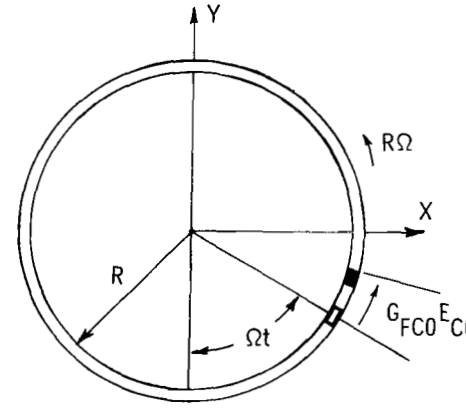

(d) $t = 3\pi/2\omega_{C0}$.

Figure 13.- Radial oscillation. $j = 0$.

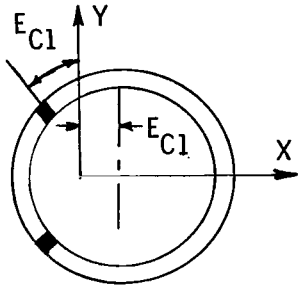

(a) $t = 0$.

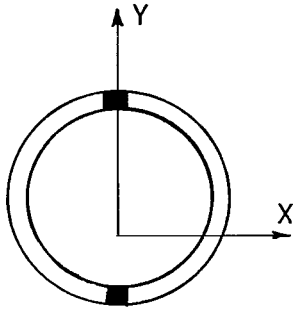

(b) $t = \pi/2\omega_{C1}$.

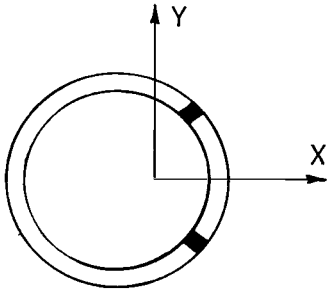

(c) $t = \pi/\omega_{C1}$.

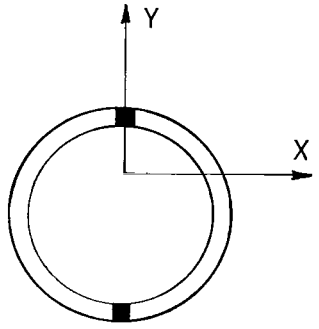

(d) $t = 3\pi/2\omega_{C1}$.

Figure 14.- In-plane compression mode. $\Omega = 0$; $j = 1$; $F_{C1} = 0$; $\omega_{C1} < 0$.

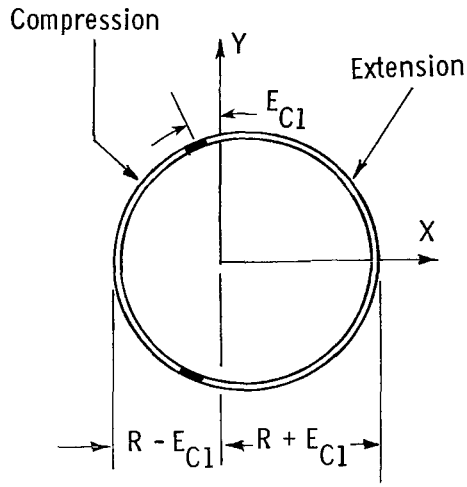

(a) t = 0.

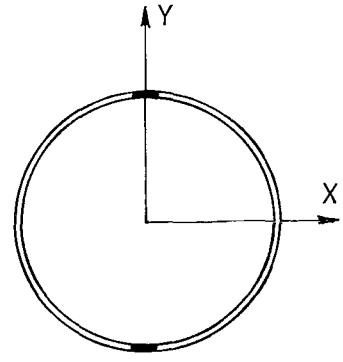

(b) $t = \pi/2\omega_{C1}$.

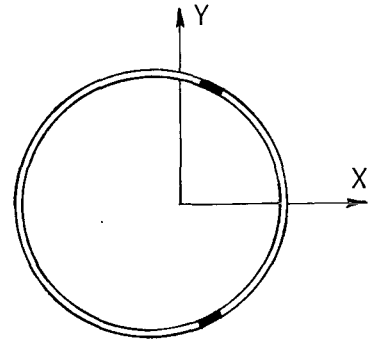

(c) $t = \pi/\omega_{C1}$.

Figure 15.- In-plane compression standing wave. $\Omega = 0$; $j = 1$; $F_{C1} = 0$.

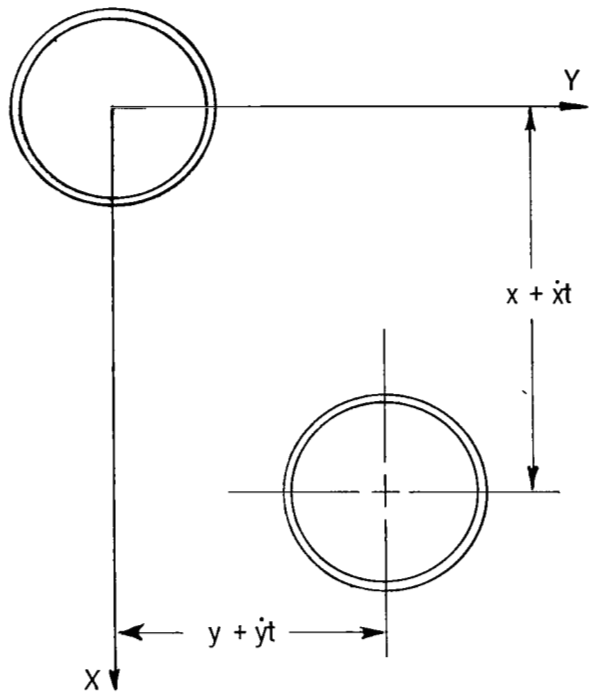

Figure 16.- In-plane translation. j = 1.

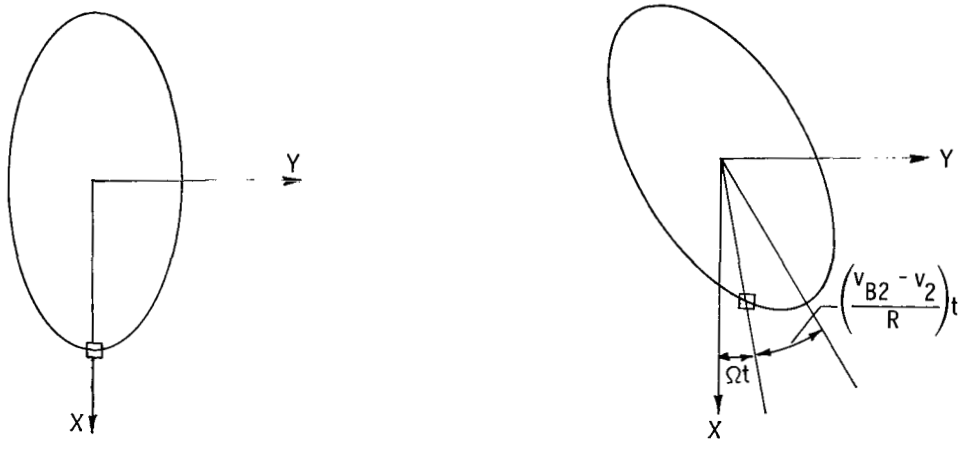

(a) t = 0. (b) t > 0.

Figure 17.- In-plane progressive bending mode for low spin rate. $\Omega << S_z\omega_s$; j = 2.

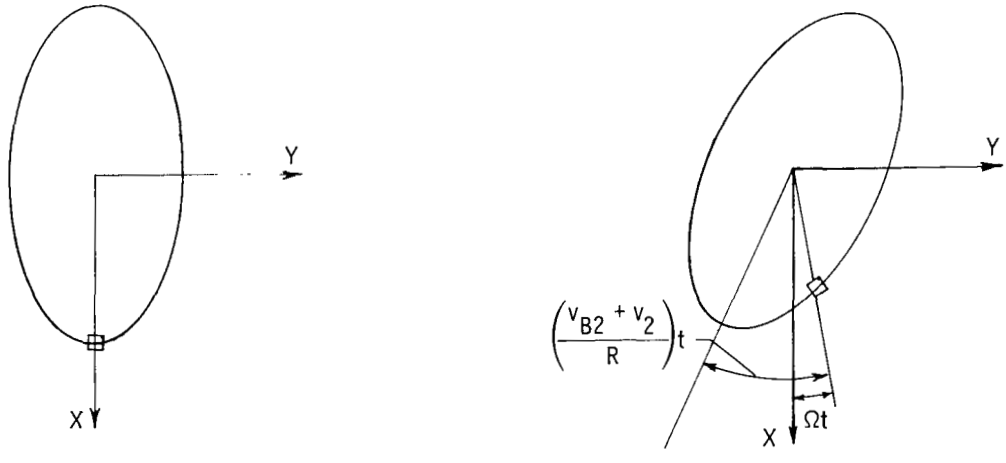

(a) t = 0. (b) t > 0.

Figure 18.- In-plane regressive bending mode for low spin rate. $\Omega << S_z\omega_s$; j = 2.

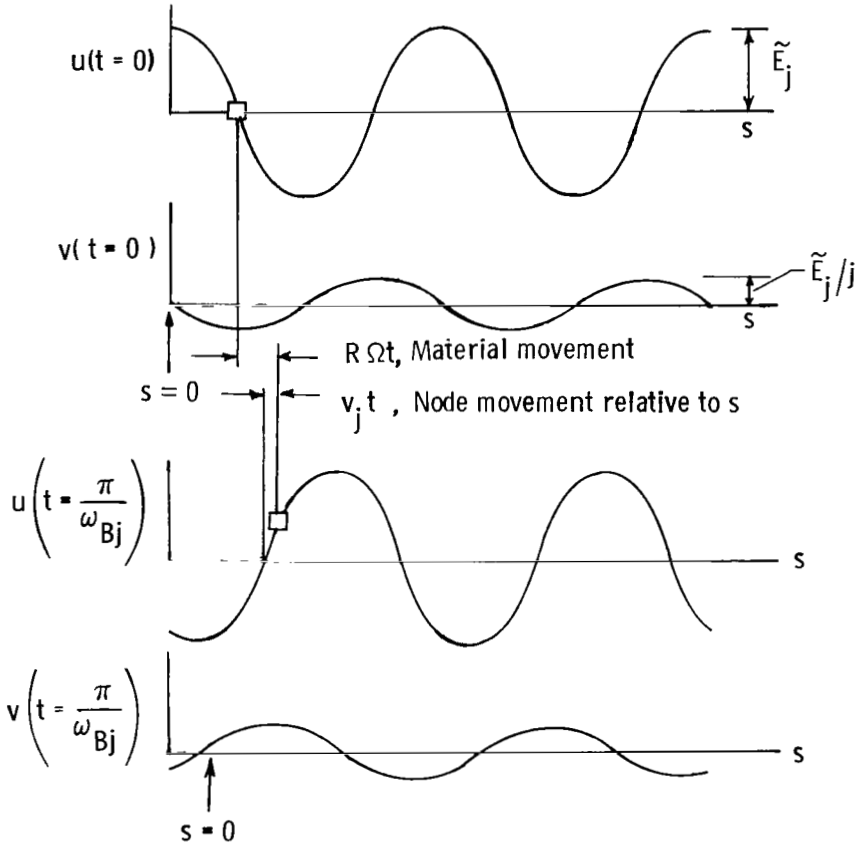

Figure 19.- In-plane bending standing wave as seen by a fixed observer for low spin rate. $\Omega << S_z\omega_s$.

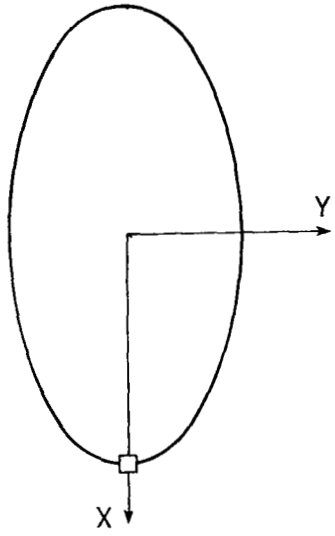

(a) $t = 0$.

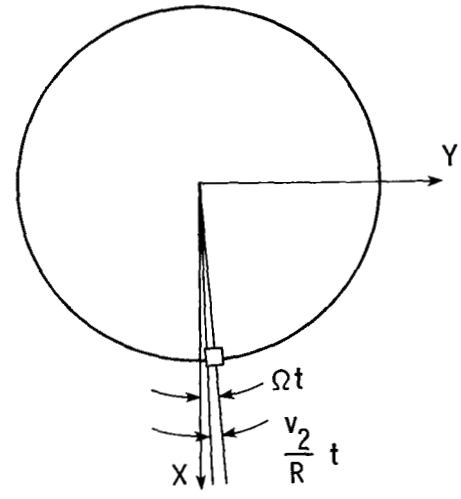

(b) $t = \pi/2\omega_{B2}$.

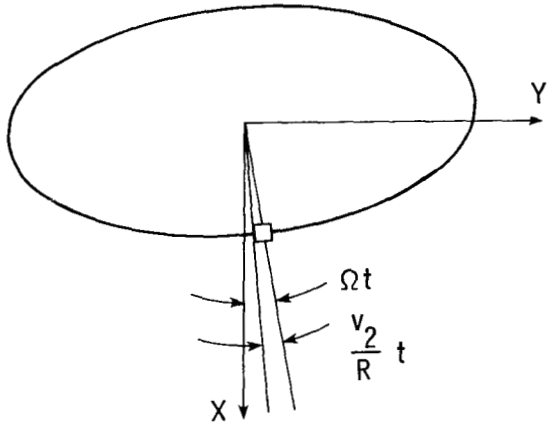

(c) $t = \pi/\omega_{B2}$.

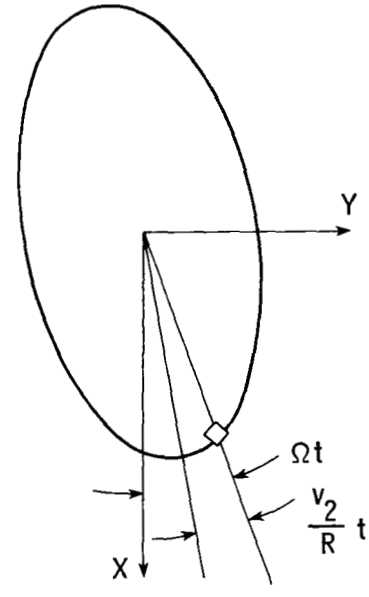

(d) $t = 2\pi/\omega_{B2}$.

Figure 20.- In-plane bending standing wave for low spin rate. $\Omega << S_z\omega_s$; $j = 2$.

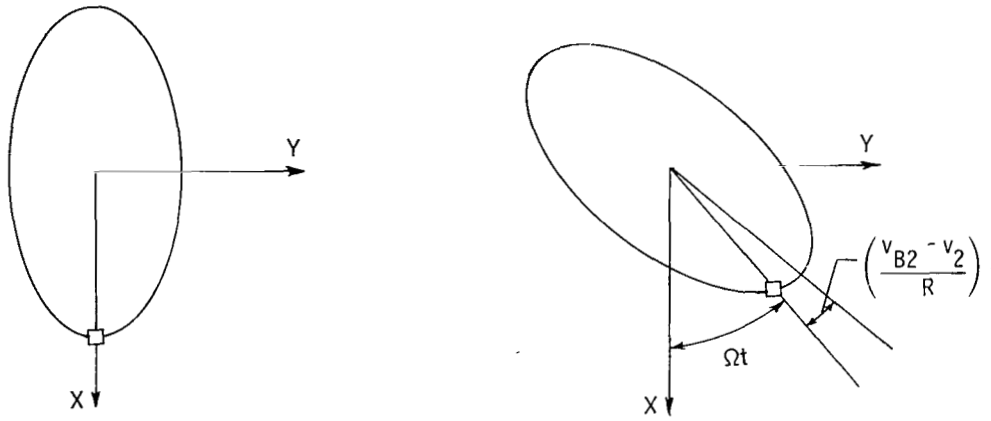

(a) t = 0. (b) t > 0.

Figure 21.- In-plane progressive bending mode for high spin rate. $S_z\omega_s << \Omega << \omega_s$; j = 2.

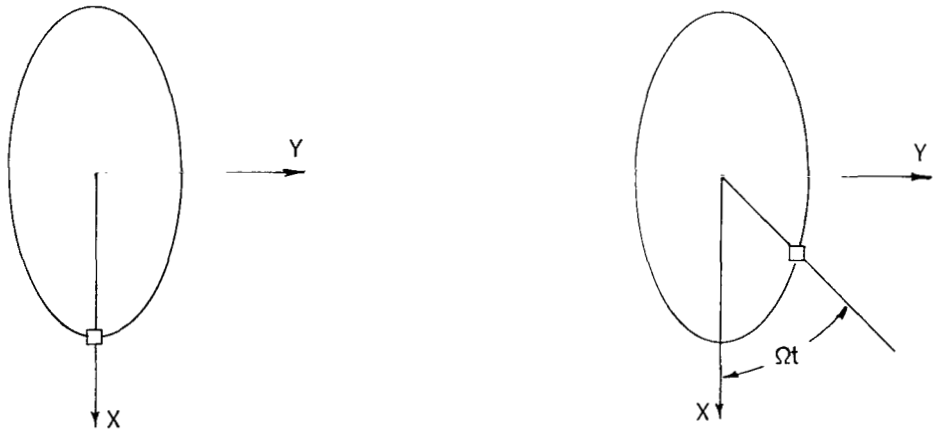

(a) t = 0. (b) t > 0.

Figure 22.- In-plane regressive bending mode for high spin rate. $S_z\omega_s << \Omega << \omega_s$; j = 2.

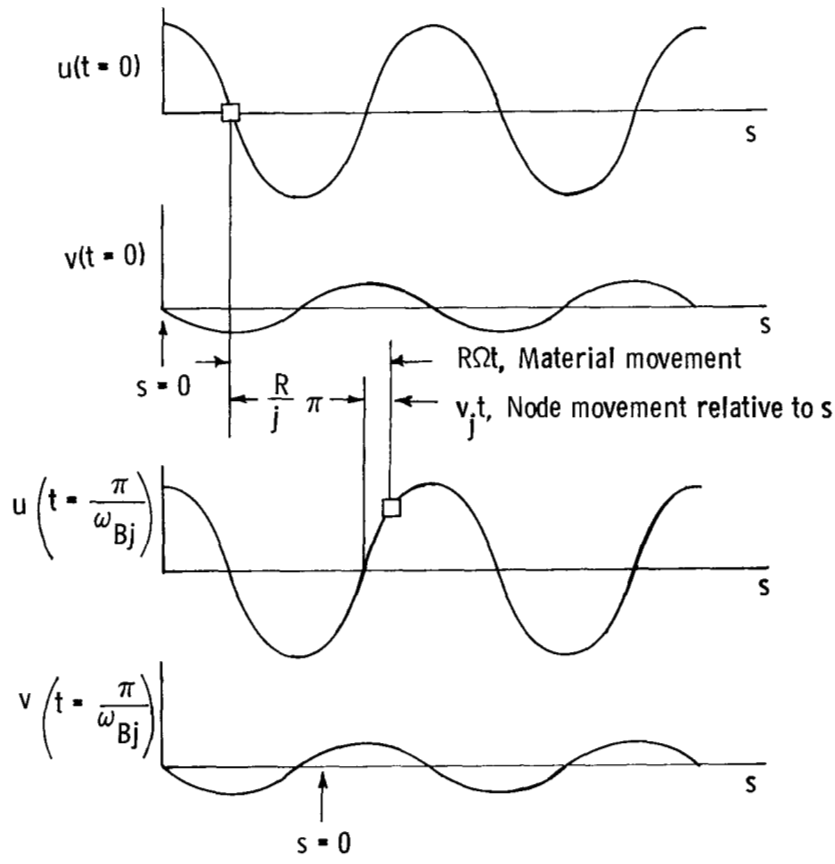

Figure 23.- In-plane bending standing wave as seen by a fixed observer for high spin rate. $S_z\omega_s \ll \Omega \ll \omega_s$.

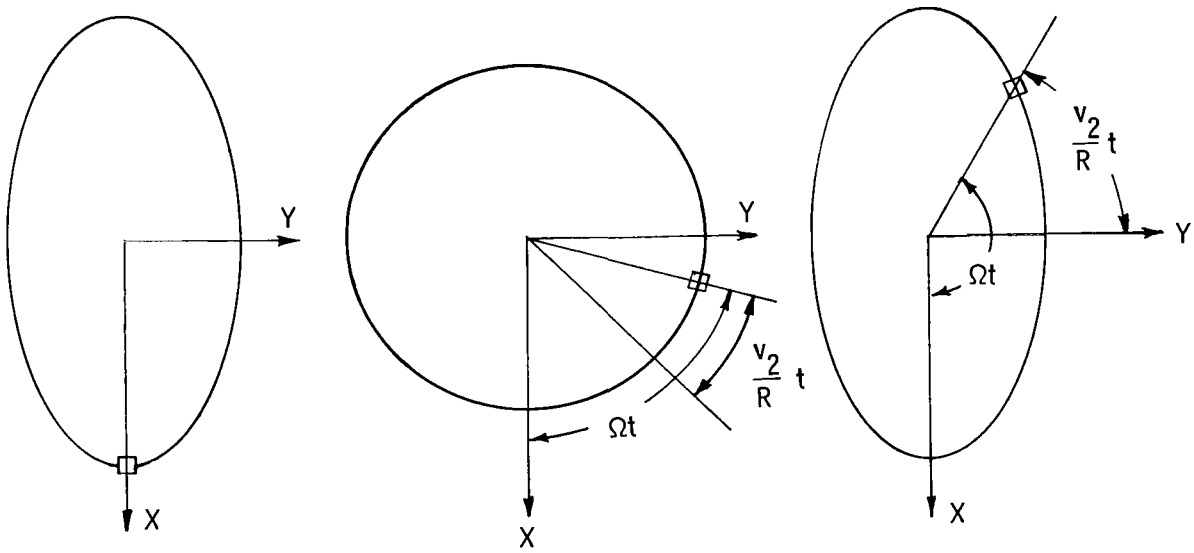

(a) $t = 0$. (b) $t = \pi/2\omega_{B2}$. (c) $t = \pi/\omega_{B2}$.

Figure 24.- In-plane bending standing wave for high spin rate. $S_z\omega_s << \Omega << \omega_s$; $j = 2$.

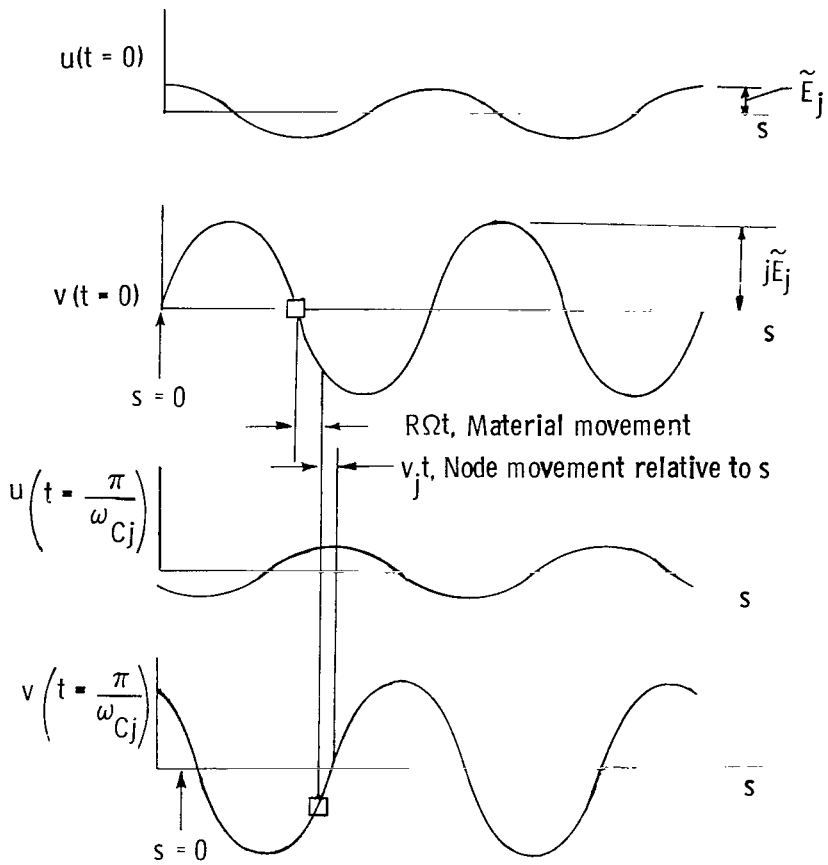

Figure 25.- In-plane compression standing wave as seen by fixed observer.

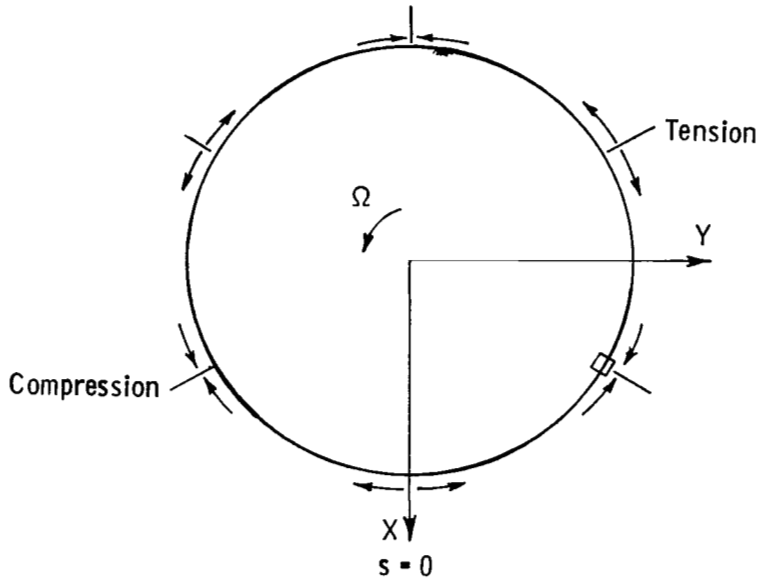

(a) t = 0.

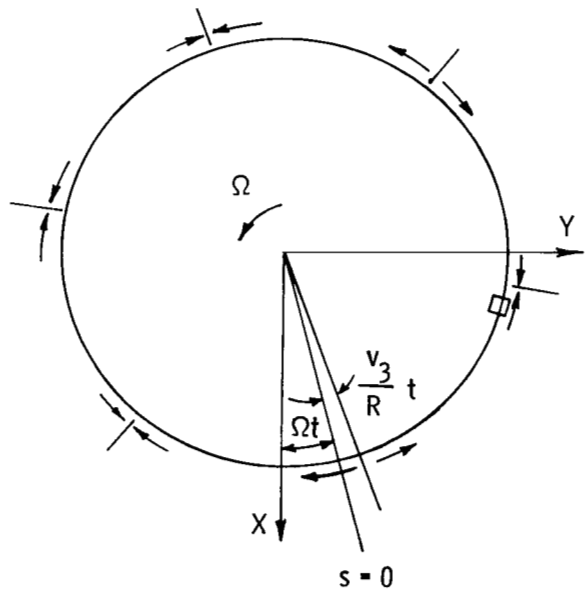

(b) $t = 2\pi/\omega_{Cj}$.

Figure 26.- In-plane compression standing wave.
$\Omega << \omega_s$; j = 3.

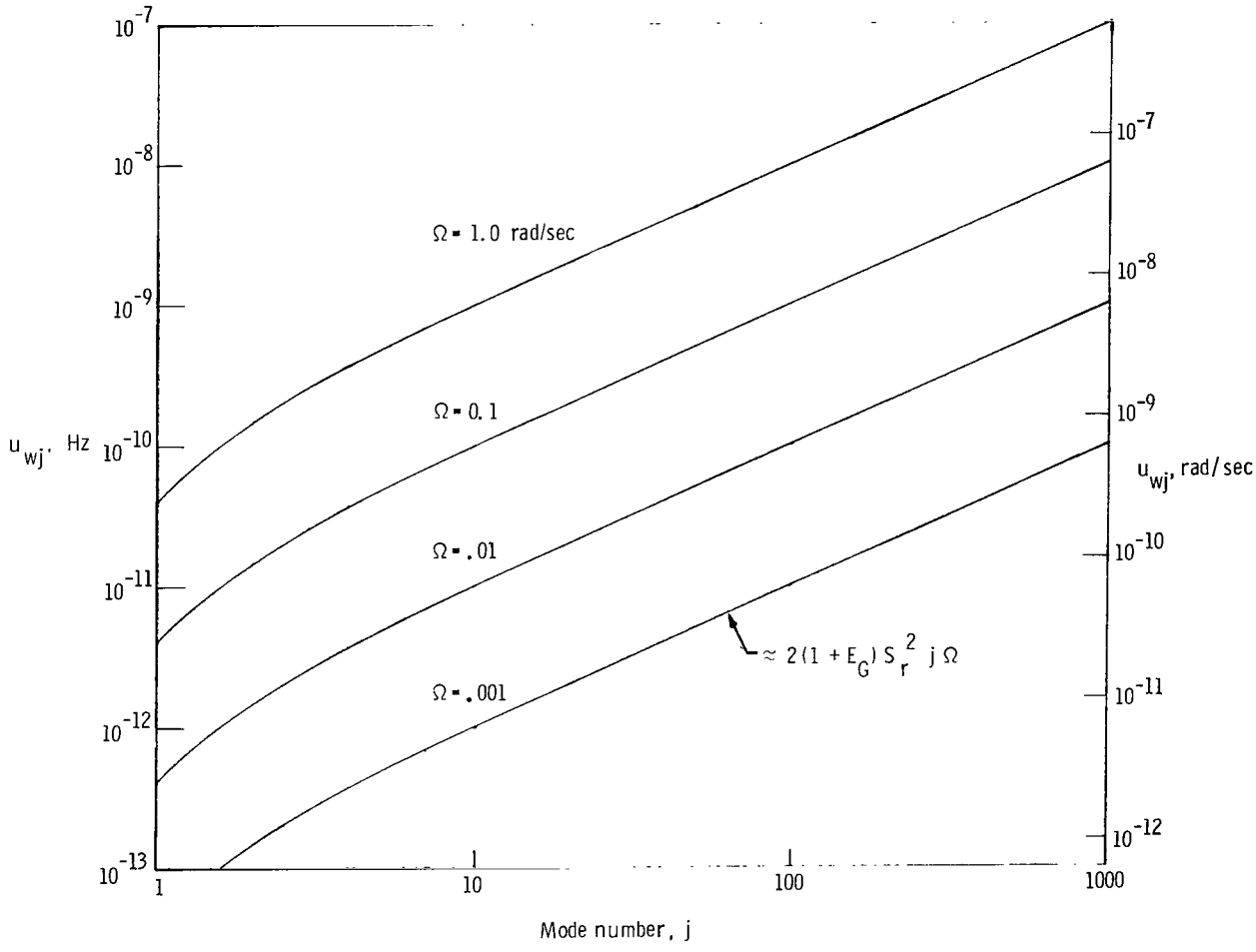

Figure 27.- Out-of-plane nodal frequencies.

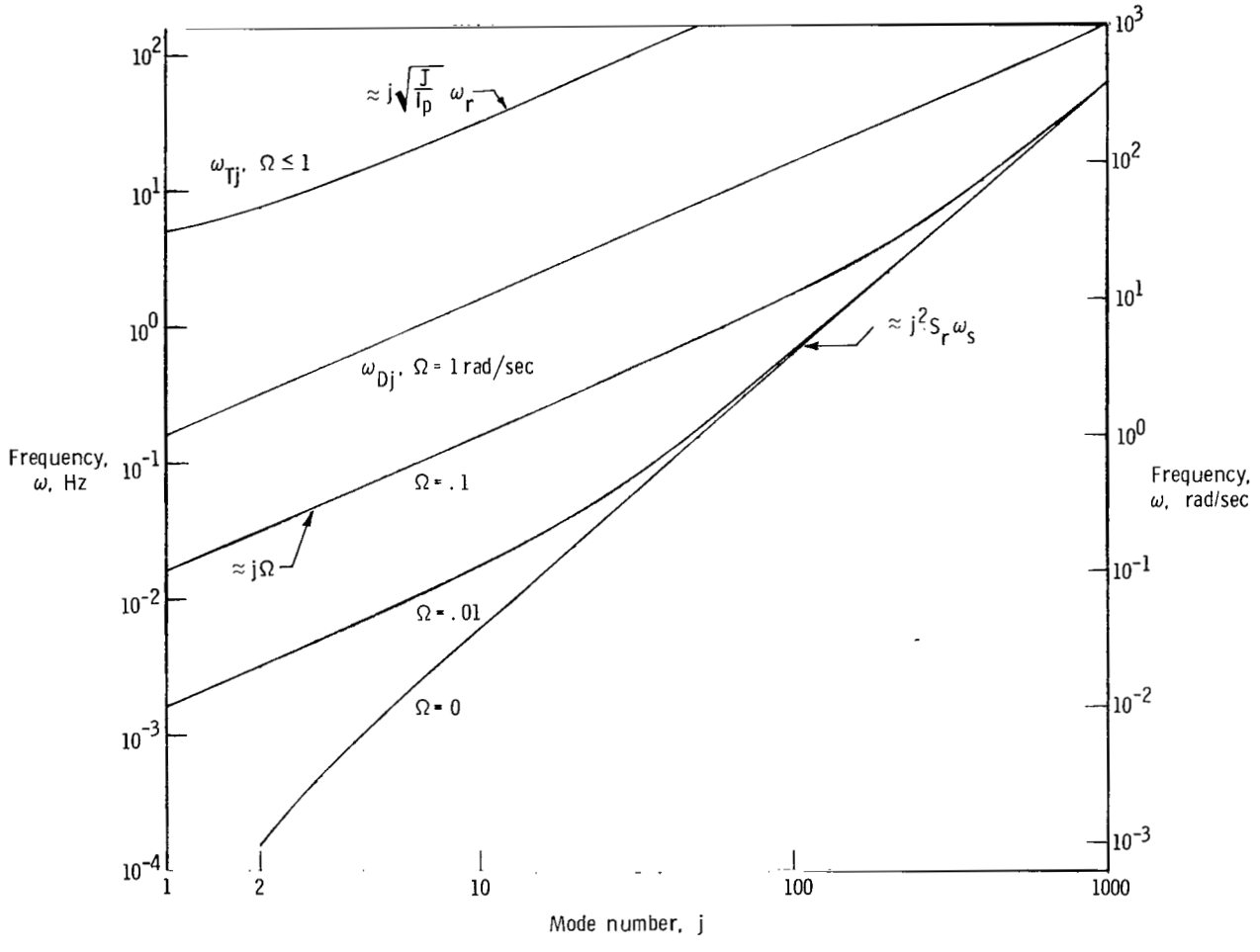

Figure 28.- Out-of-plane modal frequencies.

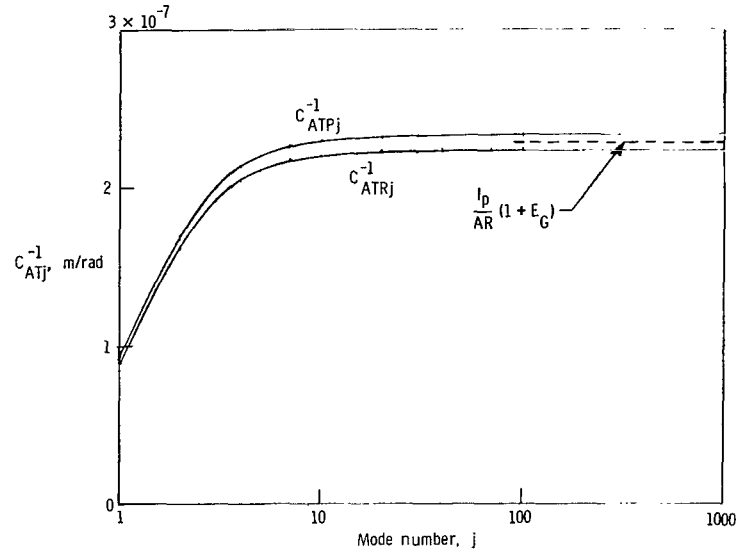

(a) Torsional mode, ratio of out-of-plane deflection to twist angle.

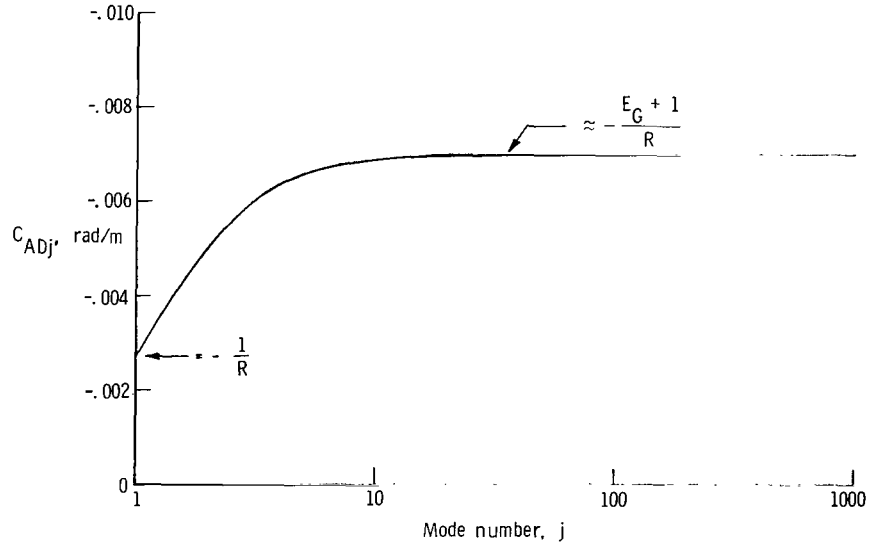

(b) Deflection mode, ratio of twist angle to out-of-plane deflection.

Figure 29.- Ratios of out-of-plane variables. Ω = 1 rad/sec.

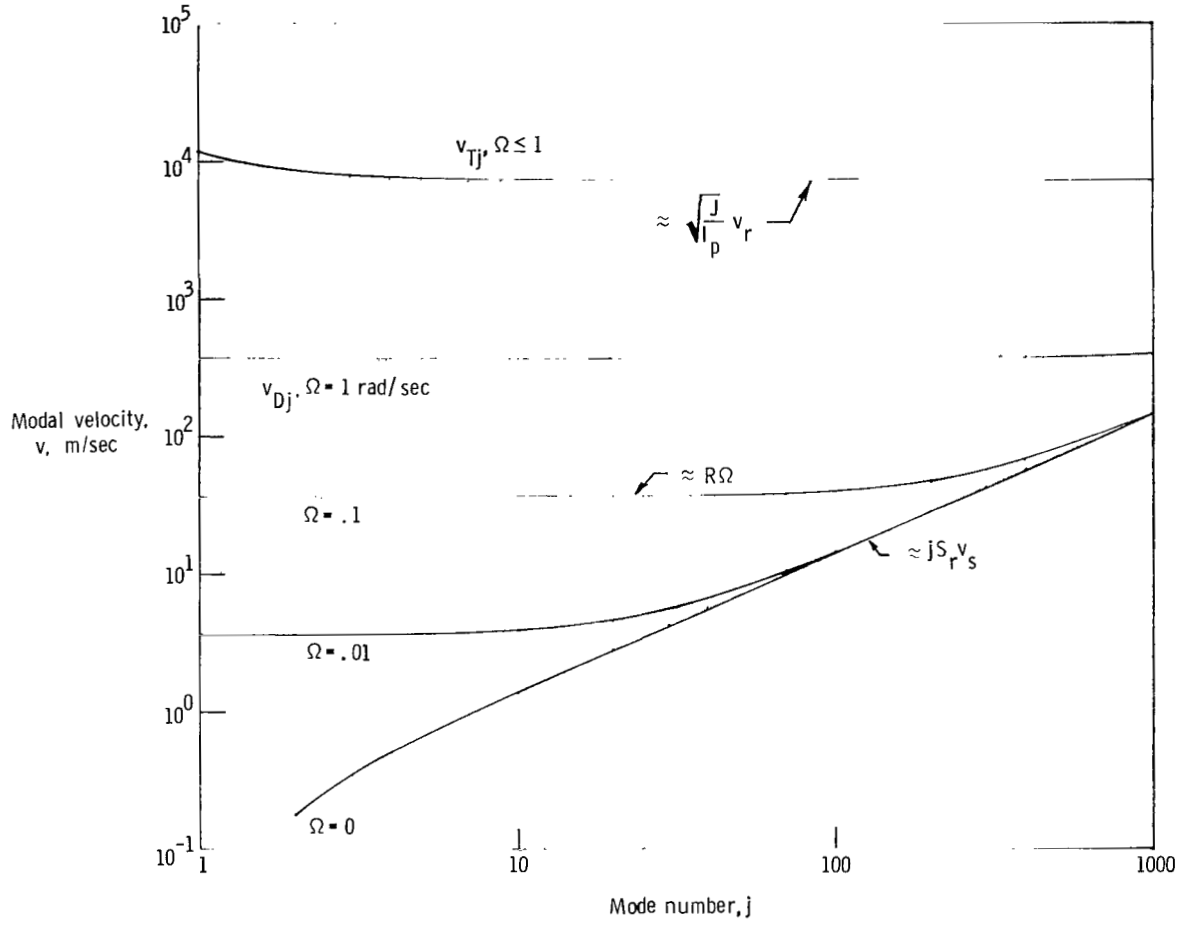

Figure 30.- Out-of-plane modal velocities versus mode number.

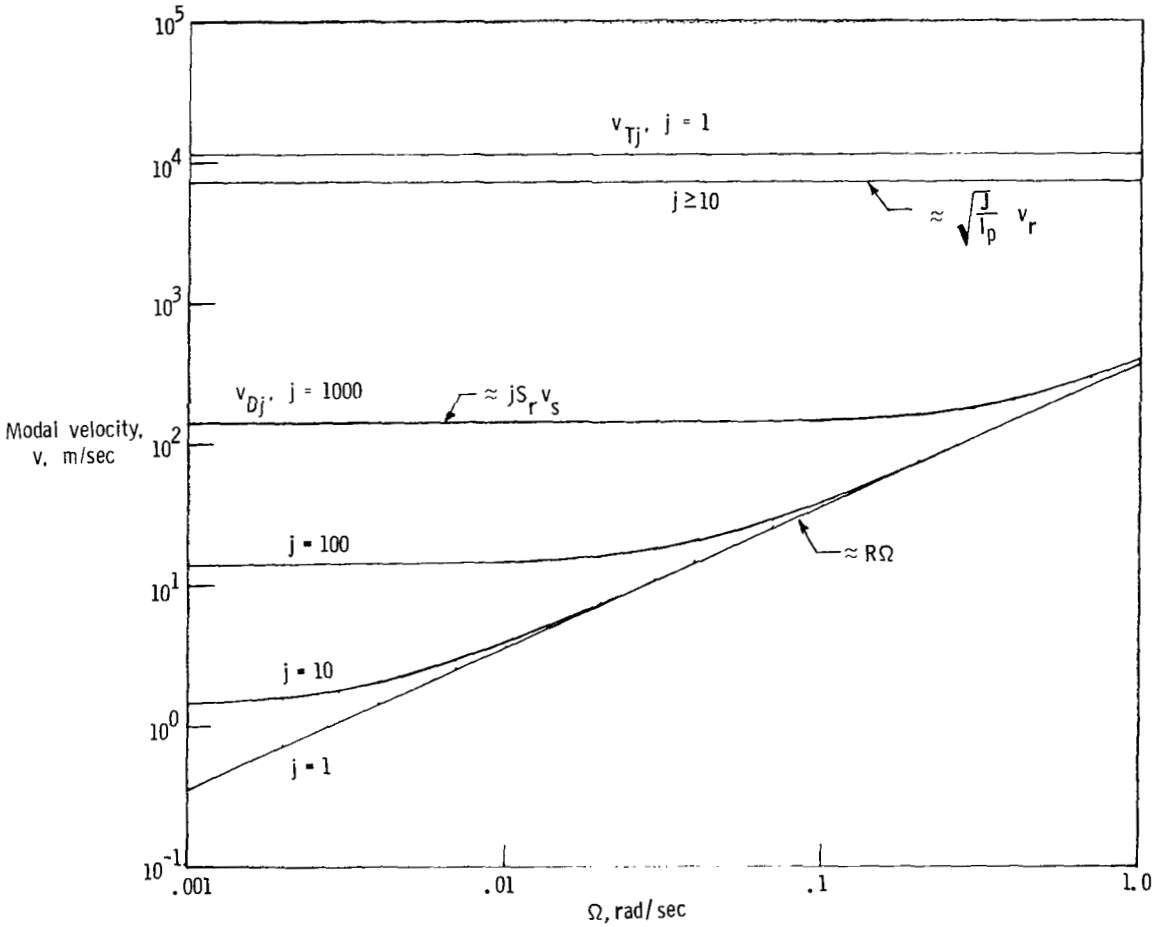

Figure 31.- Out-of-plane modal velocities versus spin rate.

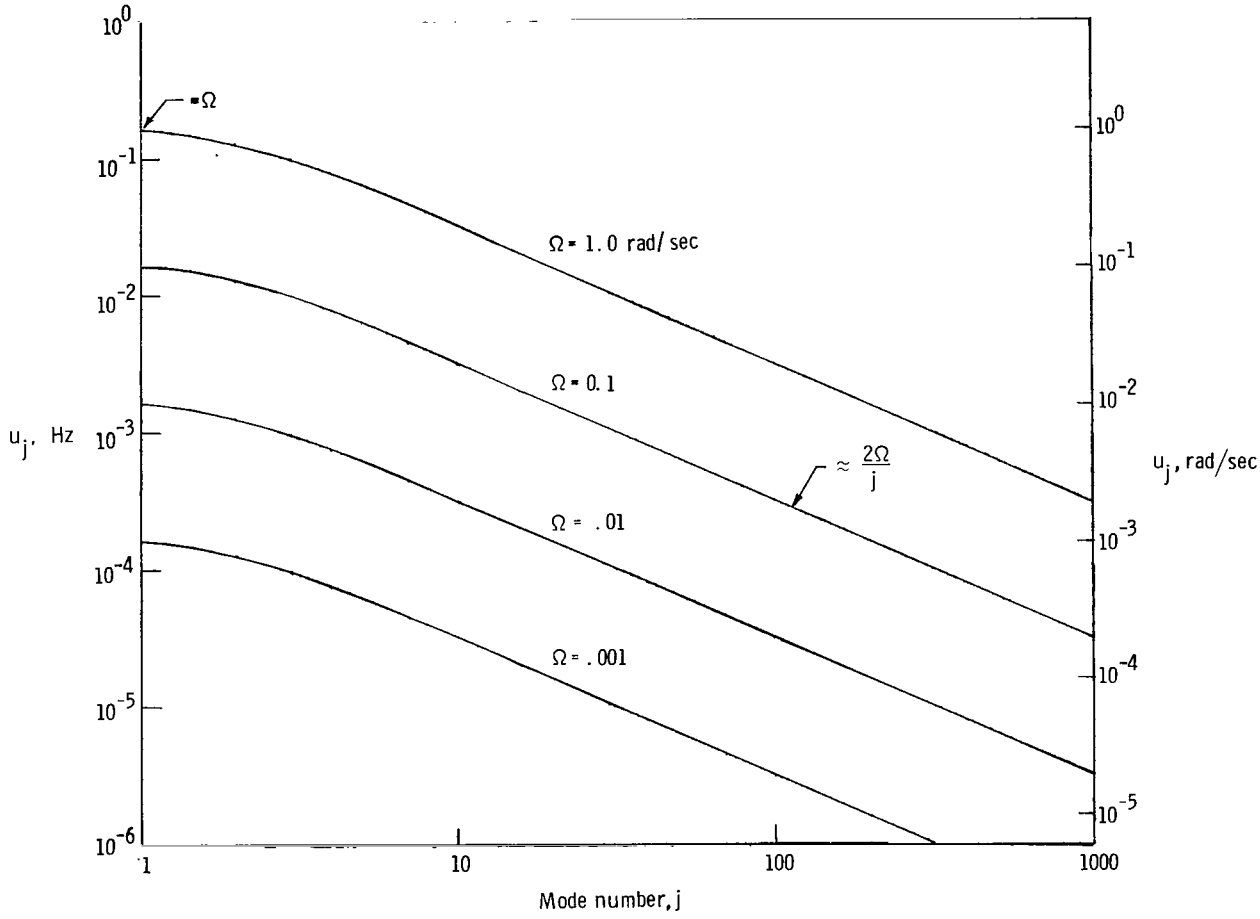

Figure 32.- In-plane nodal frequencies.

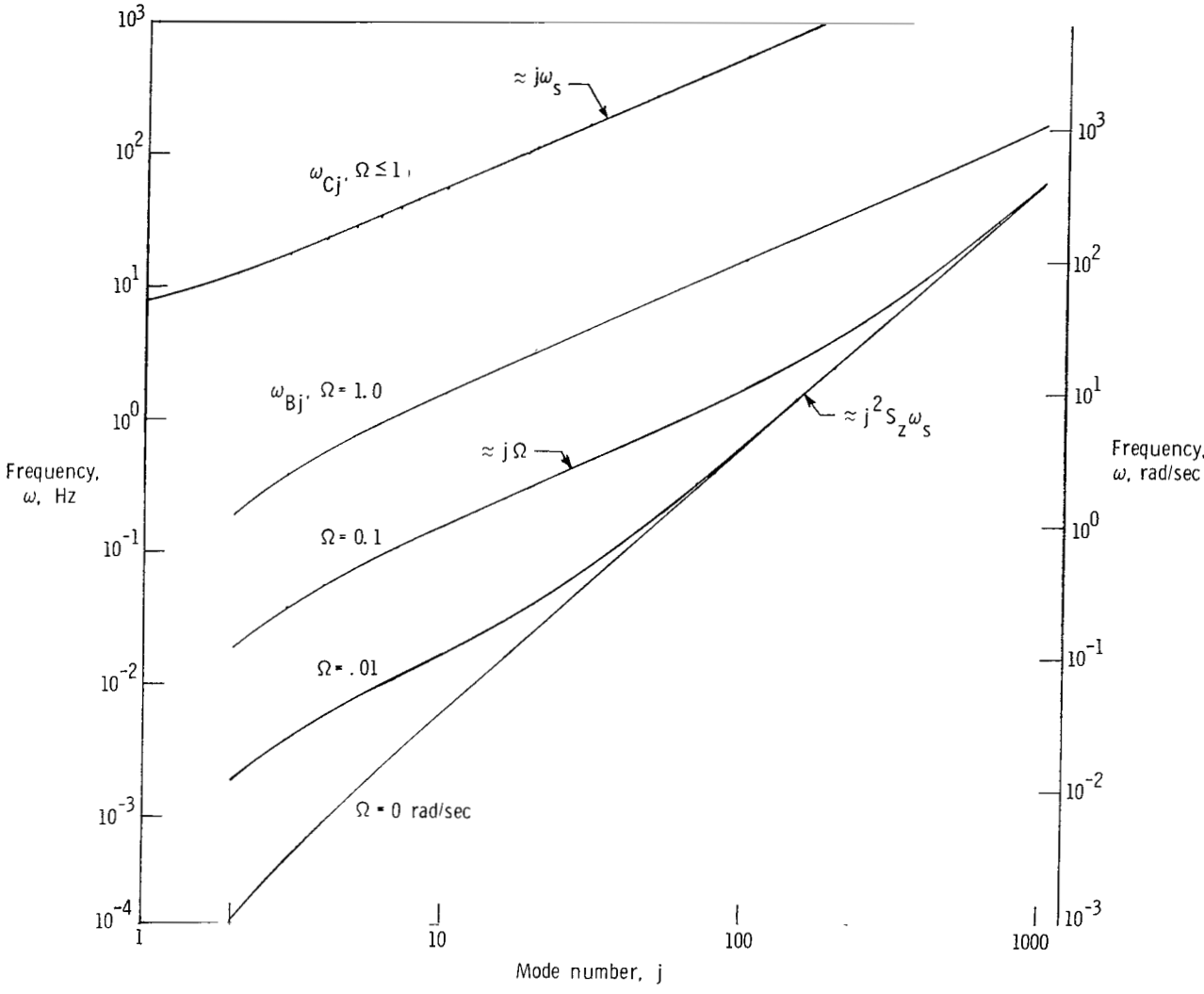

Figure 33.- In-plane modal frequencies.

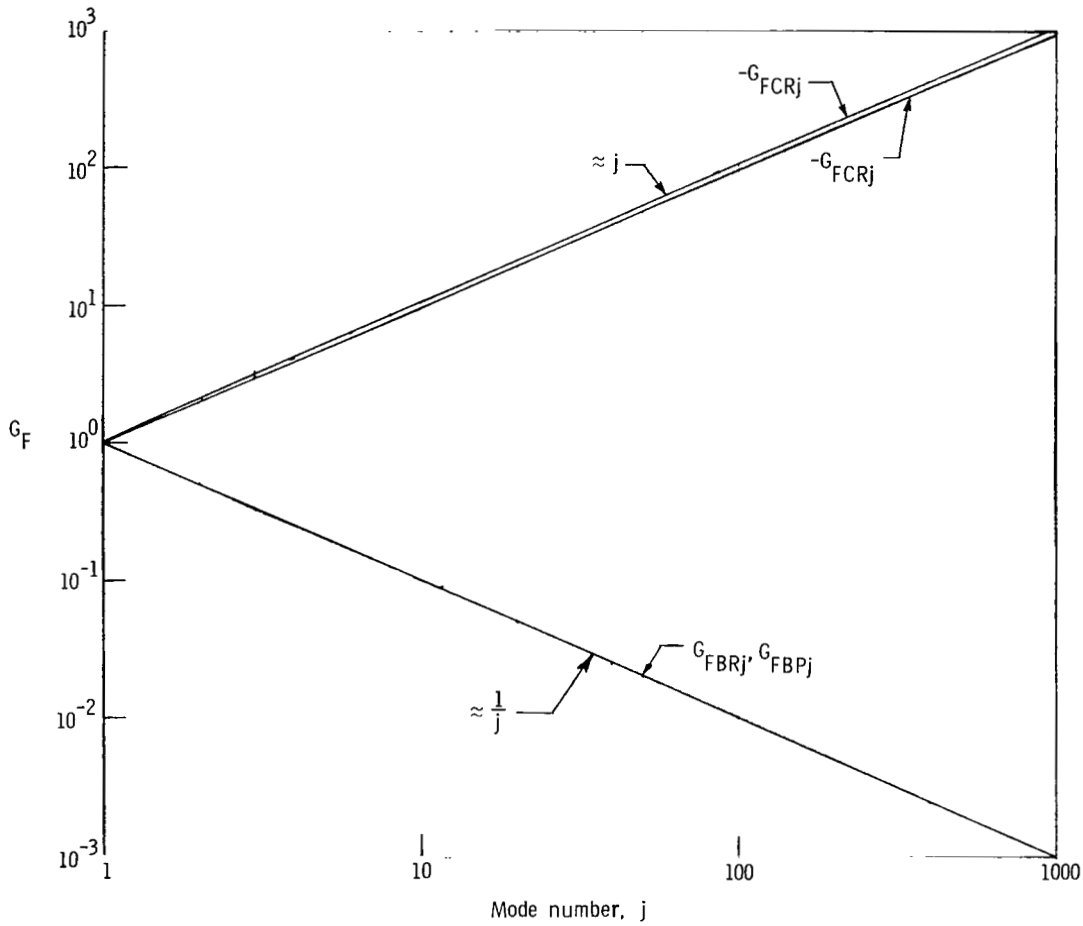

Figure 34.- Ratio of tangential motion to radial motion. Ω = 1 rad/sec.

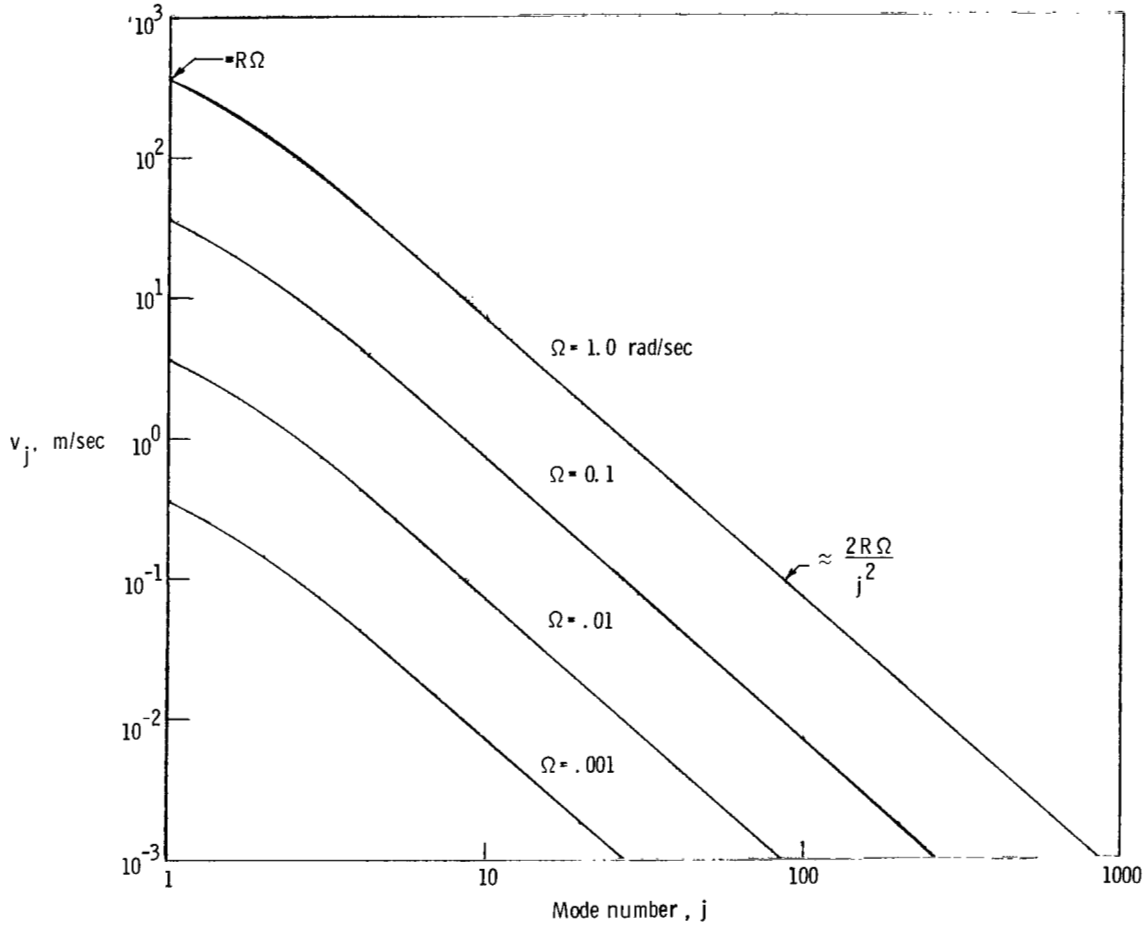

Figure 35.- In-plane nodal velocities.

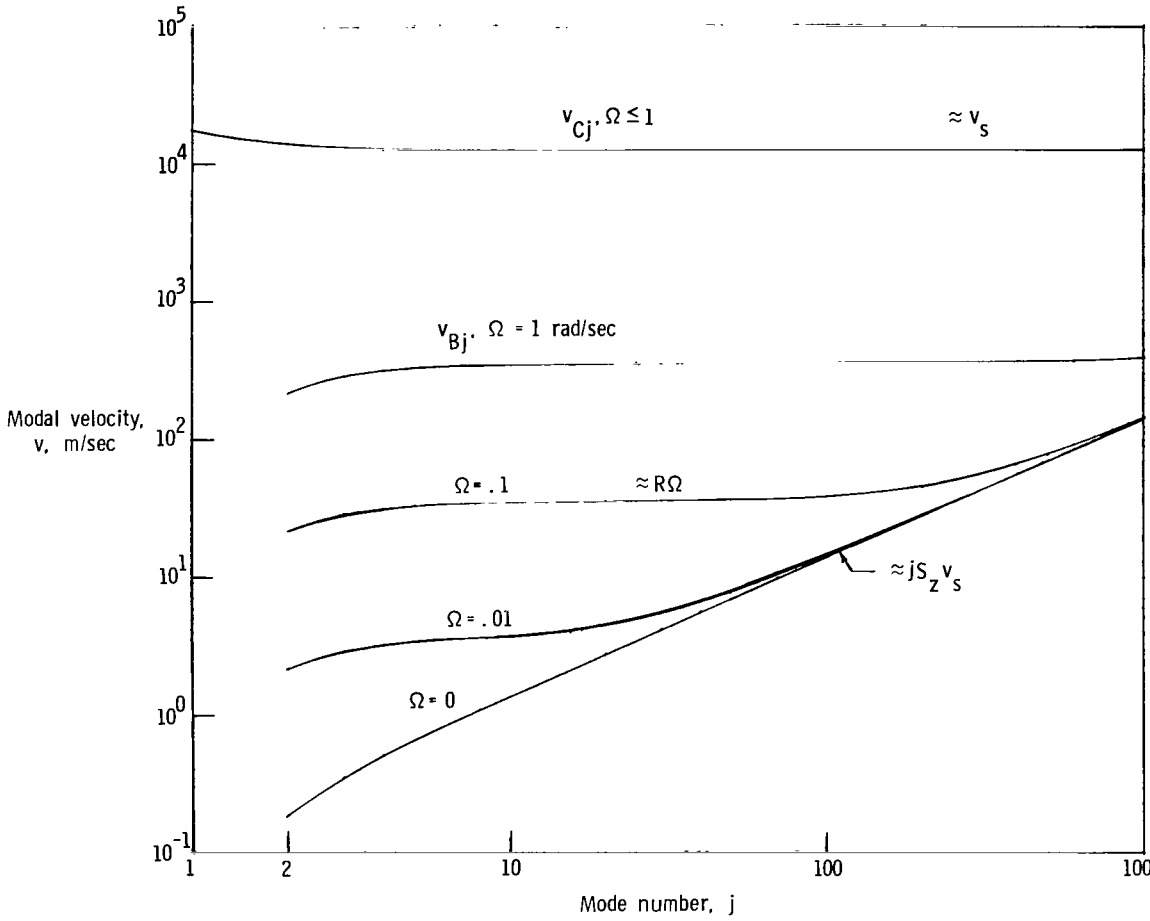

Figure 36.- In-plane modal velocities versus mode number.

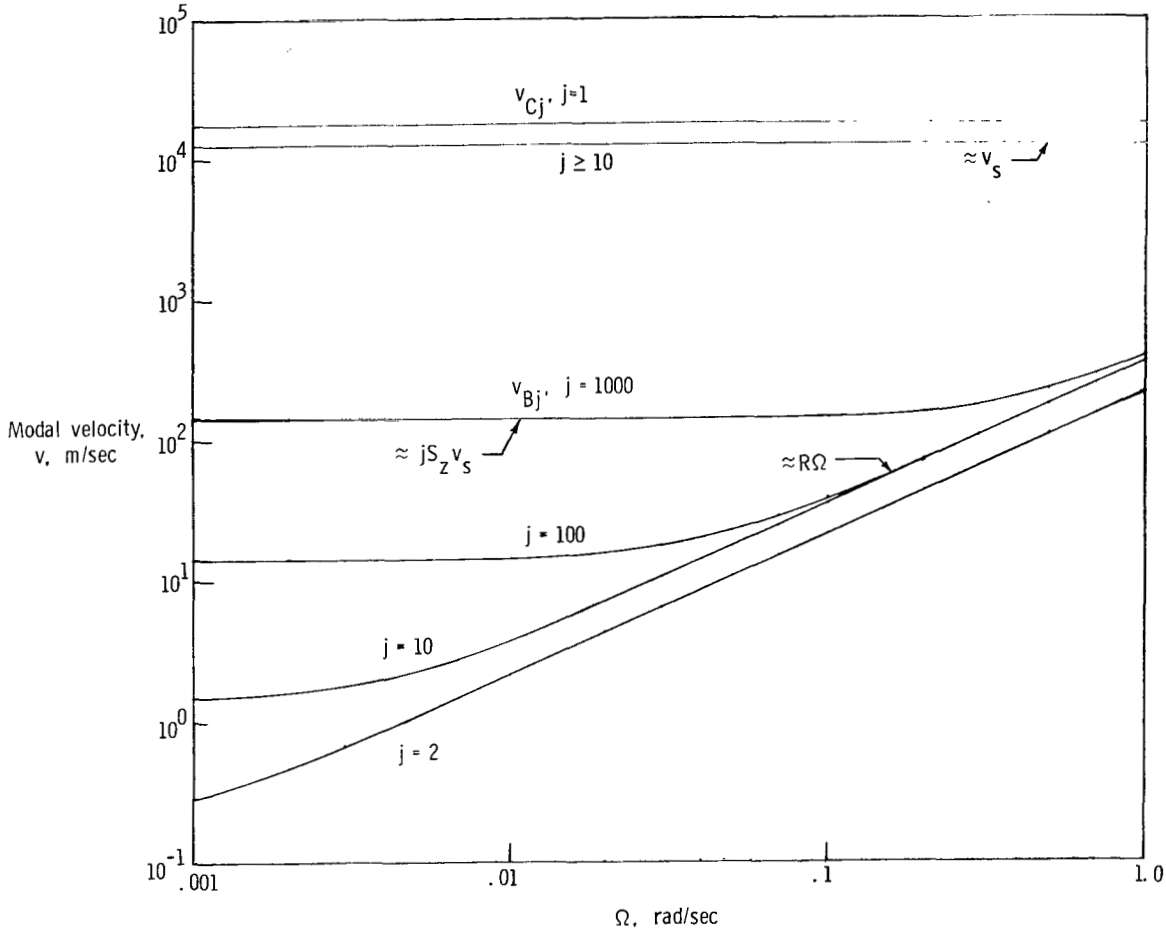

Figure 37.- In-plane modal velocities versus spin rate.

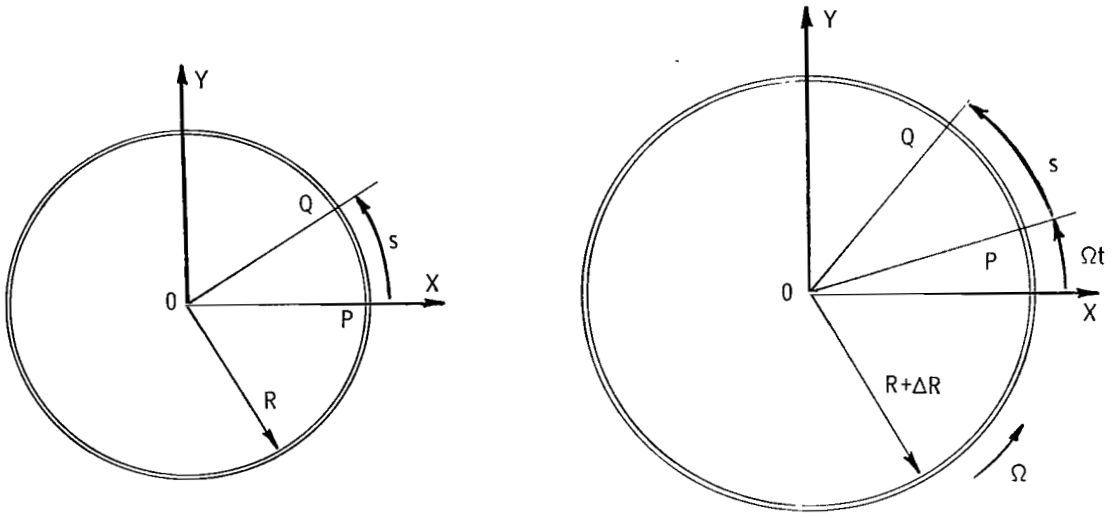

(a) Stationary ring. (b) Rotating ring.

Figure 38.- Geometry of the ring, plan view.

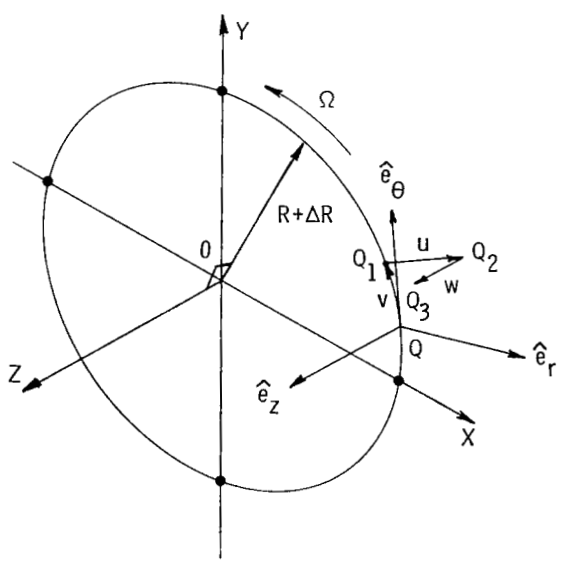

Figure 39.- Perturbation variables.

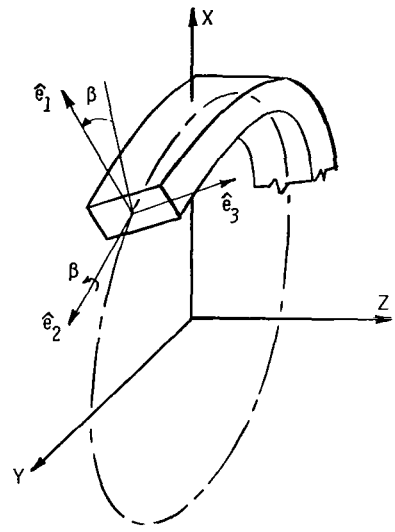

Figure 40.- Curvilinear coordinates.

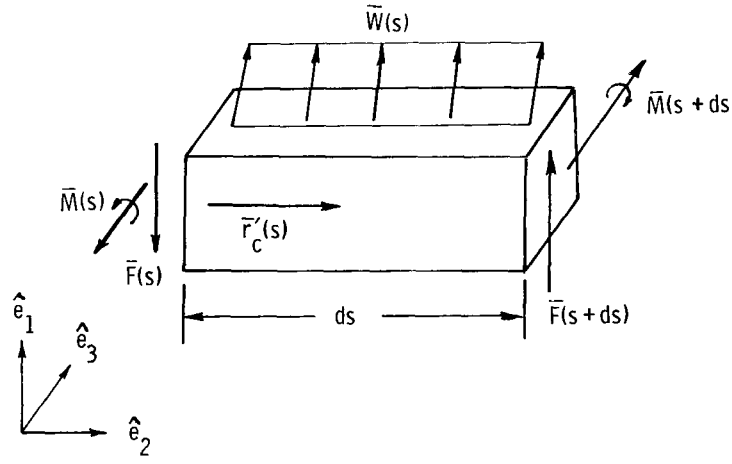

Figure 41.- Short ring segment with forces and moments acting upon it.

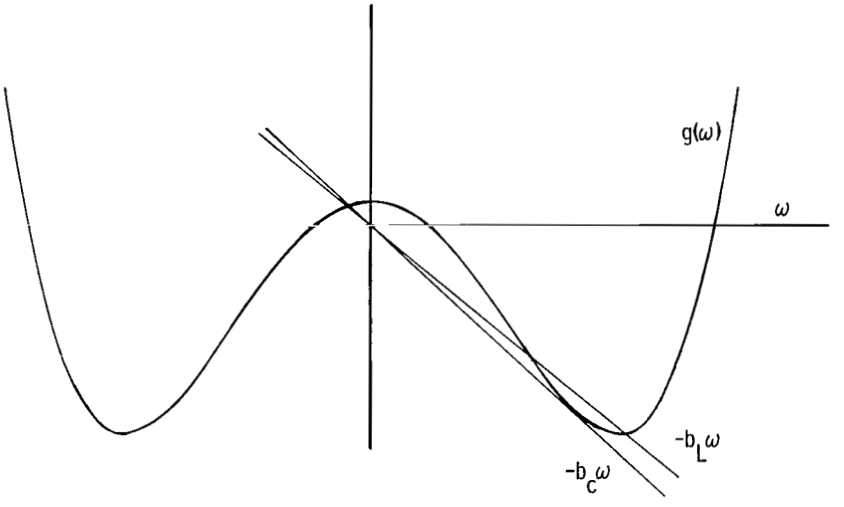

Figure 42.- Quartic polynomial.

1. Report No.	2. Government Accession No.	3. Recipient's Catalog No.
NASA TP-1775		

4. Title and Subtitle	5. Report Date
VIBRATION CHARACTERISTICS OF A STEADILY ROTATING SLENDER RING	December 1980
	6. Performing Organization Code: 506-53-63-04

7. Author(s)	8. Performing Organization Report No.
Frederick J. Lallman	L-13386
	10. Work Unit No.

9. Performing Organization Name and Address	11. Contract or Grant No.
NASA Langley Research Center Hampton, VA 23665	
	13. Type of Report and Period Covered: Technical Paper

12. Sponsoring Agency Name and Address	14. Sponsoring Agency Code
National Aeronautics and Space Administration Washington, DC 20546	

15. Supplementary Notes

16. Abstract

Partial differential equations are derived to describe the structural vibrations of a uniform homogeneous ring which is very flexible because the radius is very large compared with the cross-sectional dimensions. Elementary beam theory is used and small deflections are assumed in the derivation. Four sets of structural modes are examined: bending and compression modes in the plane of the ring, bending modes perpendicular to the plane of the ring, and twisting modes about the centroid of the ring cross section. Spatial and temporal characteristics of these modes, presented in terms of vibration frequencies and ratios between vibration amplitudes, are demonstrated in several figures. Given a sufficiently high rotational rate, the dynamics of the ring approach those of a vibrating string. In this case, the velocity of traveling waves in the material of the ring approaches the velocity of the material relative to inertial space, resulting in structural modes which are almost stationary in space.

17. Key Words (Suggested by Author(s))	18. Distribution Statement
Structural dynamics Vibrations Structural mechanics Spacecraft design Circular ring	Unclassified - Unlimited Subject Category 39

19. Security Classif. (of this report)	20. Security Classif. (of this page)	21. No. of Pages	22. Price*
Unclassified	Unclassified	97	A05

* For sale by the National Technical Information Service, Springfield, Virginia 22161

NASA-Langley, 1980

National Aeronautics and
Space Administration

Washington, D.C.
20546

Official Business
Penalty for Private Use, $300

THIRD-CLASS BULK RATE

Postage and Fees Paid
National Aeronautics and
Space Administration
NASA-451

U.S.MAIL

10 1 1U,D, 121980 S00903DS
DEPT OF THE AIR FORCE
AF WEAPONS LABORATORY
ATTN: TECHNICAL LIBRARY (SUL)
KIRTLAND AFB NM 87117

NASA

POSTMASTER: If Undeliverable (Section 158 Postal Manual) Do Not Return